Geometric morphometric variability in the supraorbital and orbital region of Middle Pleistocene hominins: Implications for the taxonomy and evolution of later *Homo*

Suzanna White [a,*], Matt Pope [b], Simon Hillson [b], Christophe Soligo [a]

[a] *Department of Anthropology, University College London, 14 Taviton Street, London, WC1H 0BW, UK*

[b] *Institute of Archaeology, University College London, 31-34 Gordon Square, London, WC1H 0PY, UK*

*Corresponding author.

E-mail address: suzanna.white@ucl.ac.uk (S. White).

Geometric morphometric variability in the supraorbital and orbital region of Middle Pleistocene hominins: Implications for the taxonomy and evolution of later *Homo*

Abstract

This study assessed variation in the supraorbital and orbital region of the Middle Pleistocene hominins, sometimes called *Homo heidelbergensis* s.l., to test whether it matched the expectations of intraspecific variation. The morphological distinctiveness and relative variation of this region, which is relatively well represented in the hominin fossil record, was analyzed quantitatively in a comparative taxonomic framework. Coordinates of 230 3D landmarks (20) and sliding semilandmarks (210) were collected from 704 specimens from species of *Homo*, *Australopithecus*, *Paranthropus*, *Gorilla*, *Pan*, *Papio*, and *Macaca*. Results showed that the Middle Pleistocene hominins had expected levels of morphological distinctiveness, intragroup, and intergroup variation in supraorbital and orbital morphology, relative to commonly recognized non-hominin catarrhine species. However, the Procrustes distances between this group and *H. sapiens* were significantly higher than expected for two closely related catarrhine species. Further, this study showed that variation within the MPH could be similarly well contained within existing hypodigms of *H. sapiens*, *H. neanderthalensis*, and *H. erectus* s.l. While quantitative assessment of supraorbital and orbital morphology did not allow differentiation between taxonomic hypotheses in later *Homo*, it could be used to test individual taxonomic affiliation and identify potentially anomalous individuals. This study confirmed a complicated pattern of supraorbital and orbital morphology in the Middle Pleistocene hominin fossil record, and raises further questions over our understanding of the speciation of *H. sapiens* and *H. neanderthalensis*, and taxonomic diversity in later *Homo*.

Keywords: *Homo heidelbergensis*; Taxonomy; Intraspecific variation; Interspecific variation; Supraorbital torus; Brow ridge

1. Introduction

1.1. Middle Pleistocene hominins

Species hypodigms form the analytical units of much biological research. Taxonomies are particularly challenging to achieve for the fossil record, however, where the data available to inform taxonomic decisions are limited. One example is the ongoing discussion over the correct taxonomic assignment of the Middle Pleistocene (or Chibanian) hominin remains (MPH), which encompass a group of specimens from this age that are more apomorphic than *Homo erectus* and more plesiomorphic than *Homo sapiens* and *Homo neanderthalensis*. MPH have been widely assumed to belong to the stem species of *H. neanderthalensis* and *H. sapiens* (Stringer, 1983, 2002, 2012; Rightmire, 1998; Mounier et al., 2009, 2011), although recent research may challenge this assumption (see below). These hominin fossils have been variably attributed to *H. erectus* or 'archaic *H. sapiens*' (Stringer et al., 1979; Rightmire, 1998; Harvati, 2007; Tattersall and Schwartz, 2009; Athreya and Hopkins, in press), yet have most frequently been assigned to *Homo heidelbergensis* in recent years (Rightmire, 1988; Stringer, 2012; Buck and Stringer, 2014).

While the name *H. heidelbergensis* is inextricably linked to its holotype, the Mauer 1 mandible (Schoetensack, 1908; Stringer, 2012), dated to 610 ka (Wagner et al., 2010), the anatomically limited nature of this specimen has complicated comparisons with craniofacial fossils and made it difficult to achieve a consensus on a hypodigm composition for this species (Rightmire, 2008; Hublin, 2009; Rak et al., 2011). Nevertheless, morphological assessment of a hominin assemblage from Caune de l'Arago, France, dated to approximately 438 ka (Falguères et al., 2004, 2015), which includes both cranial and mandibular fossils has led researchers to combine Mauer 1 and the Arago hominins with other Middle Pleistocene fossils from Africa and Europe into a single species, *Homo heidelbergensis* s.l. (Stringer et al., 1979; Seidler, 1997; Harvati, 2007; Rightmire, 2008; Schwartz and Tattersall, 2010; Guipert et al., 2014). In the most generalized view, *H. heidelbergensis* s.l. now encompasses the majority of craniofacial hominin fossils from the Middle Pleistocene of Africa and Europe showing indeterminate affinities to *H. erectus*, *H. sapiens*, and *H. neanderthalensis* (see Fabbri, 2006).

Further similarities between Asian MPH, frequently attributed to *H. erectus* s.s. or 'archaic *H. sapiens*' (e.g., Dali and Narmada), and European and African MPH (e.g., Kabwe 1 and Petralona; Groves and Mirazón Lahr, 1994; Bae, 2010; Wu and Athreya, 2013) have led some researchers to suggest the inclusion of these Asian specimens in discussions of a broad *H. heidelbergensis* s.l. hypodigm (Rightmire, 2008). In contrast, other researchers have suggested that this species should be restricted to a subset of European MPH documenting features shared with Mauer 1 and not found in other members of the wider MPH, i.e., *H. heidelbergensis* s.s. (Arsuaga et al., 1997; Bermúdez de Castro et al., 1997, 2003; Manzi, 2004; Hublin, 2009).

Despite suggestions of unifying autapomorphies (e.g., Buck et al., 2012; Stringer, 2012; Rightmire, 2013; Buck, 2014), MPH generally assigned to *H. heidelbergensis* s.l. are highly variable in craniofacial morphology (Dennell et al., 2011; Manzi, 2011), and have been argued to display a mosaic appearance of derived features (Harvati, 2007; Dennell et al., 2011; Stringer, 2012). They vary in occipital morphology, nasal profile, the relationship between the orbits and the anterior cranial fossae, the definition of the pituitary fossa, the extent of pneumatization in the cranial bones, dimensions of the neurocranium, upper facial height, facial breadth, breadth and position of the nasal aperture, inflation of the infraorbital region, and supraorbital torus form and thickness (Seidler, 1997; Rightmire, 2008; Tattersall and Schwartz, 2009; Schwartz and Tattersall, 2010). Indeed, some have argued that the amount of variation displayed by the MPH may be too great to be included in a single hominin species, potentially due to the weak morphological and theoretically questionable chronological criteria used to assign specimens to this group (Schwartz and Tattersall, 2010).

While the term *H. heidelbergensis* increased in use toward the end of the last century, following the discoveries at Arago and research by Rightmire (1996, 1998), recent developments have raised questions over its validity. Firstly, DNA analysis of fossil evidence from Sima de los Huesos, dated to 448 ka (Demuro et al., 2019), indicates that the *H. neanderthalensis* lineage had been established earlier in the Middle Pleistocene than previously thought (Meyer et al., 2016). A similar realization has occurred for *H. sapiens*, with early members from Jebel Irhoud, Morocco, now dated to 315 ka (Hublin et al., 2017; Richter et al., 2017). This places these early *H. sapiens* as contemporaneous with

the relatively more plesiomorphic Kabwe 1 fossil, recently dated to 299 ka (Grün et al., 2020), which is the holotype of the nominal species *Homo rhodesiensis* (Woodward 1921), and has been frequently included in *H. heidelbergensis* s.l. (e.g., Stringer, 1983, 2012; Prossinger, 2008; Godinho and O'Higgins, 2018). Furthermore, analyses of dental evolutionary rates suggest an earlier divergence between *H. sapiens* and *H. neanderthalensis* than indicated by previous estimates (e.g., Prüfer et al., 2014), either in the early Middle Pleistocene or possibly the late Early Pleistocene (Gómez-Robles, 2019). Taken together, these findings indicate that *H. heidelbergensis* s.l. may be polyphyletic (and therefore an invalid species), and necessitate a reassessment of the suggestion that the MPH may instead represent members of *H. sapiens*, *H. neanderthalensis*, and *H. erectus* s.l. (Stringer et al., 1979).

1.2. Aims

This study quantitatively assessed craniofacial variation within the MPH in a comparative taxonomic framework. The supraorbital and orbital region was chosen for this purpose, as it is particularly well represented across the craniofacial hominin fossils from the Middle Pleistocene of Africa, Europe, and Asia. Hominins show a diversity of supraorbital morphologies (see, e.g., Smith and Ranyard, 1980; Kimbel et al., 1984; Bookstein et al., 1999; Athreya, 2009), and this region has historically been considered important in distinguishing between late hominin groups (Weidenreich, 1947). The supraorbital and orbital region has also recently been found to preserve a suitably strong phenetic signal in the catarrhine primates, including later members of *Homo*, to allow identification of species and subspecies boundaries (White et al., 2020).

The MPH have been described as united in their supraorbital morphology (Schwartz and Tattersall, 2010), which simultaneously distinguishes them from Early and Late Pleistocene hominin species and potentially unifies them into a single group, despite considerable individual variation in supraorbital torus form and thickness (Rightmire, 2013). However, detailed analyses of MPH frontal bone profiles from Africa, Asia, and Europe have suggested that variation does not follow a simple geographical pattern of isolation by distance, and that the MPH are difficult to distinguish based on frontal bone

profiles alone (Athreya, 2006, 2009, 2012). As a group, the MPH have been described as having robust, hyperpneumatized, continuous, anteroposteriorly projecting supraorbital tori, especially in their lateral aspects (Freidline et al., 2012b; Stringer, 2012; Buck, 2014), which may be autapomorphic in features such as their lateral superoinferior thinning (Groves and Mirazón Lahr, 1994). As such, quantitative, comparative assessment of supraorbital and orbital variation within the MPH may contribute to clarification of the taxonomic status of *H. heidelbergensis* s.l.

Numerous studies have explored variation in hominin craniofacial anatomy by assessing intra- and intergroup variation within a taxonomic framework, to test species-level hypotheses. Such an approach has been applied repeatedly to *H. erectus* s.l. (e.g., Terhune, 2007; Baab, 2008; Rightmire, 2019), for instance, but has not yet been used for the MPH. The present study therefore contributes to our understanding of the MPH by using this approach to ask whether supra- and circumorbital variation within this group is compatible with expectations for variation in a single species (*H. heidelbergensis* s.l.), or whether observed patterns of variation are more compatible with the inclusion of the MPH within the existing hypodigms of *H. erectus* s.l., *H. neanderthalensis*, and *H. sapiens*. Such an assessment is necessary before consideration of factors known to affect intraspecific variation, such as sexual dimorphism, within-species evolution, static allometry, and geography.

The present study applied 3D geometric morphometric (GM) methods to record morphology in a greater area of the anterior cranium and in greater detail than previous studies of the supraorbital and orbital region in later *Homo*. GM methods have been shown to be effective at both visualizing and quantifying key morphological differences in complex structures (e.g., O'Higgins, 2000; Freidline et al., 2013; Steltzer et al., 2019; Bastir et al., 2020), and are well suited to comparative assessments of morphological variation. All analyses were performed in shape space, as this has previously been shown to be the most effective type of data for taxonomic discrimination based on supra- and circumorbital morphology in catarrhine primates (White et al., 2020).

A challenge faced by all analyses of morphological variation in the fossil record is the multi-factorial nature of influences on that variation. As with other skeletal regions, the morphology of the supraorbital and orbital region is affected by adaptive and neutral genetic processes, sexual

dimorphism (e.g., Bulygina et al., 2006; Garvin and Ruff, 2012), ontogeny and ageing (e.g., Russell, 1985; Hofbauer et al., 2003; Gonzalez et al., 2010), allometry (e.g., Rosas and Bastir, 2002; Freidline et al., 2015), and ecogeographical variables (e.g., Howells, 1973, 1989; Mirazón Lahr and Wright, 1996), with likely covariance between many of these factors. For example, biomechanical hypotheses, such as the anterior dental loading hypothesis (Oyen et al., 1970a,b; Russell, 1982, 1985), relate the evolution of the primate supraorbital torus to the need to resist masticatory-induced strain, whereas nonmechanical hypotheses, such as the neuro-orbital disjunction model (Moss and Young, 1960), incorporate structural and spatial hypotheses that focus on the integration of the supraorbital torus within the wider craniofacial complex. While there may be less support at present for a biomechanical explanation (e.g., Hylander et al., 1991; Ravosa, 1991; Picq, 1994) and slightly more support for a spatial model (e.g., Shea, 1986; Ravosa, 1988, 1991; Fiscella and Smith, 2006), with studies showing that the supraorbital region is under low-to-moderate masticatory strain (Lycett and Collard, 2005; Collard and Wood, 2007; Collard and Lycett, 2008; Kupczik et al., 2009; Tückmantel et al., 2009; von Cramon Taubadel, 2009; Godinho and O'Higgins, 2018), there is currently no consensus on the functional significance of the primate (or hominin) supraorbital torus, with alternative hypotheses including social communication also being considered (Godinho et al., 2018). Continued uncertainty regarding the factors driving morphological variation in the supraorbital region of hominins and other primates underlines the need to use multiple extant species models in order to evaluate morphological variation in MPH.

Other researchers have similarly made strong arguments for the use of multiple model species when comparing taxonomic variation between hominins and model primates (Jolly, 1970, 2001; Frost et al., 2003; Harvati et al., 2004; Baab, 2008). While *Pan* is typically used in paleoanthropological models, due to its close phylogenetic relationship with the hominins (Macho, 2018), the inclusion of a wider range of comparative model taxa is critical to building robust models of expected and maximum intraspecific variation, especially for a group such as the MPH, which occupied three continents, a variety of ecologies, and spanned over 400 kyr. Comparative model species were drawn from the Catarrhini, and include both monotypic and polytypic species to model average and maximum

expected intra- and interspecific variation (Mayr, 1969) as well as morphological (or biological) distinctiveness (Cardini et al., 2009; Cardini and Elton, 2011) across groups which vary in sexual dimorphism, temporal, and geographic range. The use of multiple model species allows for the possibility that fossil hypodigms may deviate from the pattern observed in a single, or some, model species, while falling within the recorded range for the others. Such cases can be assessed in the context of the factors known to determine patterns of variation in the model species concerned in order to refine taxonomic hypotheses in the fossil record.

1.3. Hypotheses

The present study explored two hypotheses regarding the pattern of relative variation within the supraorbital and orbital region of the MPH. The first hypothesis was that the MPH could be considered as a single species (*H. heidelbergensis* s.l.). The alternative, based on recent evidence for an earlier divergence between *H. sapiens* and *H. neanderthalensis*, and contemporaneity of more plesiomorphic and more derived hominins in the Middle Pleistocene, is a revision of an earlier suggestion: that the MPH are not a coherent species, and instead incorporate members of *H. sapiens*, *H. neanderthalensis*, and *H. erectus* s.l. lineages.

Main hypothesis When considered as a separate group, supraorbital and orbital variation in the MPH will be consistent with expectations for a single species. This hypothesis would be rejected if the morphological distinctiveness, intra-, and intergroup variation of the MPH were found to be incompatible with the expectations for a distinct species, as measured in the extant non-hominin catarrhine species (see predictions below).

Alternative hypothesis When the MPH are not considered as a separate group, and instead placed within either *H. sapiens*, *H. neanderthalensis*, or *H. erectus* s.l., supraorbital and orbital variation in these hominin species will be consistent with the expectations for distinct species. This hypothesis would be rejected if morphological distinctiveness, intra-, and intergroup variation within the expanded *H. sapiens*, *H. neanderthalensis*, and *H. erectus* s.l. hypodigms were found to be

incompatible with the expectations for separate species, as measured in the extant non-hominin catarrhine species.

The following predictions were made for species-level variation in supraorbital and orbital morphology, based on existing literature (see Simpson, 1961; Simons and Pilbeam, 1965; Mayr, 1969; Tattersall, 1986, 1992; Wood, 1991; Albrecht and Miller, 1993; Kimbel and Martin, 1993; Lockwood et al., 1999; Harvati, 2003; Harvati et al., 2004; Terhune et al., 2007; Groves, 2012; Rightmire, 2019):

Morphological distinctiveness (sensu Cardini et al., 2009; Cardini and Elton, 2011), assessed via stepwise, jackknife cross-validated linear discriminant analysis of principal component values, will be within the expected range for a species, as quantified in extant non-hominin catarrhine species.

Intraspecific variation, measured through intragroup Procrustes distances (see, e.g., Bookstein, 1996; Klingenberg, 2005), will not be statistically greater than that found in extant non-hominin catarrhine species.

Interspecific variation, measured through intergroup Procrustes distances, will not be statistically smaller than that found in extant non-hominin catarrhine species.

The magnitude of intra- relative to interspecific variation will be comparable to that found in the non-hominin catarrhine species.

2. Materials and Methods

2.1. Sample

This study included 13 MPH (Table 1), many of which have previously been assigned to *H. heidelbergensis* s.l. The Florisbad cranium from South Africa and the Zuttiyeh fossil from Israel are variably identified as 'archaic *H. sapiens*', *H. neanderthalensis*, or late *H. heidelbergensis* s.l. (Simmons et al., 1991; Rightmire, 2001, 2009; Zeitoun, 2001; Freidline et al., 2012a; Bruner et al., 2013), although Florisbad has also been used to describe a separate species, *Homo helmei* (Dreyer, 1935; McBrearty and McBrearty, 2000; Mirazón Lahr and Foley, 2001). Recent aDNA analysis of the Sima de los Huesos assemblage from Atapuerca, Spain, has indicated that these hominins form part of a wider *H. neanderthalensis* clade (Meyer et al., 2016), supporting indications from earlier

morphological analyses (e.g., Arsuaga et al., 1997, 2014; Martinón-Torres et al., 2012). Nevertheless, these hominins have also been compared to other MPH such as Petralona and Arago 21 based on their craniofacial morphology (Arsuaga et al., 1993, 1997, 2014), leading to their earlier attribution to *H. heidelbergensis* s.l. (Arsuaga et al., 1997).

The specimens included in this analysis comprised a large proportion of the MPH fossils that preserve the supraorbital and orbital region, with the exception of Ndutu, Jinniushan, Yunxian, Gruta da Aroeira, and the other crania from Sima de los Huesos. The Yunxian hominins show considerable postdepositional damage and distortion (Li and Etler, 1992; Etler, 1996; Vialet et al., 2010), and the Jinniushan cranium is fragmented and largely reconstructed in the frontal region (Wu, 1988). The Ndutu specimen has gone through multiple reconstruction efforts (Clarke, 1976, 1990) and only preserves a portion of the right frontal bone and the left supraorbital torus, and was therefore excluded from this study. The remaining specimens were excluded due to limited access opportunities, although Gruta da Aroeira is also damaged in the lateral aspects of the supraorbital torus. The sample therefore included all of the sufficiently well-preserved MPH specimens for which access could be secured, and, as such, represents the best currently available estimate of supraorbital variation in this group.

Under the alternative hypothesis, the 13 MPH were assigned to *H. erectus* s.l., *H. neanderthalensis*, or *H. sapiens*. Assignation was based on the presence of autapomorphic features (for *H. sapiens* and *H. neanderthalensis*), or the absence of these autapomorphies (for *H. erectus* s.l.), following the literature (Table 2). Due to the debate over the attribution of the Zuttiyeh specimen, two versions of this hypothesis were tested: one in which Zuttiyeh was considered *H. sapiens*, and another where it was considered *H. neanderthalensis*.

Details of the Pleistocene hominin specimens are shown in Table 3 (see also Supplementary Online Material [SOM] Table S1). The *H. sapiens* sample also included 172 Holocene, non-fossil (i.e. archaeological or historical) specimens (see SOM Table S2) from a wide geographical and temporal range. *Homo sapiens* specimens were further assigned to different groups by date and morphology: Pleistocene specimens showing a mosaic of *H. sapiens* autapomorphies (e.g., bipartite brow, canine fossa, retracted face, globular neurocranium; see Day and Stringer, 1982; Lieberman et al., 2002;

Schwartz, 2016) and plesiomorphic traits were distinguished as early *H. sapiens* (EHS, *n* = 6), while Pleistocene specimens showing all expected *H. sapiens* autapomorphies were grouped as anatomically modern *H. sapiens* (AMHS, *n* = 17), and Holocene specimens (both fossil specimens from Table 3 and archaeological and historical specimens from SOM Table S2) as recent *H. sapiens* (RHS, *n* = 184) due to evidence of increasing gracilization in this period (Mirazón Lahr, 1996; Cieri et al., 2014; Mirazón Lahr, 2016). These subgroups were used for stratified sampling in bootstrapping procedures (see Section 2.3), ensuring sampling across the time period of this species.

The MPH and *H. erectus* s.l. were divided into geographical subgroups for visualization in principal component plots. The MPH were categorized as either African, Asian, or European, due to discussion over taxonomic relationships between these groups (Harvati, 2007; Bae, 2010; Dennell et al., 2011; Manzi, 2011; Martinón-Torres et al., 2011; Stringer, 2012). *Homo erectus* s.l. specimens were divided into African, Georgian, and Asian members, due to the ongoing debate over the correct taxonomic assignment of these hominins (Kramer, 1993; Baab, 2008; Lordkipanidze et al., 2013; Baab, 2016). Specimens of *H. erectus* s.l. were chosen based on their relative preservation across the supraorbital and orbital region, to minimize the impact of reconstruction on estimates of intragroup variation in model species. While the final sample size for this group was relatively low (*n* = 7), this was one of many comparison species used to model intraspecific variation, and the specimens used ranged across much of the timespan of this species, meaning that this sample should provide a useful measure of variation caused by within-species evolution, albeit over a longer period of time than for the MPH.

The comparative sample consisted of adult specimens from species and subspecies within *Homo*, *Australopithecus*, *Paranthropus*, *Gorilla*, *Pan*, *Papio*, and *Macaca* (see White et al., 2020 and SOM Tables S1 and S2 for further details). Adult status was assessed dentally, by the full eruption of the third molars, and cranially, by full fusion of the occipital-sphenoidal synchondrosis. Specimens showing evidence of pathology or trauma affecting the region of interest were excluded. 3D surface models were collected with a NextEngine desktop laser scanner (model 2020i), with additional surface models being generated from available CT data using 3D Slicer v. 4.5 (Fedorov et al., 2012).

Research-quality casts were used when access to original fossils was limited (see Table 3 and SOM Table S1).

The final sample consisted of 704 individuals (Table 4). The proportions of total females and males were approximately equal (301 [42.8%] vs. 291 [41.3%], respectively), although this varied between groups and sex was unknown for some specimens. Sex of *H. sapiens* specimens was estimated following Buikstra and Ubelaker (1994) when known sex data were not available. Sex determination methods were not attempted on fossil or cast specimens due to issues with the applicability of standards deduced from modern reference samples across hominin evolutionary history. Sex data were taken from the museum records for non-hominin catarrhine specimens, when available.

2.2. Reconstruction

Most fossil hominin specimens included in this study were not completely preserved across the region of interest, and many specimens documented postdepositional distortion. Despite selection for the best-preserved specimens available, a number of *H. sapiens* and non-hominin catarrhine specimens also had missing data. A combination of reconstruction methods was therefore used, with specimens being assessed individually to apply the most appropriate method (SOM S1). Some surface models were reconstructed before landmarking, using digital reconstruction methods, with either the original model being reflected to reconstruct missing regions, or a suitable surface model being used as a template, and retrodeformation was used to correct distortion in two fossil hominins. Missing points were estimated using reflection across an empirical midplane estimated by orthogonal regression (for a single point in a bilateral pair), geometric reconstruction using thin-plate splines and matched reference samples (for a few missing points), or manual virtual reconstruction (for points automatically placed on endocranial surfaces on models generated from CT data; further details can be found in SOM S1).

2.3. Methods

Landmarking This study used a configuration of 230 3D landmarks and semilandmarks. This consisted of nine landmarks placed around the orbital region, along with a mesh of 221 points placed over the supraorbital and orbital region, which included 11 anchoring landmarks (SOM Table S3). Two additional landmarks (left and right auriculare) were used in the identification of defining planes (Frankfort horizontal, midsagittal, and paracoronal) for mesh placement, but were not included in the final configuration. While many of the landmarks were standard craniometric points, some definitions had to be adapted or created in order to allow homology between all primate species used, and to account for frequent damage to certain areas of the cranium (e.g., the lacrimal bones). All landmarking was conducted in Checkpoint v. 2016.06.28.0428 or 2018.09.07.0325 (Stratovan Corporation, 2016, 2018). Intraobserver error for the landmark configuration was assessed using the methods of White et al. (2020) and was found to be significantly lower than intra- and intertaxonomic distances (SOM S2; SOM Table S4; SOM Fig. S1), meaning that intraobserver error should not significantly affect the outcomes of this study.

Generalized Procrustes analysis The data were put through a generalized Procrustes analysis (GPA) with a partial Procrustes fit (Rohlf and Slice, 1990; Rohlf, 1999) using the 'gpagen' function in the 'geomorph' package v. 3.3.1 (Adams et al., 2013) in R v. 3.6.1 (R Core Team, 2014). During this process, the semilandmarks were slid to minimize bending energy. Registered configurations were visualized for the 13 MPH using 3D scatterplots for qualitative comparison. Procrustes shape coordinates were subsequently put through a principal component analysis (PCA) in Morphologika 2 v. 2.5 (O'Higgins and Jones, 1998). The first and second principal components (PCs) were used to visualize the major trends in morphological variation within the sample. This process was also repeated for a dataset consisting of just the hominin specimens.

Morphological distinctiveness Stepwise, jackknife cross-validated discriminant analyses were performed to assess morphological distinctiveness of species for the recorded region (following Cardini et al., 2009; Cardini and Elton, 2011; White et al., 2020), with the principal components accounting for over 95% of total sample variation from PCA of the entire sample being entered as

variables, and prior probabilities being calculated from group (i.e., actual and hypothesized species) numbers. Analyses were run separately on the non-hominin catarrhine and hominin datasets.

To account for differences in sample sizes between species, the process was repeated on 1000 random subsets of specimens. For the non-hominin catarrhine analysis, the subsets were comprised of the eight *Papio cynocephalus* specimens, and eight randomly selected specimens from each of the remaining species, resulting in 1000 subsets of 80 individuals. For the hominin analysis, the subsets consisted of eight randomly selected specimens from each of *H. sapiens*, *H. neanderthalensis* and the MPH, combined with all seven (under the main hypothesis) or eight randomly selected members of *H. erectus* s.l. (under the alternative hypothesis), and both *Homo habilis*, resulting in 1000 subsets of 33 or 34 individuals. Within *H. sapiens*, subsamples were set to randomly select two specimens from EHS, two from AMHS, and four from RHS, to ensure all subsamples included temporal and geographic variation across the species.

Members of *Homo naledi*, *Homo rudolfensis*, *Australopithecus africanus*, *Paranthropus boisei*, and *Paranthropus aethiopicus* were excluded from discriminant analyses due to their low sample size. *Homo habilis* was included to provide more conservative classification of the *H. erectus* s.l. specimens by further subdividing the morphospace (White et al., 2020). Discriminant analyses were performed in R using the 'stepclass' function from the 'klaR' package v. 0.6.15 (Weihs et al., 2005) and the 'lda' function from the 'MASS' package v. 7.3.51.5 (Venables and Ripley, 2002). Descriptive statistics of classification accuracy were calculated for each species across the 1000 repeats.

Intra- and intergroup variation The Procrustes distance matrix, extracted from the Procrustes residuals, was used to calculate intra- (i.e., Procrustes distances between each member of a single species to every other conspecific) and intergroup (i.e., Procrustes distances between each member of one species and each member of another species) distances. These were visualized using violin and distribution plots. Distributions of intra- and intergroup distances for the relevant hominin groups were compared to those of non-hominin catarrhine species, with subsampling being used to test for significant differences (see below). Interspecies distances were only calculated between closely

related species (i.e., within the same genus) for the non-hominin catarrhines, and between relevant hominin groups for the hypothesis being tested.

First, to directly compare the amount of intragroup variation in the 13 MPH relative to accepted species under the main hypothesis, 1000 samples of 13 individuals were selected from each comparative species (but see below). Subsamples were controlled to randomly select approximately equal numbers of individuals from each subspecies (in the case of *Pan troglodytes*, all *Gorilla* species, and *Macaca fuscata*), and equal numbers of recent vs. anatomically modern and early *H. sapiens* (Table 3; SOM Tables S1 and S2). The vectors of intragroup Procrustes distances for these subsamples were then compared to that of the 13 MPH using independent sample t-tests. Results were considered significant if $p < 0.05$ in over 95% of repeats.

Available sample sizes prevented the application of this approach for comparisons with *Pap. cynocephalus* ($n = 8$), *H. erectus* s.l. ($n = 7$ under the main hypothesis), and *H. neanderthalensis* ($n = 13$). Therefore, 1000 random subsamples of eight (for comparisons with *Pap. cynocephalus*) and seven (for comparisons with *H. erectus* s.l.) MPH were compared to a vector of Procrustes distances for the first two of these groups, using the same threshold for significance as stated above. A single independent sample t-test was used to directly compare intragroup Procrustes distances of the 13 *H. neanderthalensis* to those of the 13 MPH.

Analysis was repeated with smaller subsamples to compare intra- and intergroup variation with equal sample size across groups, under both hypotheses. Subsample numbers were set to the sample size of the smallest group: $n = 7$ for *H. erectus* s.l. under the main hypothesis, and $n = 8$ for *Pap. cynocephalus* under the alternative hypothesis (and for non-hominin catarrhine comparisons). Hominin intra- and intergroup Procrustes distances were compared to intra- and interspecific Procrustes distances across the non-hominin catarrhines using subsampling with 1000 repeats. Hominin intragroup Procrustes distances were then compared to intergroup distances for both hypotheses, and to values for non-hominin catarrhine comparisons.

3. Results

3.1. Generalized Procrustes analysis

PCA for the entire sample resulted in 687 PCs, with the first 19 accounting for over 95% of total sample variation combined, and the first eight accounting for >1% of variation individually. PC1, which accounted for 63.9% of sample variance, was the major axis along which the hominin groups were differentiated (see below), and partially separated the *Gorilla* (which had more negative values) from the other non-hominin catarrhines (Fig. 1). More negative values on this axis were associated with anteroposteriorly deep brow ridges, post-toral sulci, and wide, laterally flared supraorbital tori, with the inferior aspect of the orbit being more posteriorly positioned. As the values along this PC increased, the configurations became taller superoinferiorly, with a more bulging, vertical frontal squama, and a higher mid-frontotemporale point. The post-toral sulcus and supraorbital torus disappeared between the median and maximum values, the lateral components of the supraorbital torus moved laterally to become parallel with the edges of the frontal squama, and the inferior points of the orbit were more anteriorly positioned, lying under the frontal squama.

PC2 accounted for 8.8% of sample variation, mainly differentiating the *Gorilla* (which had more negative values) from the other taxa; hominin taxa largely overlapped in their values along this axis. Specimens with more negative values had relatively superoinferiorly shorter brow ridges that protruded mostly in the inferior aspects, taller frontal squama, narrower frontals, shorter orbits, and broader nasal columns.

Figure 2 shows the results of the PCA using only the hominin specimens from the sample, with the Middle Pleistocene hominins identified (see also SOM Fig. S2). PC1 (52.1%) separated out the hominins along a cline from more robust (negative end) to more gracile (positive end), with recent *H. sapiens* having the most positive values. PC2 (9.3%) mainly separated the *Paranthropus* specimens and Dinaledi hominin 1 from later hominins, due to their lower values along this axis, although the range of values for *H. sapiens* encompassed the variation in all other hominins along this axis. The MPH overlapped with the spaces occupied by *H. erectus* s.l., *H. neanderthalensis,* and *H. sapiens.* In this view, the 13 MPH occupied a larger area than the seven *H. erectus* s.l. and the 13 *H. neanderthalensis*, but a smaller area than the 207 *H. sapiens*.

3.2. Prediction 1: Morphological distinctiveness

Mean species classification accuracy for the non-hominin catarrhines, as measured in the discriminant analysis and taken as a proxy of morphological distinctiveness, was 72.3% across the 1000 repeats (see SOM Table S5 for ranges and standard deviation) and varied within groups from 48.6% in *Pap. cynocephalus* to 86.2% in *Papio kindae* (Table 5). Mean species classification accuracy for the hominins was 82.4% (75.2% when the value for *H. habilis* was included; Table 6; see also Table 7 and SOM Table S6). *Homo neanderthalensis* and *H. sapiens* were found to have relatively high classification accuracy (90.9% and 85.4%, respectively), while *H. habilis* had relatively low classification accuracy of 46.2%, although this figure should be interpreted cautiously due to the low sample size for this species. Classification accuracy for the MPH was 77.6%, which was similar to that of *H. erectus* s.l. (75.7%).

When the discriminant analysis was repeated without the MPH grouping (i.e., under the alternative hypothesis, where the MPH fossils were variably assigned to other late *Homo* species), mean hominin classification accuracy was 85.7%, and 80.3% or 79.9% (with Zuttiyeh classified as *H. sapiens* or *H. neanderthalensis*, respectively) when *H. habilis* were included (Table 8). Classification accuracy for *H. sapiens* was lower under this hypothesis (87.7% or 88.7%), while classification accuracy was similar for *H. neanderthalensis* (86.2% or 85.7%) and higher for both *H. erectus* s.l. (83.2% or 82.6%) and *H. habilis* (63.9% or 62.6%).

3.3. Prediction 2: Intragroup variation

Homo erectus s.l., *Pa. boisei*, and the *Gorilla* species were found to have the highest levels of intragroup variation in the supraorbital and orbital morphology, as measured by overall intragroup Procrustes distances (Fig. 3), while the lowest values were found within *Pap. kindae*. Intragroup variation for the MPH (main hypothesis) was slightly higher than that of *H. sapiens* and *H. neanderthalensis*, but lower than that for *H. erectus* s.l. Intragroup variation for *H. sapiens* and the MPH was similar to intraspecific variation across the non-hominin catarrhines (Fig. 4), while

intragroup variation for *H. neanderthalensis* and *H. erectus* s.l. was lower and higher, respectively, than found in the non-hominin catarrhines (Figs. 3 and 4). The 13 MPH were significantly less variable than equally sized subsamples of *Gorilla beringei* in 99.1% of cases, and not significantly different (i.e., $p \geq 0.05$ in 95% or more of repeats) in intragroup variation to the other model species, including *H. sapiens* and *H. erectus* s.l. (Table 9). Independent sample t-tests showed that intragroup variation (Procrustes distances) for the MPH (0.097) was significantly higher than for *H. neanderthalensis* (0.082), $t(152.2) = 4.5$, $p < 0.001$. When subsampling ($n = 7$) was applied to all groups, the MPH were found to be not significantly different to all comparison groups (SOM Table S7).

Variation within *H. sapiens* was similar under the alternative hypothesis (SOM Fig. S3), although some intragroup Procrustes distances exceeded the maximum recorded intraspecific distances in non-hominin catarrhine comparisons (SOM Fig. S4). Intragroup variation for *H. neanderthalensis* was increased, and more similar to intraspecific variation across the non-hominin catarrhines than under the main hypothesis. Variation within *H. erectus* s.l. was slightly lowered on average, but there was an increase in relatively large Procrustes distances between individuals attributed to this group.

When subsampling ($n = 8$) was used, variation within *H. sapiens* was found to be not significantly greater than any other group, regardless of the inclusion or exclusion of Zuttiyeh (SOM Table S8). *Homo neanderthalensis* were significantly less variable than *G. beringei* regardless of inclusion of Zuttiyeh, and not significantly different to all other groups. Variation within *H. erectus* s.l. was significantly greater than within *Pap. kindae*, and not significantly different to all other groups.

3.4. Prediction 3: Intergroup variation

Intergroup variation between *H. sapiens* and the MPH was found to be higher than pooled interspecies distances across the non-hominin catarrhines (Fig. 5), and significantly larger than interspecific distances in a number of non-hominin catarrhine comparisons (Table 10). Intergroup variation between the MPH and *H. neanderthalensis* was broadly comparable to pooled interspecies distances within non-hominin catarrhines, while variation between the MPH and *H. erectus* s.l. was slightly

higher, and both were not significantly different to interspecific distances between closely related non-hominin catarrhines.

Under the alternative hypothesis, pooled distances between subsamples of *H. sapiens* and *H. erectus* s.l. were larger than interspecies values for non-hominin catarrhines, while distances between *H. neanderthalensis* and *H. erectus* s.l. were more comparable to values for the non-hominin catarrhine models (SOM Fig. S5). Procrustes distances between subsamples of *H. sapiens* and *H. erectus* s.l. were significantly larger than those for all non-hominin catarrhine interspecific comparisons (SOM Table S9). In contrast, distances between *H. neanderthalensis* and *H. erectus* s.l. were only significantly different in comparison to interspecific distances between *Pap. kindae* and *Pap. cynocephalus*.

3.5. Prediction 4: Intra- vs. intergroup variation

Pooled intraspecific distances were found to be significantly lower on average than interspecific distances for non-hominin catarrhines ($\overline{x}$ = 0.097 vs. $\overline{x}$ = 0.106, t(28236) = -35.7, $p < 0.001$; see also SOM Fig. S6). However, when subsampling (n = 8) was used to directly compare intra- and interspecific Procrustes distances between closely related (i.e., same genus) non-hominin catarrhine species, significant differences were only found for *Pap. kindae* when compared to *Papio anubis* (SOM Table S10). Nevertheless, examination of t values showed that intraspecific distances were lower than interspecific distances in the majority of repeats in all subsampling comparisons (see also SOM Fig. S7).

Intragroup Procrustes distances for the MPH (under the main hypothesis) were found to be lower than the distances between the MPH and both *H. sapiens* and *H. erectus* s.l. (Fig. 6), but similar to those between the MPH and *H. neanderthalensis*. The only significant difference was noted when comparing variation within the MPH to variation between the MPH and *H. sapiens*, with the former being lower than the latter in 100.0% of cases. However, within-group variation was generally lower than intergroup variation between all hominin comparisons (Table 11).

Under the alternative hypothesis, intragroup distances for *H. sapiens* were significantly smaller than intergroup distances in comparisons to both *H. erectus* s.l. and *H. neanderthalensis* (SOM Fig. S8; SOM Table S11). The majority of intragroup distances were smaller than intergroup distances for *H. neanderthalensis* comparisons. Distances within *H. erectus* s.l. were found to be significantly smaller than distances between this group and *H. sapiens*. No significant difference was found between intragroup distances for *H. erectus* s.l. and intergroup distances with *H. neanderthalensis*, and t values showed that intragroup distances were larger than intergroup distances in the majority of cases in this comparison.

4. Discussion

This study quantitatively assessed variation in the supraorbital and orbital morphology of the MPH under two competing taxonomic hypotheses: one where they are considered a distinct species (*H. heidelbergensis* s.l.); and another where they are not, and are instead included as members of *H. erectus* s.l., *H. neanderthalensis*, and *H. sapiens*. The results indicated that supraorbital and orbital variation within late *Homo* groups is compatible with the expectations for catarrhine species under both taxonomic hypotheses. This result cannot be simply dismissed as a consequence of limited anatomical coverage, as the recorded morphology can successfully delineate a range of other, widely accepted hominin and non-hominin catarrhine species at relatively high accuracy (see also White et al., 2020).

4.1. Morphological distinctiveness

The morphological distinctiveness of the MPH supraorbital and orbital morphology was within the expected range for a catarrhine species (Tables 5 and 6), although it was relatively low in comparison to *H. neanderthalensis* and *H. sapiens*. The high morphological distinctiveness of this region of *H. neanderthalensis* and *H. sapiens* (Table 6), despite their close phylogenetic relationship and multiple recorded interbreeding events (Green et al., 2010; Prüfer et al., 2014; Sankararaman et al., 2014; Fu et al., 2015; Racimo et al., 2015; Sánchez-Quinto and Lalueza-Fox, 2015), supports the taxonomic and

morphological distinction between these species (Harvati, 2003; Harvati et al., 2004; Tattersall, 2005; Tattersall and Schwartz, 2006, 2008; Bruner et al., 2013; White et al., 2014, 2020).

The MPH had comparable morphological distinctiveness to the sample of *H. erectus* s.l. (Table 6), despite a previous study noting relatively higher morphological distinctiveness in the supraorbital and orbital region of the latter group (White et al., 2020); this difference is likely due to the inclusion of more members of the MPH in the present study, increasing the morphological cohesion of this group. The debate over the taxonomic attribution of *H. erectus* s.l. is complex (Antón, 2003; Etler, 2004; Bilsborough, 2005; Rightmire et al., 2006; Baab, 2008, 2016; Lordkipanidze et al., 2013). The acceptance by some of *H. erectus* s.l. as a single species is based on the premise that this group maintains morphological cohesion despite having a high degree of morphological variability (Baab, 2008, 2016), which would be supported by the morphological distinctiveness of the supraorbital and orbital region reported for this group here.

Assessment of morphological distinctiveness under the alternative hypothesis, where the MPH were assigned to *H. sapiens*, *H. neanderthalensis*, or *H. erectus* s.l., indicated that these groups were also relatively distinct in their supraorbital and orbital morphology, under the expectations set by the non-hominin catarrhines. Overall, the morphological distinctiveness under both hypotheses confirms the discriminatory power, and therefore taxonomic utility, of the supraorbital and orbital region in these late hominins (Weidenreich, 1947, Athreya, 2009).

4.2. Intragroup variation

Intragroup variation for the MPH did not differ significantly from that found in most other catarrhine species in our sample, including the geographically and temporally broad samples of *H. sapiens* and *H. erectus* s.l. While the recorded variation within the MPH may be an underestimate, due to the limited number of fossils in this group, this applies similarly to *H. erectus* s.l. and *H. neanderthalensis*, and methods employed controlled for the potential impact of different sample sizes. As such, this study provides quantitative evidence that variation within the supraorbital and orbital

region is not too high for the MPH to be considered as a single species (contra Schwartz and Tattersall, 2010).

Some of the recorded variation within the supraorbital and orbital region of the MPH could be due to spatiotemporal effects, which are accounted for through the use of multiple model species with different geographic and temporal ranges. While some researchers have argued for the presence of potential regional traits within the MPH (Manzi, 2011, 2016), to date no or only weak correlation has been described between morphological distance in the MPH frontal bone and temporal and geographic distance (Athreya, 2006). While within-species evolution and geographic separation undoubtedly contribute to variation within the supraorbital and orbital morphology of the MPH, they are intraspecific factors (Albrecht and Miller, 1993; Albrecht et al., 2002) meaning that their study, as well as that of the effects of other infraspecific factors such as static allometry and sexual dimorphism, are dependent on a consensus as to the classification taxonomic attribution of the MPH at the species level.

H. neanderthalensis were recorded as having particularly low intraspecific variation in the study region, supporting the results of previous studies (e.g., Hawks and Wolpoff, 2001; Gunz et al., 2009). The sample of this group covered a relatively short time period of~125 ka for the Krapina individuals (Rink et al., 1995) to ~40 ka for Spy 1 (Devièse et al., 2021), and was composed mainly of 'classic' Neanderthals (Dean, 1998). As such, their low recorded variation is possibly due to the effects of population bottlenecks, small population sizes, and inbreeding, particularly in the case of later populations (Briggs et al., 2009; Prüfer et al., 2014; Sánchez-Quinto and Lalueza-Fox, 2015; Prüfer et al., 2017). As with *H. sapiens*, inclusion of some MPH within *H. neanderthalensis* under the alternative hypothesis did not increase intraspecific variation beyond the expectations set by the non-hominin primate models.

Variation within *H. erectus* s.l. was particularly high, supporting the recent results of Baab (2021). Intragroup variation for this group was most comparable to *Pa. boisei* and the *Gorilla* species, which may indicate a similar effect of relatively high sexual dimorphism (Wood et al., 1991; Aiello and Wood, 1994; Silverman et al., 2001); however, estimates of sexual dimorphism for *H. erectus* s.l.,

while variable, are not comparable to those of *Gorilla* (e.g., Plavcan, 2012; but see debate over Dmanisi hominins, e.g., Bermúdez de Castro et al., 2014; Rightmire et al., 2019). The *H. erectus* s.l. sample covered a long temporal range—1.78–1.85 Ma for the Dmanisi hominins (Ferring et al., 2011) to 108–117 ka for Ngandong (Rizal et al., 2020). As such, the high variability of this group is likely to be partially explained by within-species evolution. Interestingly, average variability within *H. erectus* s.l. decreased when the MPH were included under the alternative hypothesis, underlining the pronounced variability of the original *H. erectus* s.l. sample and the plesiomorphic nature of the MPH (Stringer et al., 1979; Harvati, 2007).

4.3. Intergroup variation

Intergroup distances between the MPH and *H. sapiens*, under the main hypothesis, and *H. erectus* s.l. and *H. sapiens*, under the alternative hypothesis, were higher than expected based on the non-hominin catarrhine comparisons. This is likely due to the highly distinctive supraorbital and orbital morphology of the later members of *H. sapiens*, reflected in the PCA plots: with the exception of three EHS (Jebel Irhoud 1, Omo 1, and Skhūl V; see below), there is a relatively clear separation between *H. sapiens* and other hominins, although this result should be interpreted with caution as it only relates to the two key axes of variation within the sample.

Later *H. sapiens* are pedomorphic in their lack of 'true' supraorbital tori. Instead, they most commonly have non-continuous tori with small supraciliary arches, and small glabellae that lie below them (the 'glabellar butterfly'; Kurten, 1979; Smith and Ranyard, 1980; Russell, 1985; Lieberman, 2000; Schwartz and Tattersall, 2010), as well as high, rounded, bulging frontal squamae (Lieberman et al., 2002; Bruner et al., 2013). Jebel Irhoud 1, Omo 1, and Skhūl V are all notable for their lack of a glabellar butterfly or a bipartite supraorbital torus (Schwartz and Tattersall, 2010). These specimens overlapped with *H. neanderthalensis* and MPH in the present study in terms of their less bulging foreheads and more klinorhynchic faces, with the former two being misclassified as *H. neanderthalensis* in the discriminant analyses, while the latter was misclassified as an MPH.

Other studies have found similar results, particularly regarding the similarities between Jebel Irhoud 1 and *H. neanderthalensis* (e.g., Gunz et al., 2009; Freidline et al., 2012b; Mounier and Mirazón Lahr,

2019; Stelzer et al., 2019). One suggested interpretation of this is that Jebel Irhoud 1 is more closely related to the early *H. sapiens* which expanded out of Africa and interbred with early *H. neanderthalensis*, impacting the evolution of the 'classic' Neanderthal morphology (Mounier and Mirazón Lahr, 2019), aligning with suggestions of deep population substructure within early *H. sapiens* (Gunz et al., 2009; Sankararaman et al., 2012; Scerri et al., 2018, 2019; Bergström et al., 2021). This argument might be supported by the greater similarity in supraorbital and orbital morphology between SH5 (an early member of the Neanderthal clade) and *H. erectus* s.l. than later *H. neanderthalensis* (see Section 4.5), and the relatively small difference between the MPH and *H. neanderthalensis*, although a similar pattern may not be found in other craniofacial regions.

4.4. Intra- vs. intergroup variation

A pattern of greater interspecific variation than intraspecific variation was predicted based on expectations of morphological differentiation of species, although this pattern is acknowledged as not universal to all species and all regions, and within-species variation has frequently been noted to be greater than that between species (Simpson, 1951). Nevertheless, the results of the present study found that interspecific variation in supraorbital and orbital morphology was generally higher than intraspecific variation for the non-hominin catarrhines, although not significantly so in most cases.

4.5. Implications for the classification of the Middle Pleistocene hominins

The results of the present study indicated that Florisbad and Kabwe 1 are potentially anomalous members of the MPH group in terms of their orbital and supraorbital morphology, based on misclassifications from the discriminant analyses (Table 7) and the PCA plot. Florisbad, currently dated to 260 ka (Grün et al., 1996), is considered by some as an early *H. sapiens* (Stringer, 2016; Hublin et al., 2017), especially given the recently published dates of 315 ka for the Jebel Irhoud assemblage (Richter et al., 2017), although the supraorbital and orbital morphology of this specimen showed a closer affinity with *H. neanderthalensis* in the present study. Unlike Florisbad, Kabwe 1 is considered as unlikely to be a member of the *H. sapiens* lineage due to its recent age of 299 ka

combined with its morphology, which shows no *H. sapiens* autapomorphies (Grün et al., 2020; but see Rightmire, 2001) and a more plesiomorphic supraorbital and orbital region relative to earlier members of the MPH (e.g., Bodo; this study).

The present study included Asian fossils in its broad definition of the MPH, despite discussion over whether specimens such as Narmada, Maba, and Dali may represent early members of *H. sapiens*, *H. neanderthalensis*, Denisovans (Stringer, 2012; Hublin, 2013), or a sister lineage to early *H. sapiens* (Ji et al., in press; Ni et al., in press). While Narmada and Dali clustered towards *H. neanderthalensis* in the PCA, Maba was located more towards *H. sapiens*, due to its bulging frontal squama (Figure 2); all, however, were classified within the MPH when more aspects of supraorbital variation were taken into consideration (Table 7). The present study therefore leaves open the possibility of multiple affiliations within the Asian MPH record while providing support for inclusion of those specimens in the *H. heidelbergensis* s.l. hypodigm.

Zuttiyeh was slightly more problematic, plotting at the edge of the *H. sapiens* cluster in the PCA, yet being classified with the other MPH in the discriminant analysis. Exploration of the alternative hypothesis assigned this specimen to either *H. sapiens* or *H. neanderthalensis*, with minimal difference being found in terms of intra- and intergroup variation between these two schemes. The potentially late date of this fossil (Freidline et al., 2012a), along with its mixed morphology and geographic location, suggest that it needs to be reassessed, especially given discussions over the reticulated history of these later *Homo* species and recent arguments of a late Middle Pleistocene paleo-deme of early Neanderthals in the Levant showing more intermediate morphology relative to other late *Homo* (Hershkovitz et al., 2021).

A relatively early presence of members of the *H. neanderthalensis* clade has been recorded at Sima de los Huesos (Meyer et al., 2016; Demuro et., 2019), and evidence at Gran Dolina, also at Atapuerca, may indicate a late Early Pleistocene appearance of some *H. neanderthalensis* autapomorphies (Arsuaga et al., 1999). Despite this, the present study indicates that the recorded morphology of at least one of the Sima de los Huesos hominins (SH5) is more similar to that of the MPH and *H. erectus* s.l. than later *H. neanderthalensis*, indicating that the 'classic' Neanderthal supraorbital and orbital

morphology appeared in the late Middle Pleistocene. This may complicate the identification of other early members of the *H. neanderthalensis* clade through supraorbital and orbital morphology alone. Indeed, none of the European MPH clustered with *H. neanderthalensis*, with Florisbad being the only MPH misclassified within this group.

5. Conclusions

This study assessed the relative morphological variation in the supraorbital and orbital region of the MPH within a comparative taxonomic framework. It tested predictions of expected intra- and interspecific morphological variation under two hypotheses, contributing quantitative data to the debate over the taxonomy of these hominins. Variation within the supraorbital and orbital region of the MPH fulfills most of the expectations for a single, distinct species, despite recent evidence which would question the likelihood of a multicontinental *H. heidelbergensis* s.l. hypodigm. This study also showed, however, that supraorbital and orbital variation within the MPH could be similarly well-accommodated within the expectations of intraspecific variation by placing specimens within existing hypodigms of *H. erectus* s.l., *H. neanderthalensis*, and *H. sapiens*.

Despite the importance that has been given to the hominin supraorbital region in previous research, and the high discriminatory power recorded for this region in this study, in-depth analysis of morphological variation in this region does not allow differentiation between taxonomic hypotheses in the MPH. While this study therefore cannot provide a definite answer to the question of the taxonomy of the MPH, it confirms the emerging perspective that the MPH are the product of a complex, mosaic pattern of morphological variation. It is likely that the Middle Pleistocene documents the speciation, coexistence, and interbreeding of multiple hominin groups, which may be separated by more complicated factors than geography alone.

3D quantitative analysis of the supraorbital and orbital region contributes useful data for determining the taxonomic affiliation of individual later *Homo* fossils, and for the potential identification of atypical specimens. As such, the present study provides important insights into the relatively late morphological divergence of early *H. sapiens* and classic *H. neanderthalensis* from the Middle

Pleistocene hominins in at least one craniofacial region, as well as possible supporting evidence of population substructure within our species and the impact of interbreeding between early *H. sapiens* and *H. neanderthalensis*.

Acknowledgements

We would like to thank the following curators for allowing access to the specimens in their collections: C. Stringer and R. Kruszynski (Natural History Museum, London); M. Mirazón Lahr and M. Belatti (Duckworth Laboratory, University of Cambridge); G. Garcia and E. Hoeger (American Museum of Natural History, New York); E. Gilissen (Royal Museum for Central Africa, Tervuren); K. Hussey and C. Phillips (Royal College of Surgeons, London); I. Livne (Powell Cotton Museum, Kent); H. Hashimoto (Kyoto University Museum, Kyoto); D. Shimizu (Kyoto University Primate Research Institute, Kyoto); P. Semal (Royal Belgian Institute of Natural Sciences, Brussels); S. Bond (Institute of Archaeology, UCL, London); G. Price (Biological Anthropology Collection, UCL, London); K. Helgen (Division of Mammals, Smithsonian, Washington, DC); and M. Tocheri (Human Origins Program, Smithsonian, Washington, DC). We would like to acknowledge the help of A. Gleeson in the development of the scripts for some of the analyses, and A. Lockey, N. Barber and A. Gómez-Robles for their helpful comments during the development of this manuscript. We are also grateful to D. Alba, C. Zanolli, an anonymous associate editor, and the anonymous reviewers for their constructive and extensive comments on earlier versions of this paper. This research was supported by an AHRC/LAHP-funded studentship, grant reference number AH/L503873/1.

References

Adams, D.C., Otárola-Castillo, E., Paradis, E., 2013. Geomorph: An R package for the collection and analysis of geometric morphometric shape data. Methods in Ecology and Evolution 4, 393-399.

Aiello, L.C., Wood, B.A., 1994. Cranial variables as predictors of hominine body mass. American Journal of Physical Anthropology 95, 409-426.

Albrecht, G.H., Miller, J.M.A., 1993. Geographic variation in primates: A review with implications for interpreting fossils. In: Kimbel, W.H., Martin, L.B. (Eds.), Species, Species Concepts and Primate Evolution. Plenum Press, New York, pp. 123-162.

Antón, S.C., 2003. Natural history of *Homo erectus*. American Journal of Physical Anthropology 122, 126-170.

Arsuaga, J.L., Martínez, I., Arnold, L.J., Aranburu, A., Gracia-Téllez, A., Sharp, W.D., Quam, R.M., Falguères, C., Pantoja-Pérez, A., Bischoff, J., Poza-Rey, E., Parés, J.M., Carretero, J.M., Demuro, M., Lorenzo, C., Sala, N., Martinón-Torres, M., García, N., Alcázar de Velasco, A., Cuenca-Bescós, G., Gómez-Olivencia, A., Moreno, D., Pablos, A., Shen, C.-C., Rodríguez, L., Ortega, A.I., García, R., Bonmatí, A., Bermúdez de Castro, J.M., Carbonell, E., 2014. Neandertal roots: Cranial and chronological evidence from Sima de los Huesos. Science 344, 1358-1363.

Arsuaga, J.L., Martínez, I., Gracia, A., Carretero, J.M., Carbonell, E., 1993. Three new human skulls from the Sima de los Huesos Middle Pleistocene site in Sierra de Atapuerca, Spain. Nature 362, 534-537.

Arsuaga, J.L., Martínez, I., Gracia, A., Lorenzo, C., 1997. The Sima de los Huesos crania (Sierra de Atapuerca, Spain). A comparative study. Journal of Human Evolution 33, 219-281.

Arsuaga, J.L., Martínez, I., Lorenzo, C., Gracia, A., Muñoz, A., Alonso, O., Gallego, J.S., 1999. The human cranial remains from Gran Dolina Lower Pleistocene site (Sierra de Atapuerca, Spain). Journal of Human Evolution 37, 431-457.

Athreya, S., 2006. Patterning of geographic variation in Middle Pleistocene *Homo* frontal bone morphology. Journal of Human Evolution 50, 627-643.

Athreya, S., 2009. A comparative study of frontal bone morphology among Pleistocene hominin fossil groups. Journal of Human Evolution 57, 786-804.

Athreya, S., 2012. The frontal bone in the genus *Homo*: a survey of functional and phylogenetic sources of variation. Journal of Anthropological Science 90, 59-80.

Athreya, S., Hopkins, A. (in press). Conceptual issues in hominin taxonomy: *Homo heidelbergensis* and an ethnobiological reframing of species. American Journal of Physical Anthropology. DOI: 10.1002/ajpa.24330.

Baab, K.L., 2008. The taxonomic implications of cranial shape variation in *Homo erectus*. Journal of Human Evolution 54, 827-847.

Baab, K.L., 2016. The role of neurocranial shape in defining the boundaries of an expanded *Homo erectus* hypodigm. Journal of Human Evolution 92, 1-21.

Baab, K.L., 2021. Reconstructing cranial evolution in an extinct hominin. Proceedings of the Royal Society B: Biological Sciences 288, 20202604.

Bae, C.J., 2010. The late Middle Pleistocene hominin fossil record of eastern Asia: Synthesis and review. American Journal of Physical Anthropology 143, 75-93.

Bastir, M., García-Martínez, D., Torres-Tamayo, N., Palancar, C.A., Beyer, B., Barash, A., Villa, C., Sanchis-Gimeno, J.A., Riesco-López, A., Nalla, S., Torres-Sánchez, I., García-Río, F., Been, E., Gómez-Olivencia, A., Haeusler, M., Williams, S.A., Spoor, F., 2020. Rib cage anatomy in *Homo erectus* suggests a recent evolutionary origin of modern human body shape. Nature Ecology & Evolution 4, 1178-1187.

Bergström, A., Stringer, C., Hajdinjak, M., Scerri, E.M.L., Skoglund, P., 2021. Origins of modern human ancestry. Nature 590, 229-237.

Bermúdez de Castro, J.M., Arsuaga, J.L., Carbonell, E., Rosas, A., Martínez, I., Mosquera, M., 1997. A hominid from the lower Pleistocene of Atapuerca, Spain: Possible ancestor to Neandertals and modern humans. Science 276, 1392-1395.

Bermúdez de Castro, J.M., Martinón-Torres, M., Sarmiento, S., Lozano, M., 2003. Gran Dolina-TD6 versus Sima de los Huesos dental samples from Atapuerca: Evidence of discontinuity in the European Pleistocene population? Journal of Archaeological Science 30, 1421-1428.

Bermúdez de Castro, J.M., Martinón-Torres, M., Sier, M.J., Martín-Francés, L., 2014. On the variability of the Dmanisi mandibles. PLoS One 9, e88212.

Bilsborough, A., 2005. *Homo erectus* revisited: Aspects of affinity and diversity in a Pleistocene hominin species. Anthropologie 43, 129-158.

Bookstein, F.L., 1996. Biometrics, biomathematics and the morphometric synthesis. Bulletin of Mathematical Biology 58, 313.

Bookstein, F., Schäfer, K., Prossinger, H., Seidler, H., Fieder, M., Stringer, C., Weber, G.W., Arsuaga, J.L., Slice, D.E., Rohlf, F.J., Recheis, W., Mariam, A.J., Marcus, L.F., 1999. Comparing frontal cranial profiles in archaic and modern *Homo* by morphometric analysis. The Anatomical Record Part B: The New Anatomist 257, 217-224.

Briggs, A.W., Good, J.M., Green, R.E., Krause, J., Maricic, T., Stenzel, U., Lalueza-Fox, C., Rudan, P., Brajkovic, D., Kucan, Z., Gusic, I., Schmitz, R., Doronichev, V.B., Golovanova, L.V., de la Rasilla, M., Fortea, J., Rosas, A., Pääbo, S., 2009. Targeted retrieval and analysis of five Neandertal mtDNA genomes. Science 325, 318-321.

Bruner, E., Athreya, S., de la Cuétara, J.M., Marks, T., 2013. Geometric variation of the frontal squama in the genus *Homo*: Frontal bulging and the origin of modern human morphology. American Journal of Physical Anthropology 150, 313-323.

Buck, L.T., 2014. Craniofacial morphology, adaptation, and paranasal pneumatisation in Pleistocene hominins. Ph.D. Dissertation, University of Roehampton.

Buck, L.T., Stringer, C.B., 2014. *Homo heidelbergensis*. Current Biology 24, R214-R215.

Buck, L.T., Stringer, C.B., MacLarnon, A.M., Rae, T.C., 2012. Paranasal sinus shape in Pleistocene hominins. American Journal of Physical Anthropology S54, 108.

Buikstra, J.E., Ubelaker, D.H., 1994. Standards for Data Collection from Human Skeletal Remains: Proceedings of a Seminar at the Field Museum of Natural History, Organized by Jonathan Haas. Arkansas Archaeological Survey, Fayetteville.

Bulygina, E., Mitteroecker, P., Aiello, L., 2006. Ontogeny of facial dimorphism and patterns of individual development within one human population. American Journal of Physical Anthropology 131, 432-443.

Cameron, D., Patnaik, R., Sahni, A., 2004. The phylogenetic significance of the Middle Pleistocene Narmada hominin cranium from central India. International Journal of Osteoarchaeology 14, 419-447.

Cardini, A., Elton, S., 2011. GeMBiD, a geometric morphometric approach to the study of biological diversity: An example study of the red colobus (*Procolobus* [*Piliocolobus*]) species complex. International Journal of Primatology 32, 377-389.

Cardini, A., Nagorsen, D., O'Higgins, P., Polly, P.D., Thorington, R.W., Tongiorgi, P., 2009. Detecting biological distinctiveness using geometric morphometrics: An example case from the Vancouver Island marmot. Ethology Ecology & Evolution 21, 209-223.

Cieri, R.L., Churchill, S.E., Franciscus, R.G., Tan, J., Hare, B., 2014. Craniofacial feminization, social tolerance, and the origins of behavioral modernity. Current Anthropology 55, 419-443.

Clark, J.D., 1994. African *Homo erectus* - Old radiometric ages and young Oldowan assemblages in the Middle Awash Valley, Ethiopia. Science 264, 1907-1910.

Clarke, R.J., 1976. New cranium of *Homo erectus* from Lake Ndutu, Tanzania. Nature 262, 485-487.

Clarke, R.J., 1990. The Ndutu cranium and the origin of *Homo sapiens*. Journal of Human Evolution 19, 699-736.

Collard, M., Wood, B., 2007. Hominin homoiology: An assessment of the impact of phenotypic plasticity on phylogenetic analyses of humans and their fossil relatives. Journal of Human Evolution 52, 573-584.

Collard, M., Lycett, S.J., 2008. Does phenotypic plasticity confound attempts to identify hominin fossil species? Folia Primatologica 79, 111-122.

Czarnetzki, A., 1983. Zur Entwicklung des Menschen in Südwestdeutschland. In: Müller-Beck, H. (Ed.), Urgeschichte in Baden-Württemberg. Konrad Theiss, Stuttgart, pp. 217-240.

Day, M., Stringer, C.B. (1982). A reconsideration of the Omo-Kibish remains and the *erectus-sapiens* transition. In: de Lumley, H. (Ed.), L'*Homo erectus* et la Place de L'Homme de Tautavel Parmi les Hominidés Fossiles 2 (1982). Centre National de la Recherche Scientifique, Nice, pp. 814-846.

Dean, D., 1998. On the phylogenetic position of the pre-Neandertal specimen from Reilingen, Germany. Journal of Human Evolution 34, 485-508.

Demuro, M., Arnold, L.J., Aranburu, A., Sala, N., Arsuaga, J.-L., 2019. New bracketing luminescence ages constrain the Sima de los Huesos hominin fossils (Atapuerca, Spain) to MIS 12. Journal of Human Evolution 131, 76-95.

Dennell, R.W., Martinón-Torres, M., Bermúdez de Castro, J.M., 2011. Hominin variability, climatic instability and population demography in Middle Pleistocene Europe. Quaternary Science Reviews 30, 1511-1524.

Devièse, T., Abrams, G., Hajdinjak, M., Pirson, S., De Groote, I., Di Modica, K., Toussaint, M., Fischer, V., Comeskey, D., Spindler, L., Meyer, M., Semal, P., Higham, T., 2021. Reevaluating the timing of Neanderthal disappearance in Northwest Europe. Proceedings of the National Academy of Sciences USA 118, e2022466118.

Dreyer, T., 1935. A human skull from Florisbad. Proceedings of the Royal Academy of Science Amsterdam 38, 119-128.

Etler, D., 1996. The fossil evidence for human evolution in Asia. Annual Review of Anthropology 25, 275-301.

Etler, D.A., 2004. *Homo erectus* in East Asia: Human ancestor or evolutionary dead-end? Athena Review 4, 37-50.

Fabbri, P.F., 2006. Mandible and taxonomy of the earliest European *Homo*. Human Evolution 21, 289-300.

Falguères, C., Shao, Q., Han, F., Bahain, J.J., Richard, M., Perrenoud, C., Moigne, A.M., Lumley de, H., 2015. New ESR and U-series dating at Caune de l'Arago, France: A key-site for European Middle Pleistocene. Quaternary Geochronology 30B, 547-553.

Falguères, C., Yokoyama, Y., Shen, G., Bischoff, J.L., Ku, T.-L., de Lumley, H., 2004. New U-series dates at the Caune de l'Arago, France. Journal of Archaeological Science 31, 941-952.

Fedorov, A., Beichel, R., Kalpathy-Cramer, J., Finet, J., Fillion-Robin, J.C., Pujol, S., Bauer, C., Jennings, D., Fennessy, F., Sonka, M., Buatti, J., Aylward, S., Miller, J.V., Pieper, S., Kikinis, R., 2012. 3D Slicer as an image computing platform for the Quantitative Imaging Network. Magnetic Resonance Imaging 30, 1323-1341.

Ferring, R., Oms, O., Agustí, J., Berna, F., Nioradze, M., Shelia, T., Tappen, M., Vekua, A., Zhvania, D., Lordkipanidze, D., 2011. Earliest human occupations at Dmanisi (Georgian Caucasus) dated to 1.85–1.78 Ma. Proceedings of the National Academy of Sciences USA 108, 10432-10436.

Fiscella, G.N., Smith, F.H., 2006. Ontogenetic study of the supraorbital region in modern humans: A longitudinal test of the spatial model. Anthropologischer Anzeiger 64, 147-160.

Freidline, S.E., Gunz, P., Harvati, K., Hublin, J.J., 2012a. Middle Pleistocene human facial morphology in an evolutionary and developmental context. Journal of Human Evolution 63, 723-740.

Freidline, S.E., Gunz, P., Jankovic, I., Harvati, K., Hublin, J.J., 2012b. A comprehensive morphometric analysis of the frontal and zygomatic bone of the Zuttiyeh fossil from Israel. Journal of Human Evolution 62, 225-241.

Freidline, S.E., Gunz, P., Harvati, K., Hublin, J.J., 2013. Evaluating developmental shape changes in *Homo antecessor* subadult facial morphology. Journal of Human Evolution 65, 404-423.

Freidline, S.E., Gunz, P., Hublin, J.J., 2015. Ontogenetic and static allometry in the human face: Contrasting Khoisan and Inuit. American Journal of Physical Anthropology 158, 116-131.

Freidline, S.E., Gunz, P., Jankovic, I., Harvati, K., Hublin, J.J., 2012b. A comprehensive morphometric analysis of the frontal and zygomatic bone of the Zuttiyeh fossil from Israel. Journal of Human Evolution 62, 225-241.

Frost, S.R., Marcus, L.F., Bookstein, F.L., Reddy, D.P., Delson, E., 2003. Cranial allometry, phylogeography, and systematics of large-bodied papionins (Primates: Cercopithecinae) inferred from geometric morphometric analysis of landmark data. The Anatomical Record Part A: Discoveries in Molecular, Cellular, and Evolutionary Biology 275, 1048-1072.

Fu, Q., Hajdinjak, M., Moldovan, O.T., Constantin, S., Mallick, S., Skoglund, P., Patterson, N., Rohland, N., Lazaridis, I., Nickel, B., Viola, B., Prufer, K., Meyer, M., Kelso, J., Reich, D., Pääbo, S., 2015. An early modern human from Romania with a recent Neanderthal ancestor. Nature 524, 216-219.

Garvin, H.M., Ruff, C.B., 2012. Sexual dimorphism in skeletal browridge and chin morphologies determined using a new quantitative method. American Journal of Physical Anthropology 147, 661-670.

Godinho, R.M., O'Higgins, P., 2018. The biomechanical significance of the frontal sinus in Kabwe 1 (*Homo heidelbergensis*). Journal of Human Evolution 114, 141-153.

Godinho, R.M., Spikins, P., O'Higgins, P., 2018. Supraorbital morphology and social dynamics in human evolution. Nature Ecology & Evolution 2, 956-961.

Gómez-Robles, A., 2019. Dental evolutionary rates and its implications for the Neanderthal–modern human divergence. Science Advances 5, eaaw1268.

Gonzalez, P.N., Perez, S.I., Bernal, V., 2010. Ontogeny of robusticity of craniofacial traits in modern humans: A study of South American populations. American Journal of Physical Anthropology 142, 367-379.

Green, R.E., Green, J., Krause, A.W., Briggs, T., Maricic, U., Stenzel, M., Kircher, N., Patterson, H., Li, W., Fritz, N.F., Fritz, N.F., Hansen, E.Y., Durand, A.S., Malaspinas, J.D., Jensen, T., Marques Bonet, C., Alkan, K., Prufer, M., Meyer, H.A., Burbano, J.M., Good, R., Schultz, A., Aximu Petri, A., Butthof, B., Hober, B., Hoffner, M., Siegemund, A., Weihmann, C., Nusbaum, E.S., Lander, C., Russ, N., Novod, J., Affourtit, M., Egholm, C., Verna, P., Rudan, D., Brajkovic, Z., Kucan, I., Gusic, V.B., Doronichev, L.V., Golovanova, C., Lalueza Fox, M., Fortea, A., Fortea, A., Rosas, R.W., Johnson, E.E., Johnson, E.E., Eichler, D., Falush, E., Birney, J.C., Mullikin, M., Slatkin, R., Nielsen, J., Kelso,

M., Lachmann, D., Reich, S., 2010. A draft sequence of the Neandertal genome. Science 328, 710-722.

Groves, C.P., Mirazón Lahr, M., 1994. A bush not a ladder: Speciation and replacement in human evolution. In: Freedman, L., Jablonski, N., Bruce, N. (Eds.) Perspectives in Human Biology 4 (1994). UWA Centre for Human Biology, Perth, Australia, 1-11.

Groves, C., 2012. Speciation in hominin evolution. In: Gallagher, A., Reynolds, S.C. (Eds.), African Genesis: Perspectives on Hominin Evolution. Cambridge University Press, Cambridge, pp. 45-62.

Grün, R., 1996. A re-analysis of electron spin resonance dating results associated with the Petralona hominid. Journal of Human Evolution 30, 227-241.

Grün, R., Brink, J.S., Spooner, N.A., Taylor, L., Stringer, C.B., Franciscus, R.G., Murray, A.S., 1996. Direct dating of Florisbad hominid. Nature 382, 500-501.

Grün, R., Pike, A., McDermott, F., Eggins, S., Mortimer, G., Aubert, M., Kinsley, L., Joannes-Boyau, R., Rumsey, M., Denys, C., Brink, J., Clark, T., Stringer, C., 2020. Dating the skull from Broken Hill, Zambia, and its position in human evolution. Nature 580, 372-375.

Guipert, G., de Lumley, M.-A., de Lumley, H., 2014. Restauration virtuelle d'Arago 21. Comptes Rendus Palevol 13, 51-59.

Gunz, P., Bookstein, F.L., Mitteroecker, P., Stadlmayr, A., Seidler, H., Weber, G.W., 2009. Early modern human diversity suggests subdivided population structure and a complex out-of-Africa scenario. Proceedings of the National Academy of Sciences USA 106, 6094-6098.

Harvati, K., 2003. The Neanderthal taxonomic position: Models of intra- and inter-specific craniofacial variation. Journal of Human Evolution 44, 107-132.

Harvati, K., 2007. 100 years of *Homo heidelbergensis* – Life and times of a controversial taxon. Mitteilungen der Gesellschaft für Urgeschichte 16, 85-94.

Harvati, K., Frost, S.R., McNulty, K.P., 2004. Neanderthal taxonomy reconsidered: Implications of 3D primate models of intra- and interspecific differences. Proceedings of the National Academy of Sciences USA 101, 1147-1152.

Hawks, J.D., Wolpoff, M.H., 2001. The accretion model of Neandertal evolution. Evolution 55, 1474-1485.

Hershkovitz, I., May, H., Sarig, R., Pokhojaev, A., Grimaud-Hervé, D., Bruner, E., Fornai, C., Quam, R., Arsuaga, J.L., Krenn, V.A., Martinón-Torres, M., de Castro, J.M.B., Martín-Francés, L., Slon, V., Albessard-Ball, L., Vialet, A., Schüler, T., Manzi, G., Profico, A., Di Vincenzo, F., Weber, G.W., Zaidner, Y., 2021. A Middle Pleistocene *Homo* from Nesher Ramla, Israel. Science 372, 1424-1428.

Hofbauer, A., Ahern, J.C.M., Lee, S.H., 2003. Craniofacial remodeling during adulthood: The supraorbital region. American Journal of Physical Anthropology S36, 115.

Howells, W.W., 1973. Cranial Variation in Man: A Study by Multivariate Analysis of Patterns of Differences among Recent Human Populations. Papers of the Peabody Museum, Harvard, Cambridge.

Howells, W.W., 1989. Skull Shapes and the Map. Papers of the Peabody Museum, Harvard, Cambridge.

Hublin, J.J., 2009. The origin of Neandertals. Proceedings of the National Academy of Sciences USA 106, 16022-16027.

Hublin, J.J., 2013. The Middle Pleistocene record: On the ancestry of Neandertals, modern humans and others. In: Begun, D. (Ed.) A Companion to Paleoanthropology. Blackwell Publishing Ltd, Chichester, pp. 517-537.

Hublin, J.J., Ben-Ncer, A., Bailey, S.E., Freidline, S.E., Neubauer, S., Skinner, M.M., Bergmann, I., Le Cabec, A., Benazzi, S., Harvati, K., Gunz, P., 2017. New fossils from Jebel Irhoud, Morocco and the pan-African origin of *Homo sapiens*. Nature 546, 289-292.

Hylander, W.L., Johnson, K.R., Picq, P.G., 1991. Masticatory-stress hypotheses and the supraorbital region of primates. American Journal of Physical Anthropology 86, 1-36.

Ji, Q., Wu, W., Ji, Y., Li, Q., Ni, X., in press. Late Middle Pleistocene Harbin cranium represents a new *Homo* species. The Innovation. DOI: 10.1016/j.xinn.2021.100132.

Jolly, C., 1970. The seed-eaters: A new model of hominid differentiation based on a baboon analogy. Man 5, 5-26.

Jolly, C.J., 2001. A proper study for mankind: Analogies from the papionin monkeys and their implications for human evolution. American Journal of Physical Anthropology 116, 177-204.

Kimbel, W.H., Martin, L.B., 1993. Species and speciation conceptual issues and their relevance for primate evolutionary biology. In: Kimbel, W.H., Martin, L.B. (Eds.), Species, Species Concepts, and Primate Evolution. Plenum Press, New York, pp. 539-553.

Kimbel, W.H., White, T.D., Johanson, D.C., 1984. Cranial morphology of *Australopithecus afarensis*: A comparative study based on a composite reconstruction of the adult skull. American Journal of Physical Anthropology 64, 337-388.

Klein, R.G., Avery, G., Cruz-Uribe, K., Steele, T.E., 2007. The mammalian fauna associated with an archaic hominin skullcap and later Acheulean artifacts at Elandsfontein, Western Cape Province, South Africa. Journal of Human Evolution 52, 164-186.

Klingenberg, C.P., Monteiro, L.R., 2005. Distances and directions in multidimensional shape spaces: Implications for morphometric applications. Systematic Biology 54, 678-688.

Kramer, A., 1993. Human taxonomic diversity in the pleistocene: Does *Homo erectus* represent multiple hominid species? American Journal of Physical Anthropology 91, 161-171.

Kuman, K., 1999. Palaeoenvironments and cultural sequence of the Florisbad Middle Stone Age hominid site, South Africa. Journal of Archaeological Science 26, 1409-1425.

Kupczik, K., Dobson, C.A., Crompton, R.H., Phillips, R., Oxnard, C.E., Fagan, M.J., O'Higgins, P., 2009. Masticatory loading and bone adaptation in the supraorbital torus of developing macaques. American Journal of Physical Anthropology 139, 193-203.

Kurten, B., 1979. The shadow of the brow. Current Anthropology 20, 229-230.

Li, T., Etler, D.A., 1992. New Middle Pleistocene hominid crania from Yunxian in China. Nature 357, 404-407.

Lieberman, D., 2000. Ontogeny, homology, and phylogeny in the hominid craniofacial skeleton: The problem of the browridge. In: O'Higgins, P., Cohn, M.J. (Eds.), Development, Growth and Evolution. Academic Press, London, pp. 85-122.

Lieberman, D.E., McBratney, B.M., Krovitz, G. (2002). The evolution and development of cranial form in *Homo sapiens*. Proceedings of the National Academy of Sciences USA 99, 1134-1139

Lockwood, C.A., 1999. Sexual dimorphism in the face of *Australopithecus africanus*. American Journal of Physical Anthropology 108, 97-127.

Lordkipanidze, D., Lordkipanidze, M.S., Margvelashvili, Y., Margvelashvili, Y., Rak, G.P., Rightmire, A., Zollikofer, 2013. A complete skull from Dmanisi, Georgia, and the evolutionary biology of early *Homo*. Science 342, 326-331.

Lycett, S.J., Collard, M., 2005. Do homoiologies impede phylogenetic analyses of the fossil hominids? An assessment based on extant papionin craniodental morphology. Journal of Human Evolution 49, 618-642.

Macho, G., 2018. Referential models for the study of hominin evolution: How many do we need? In: Schwartz, J.H. (Ed.), Rethinking Human Evolution. The MIT Press, Cambridge, pp. 251-266.

Manzi, G., 2004. Human evolution at the Matuyama-Brunhes boundary. Evolutionary Anthropology 13, 11-24.

Manzi, G., 2011. Before the emergence of *Homo sapiens*: Overview on the Early-to-Middle Pleistocene fossil record (with a proposal about *Homo heidelbergensis* at the subspecific level). International Journal of Evolutionary Biology 2011, 582678.

Manzi, G., 2016. Humans of the Middle Pleistocene: The controversial calvarium from Ceprano (Italy) and its significance for the origin and variability of *Homo heidelbergensis*. Quaternary International 411, Part B, 254-261.

Manzi, G., Magri, D., Milli, S., Palombo, M.R., Margari, V., Celiberti, V., Barbieri, M., Barbieri, M., Melis, R.T., Rubini, M., Ruffo, M., Saracino, B., Tzedakis, P.C., Zarattini, A., Biddittu, I., 2010. The new chronology of the Ceprano calvarium (Italy). Journal of Human Evolution 59, 580-585.

Martinón-Torres, M., Bermúdez de Castro, J.M., Gómez-Robles, A., Prado-Simon, L., Arsuaga, J.L., 2012. Morphological description and comparison of the dental remains from Atapuerca-Sima de los Huesos site (Spain). Journal of Human Evolution 62, 7-58.

Martinón-Torres, M., Dennell, R., Bermúdez de Castro, J.M., 2011. The Denisova hominin need not be an out of Africa story. Journal of Human Evolution 60, 251-255.

Mayr, E., 1969. Principles of Systematic Zoology. McGraw-Hill, New York.

McBrearty, S., McBrearty, A., 2000. The revolution that wasn't: A new interpretation of the origin of modern human behavior. Journal of Human Evolution 39, 453-563.

Meyer, M., Arsuaga, J.L., de Filippo, C., Nagel, S., Aximu-Petri, A., Nickel, B., Martínez, I., Gracia, A., Bermúdez de Castro, J.M., Carbonell, E., Viola, B., Kelso, J., Prüfer, K., Pääbo, S., 2016. Nuclear DNA sequences from the Middle Pleistocene Sima de los Huesos hominins. Nature 531, 504-507.

Mirazón Lahr, M., 1996. The Evolution of Modern Human Diversity: A Study of Cranial Variation. Cambridge University Press, Cambridge

Mirazón Lahr, M., 2016. The shaping of human diversity: Filters, boundaries and transitions. Philosophical Transactions of the Royal Society B: Biological Sciences 371, 20150241.

Mirazón Lahr, M., Foley, R., 2001. Mode 3, *H. helmei*, and the pattern of human evolution in the Middle Pleistocene. In: Barham, L., Robson-Brown, K. (Eds.), Human Roots: Africa and Asia in the Middle Pleistocene. Western Academic and Specialist Print, Bristol, pp. 23-40.

Mirazón Lahr, M., Wright, R.V.S., 1996. The question of robusticity and the relationship between cranial size and shape in *Homo sapiens*. Journal of Human Evolution 31, 157-191.

Moss, M.L., Young, R.W., 1960. A functional approach to craniology. American Journal of Physical Anthropology 18, 281-292.

Mounier, A., Condemi, S., Manzi, G., 2011. The stem species of our species: A place for the archaic human cranium from Ceprano, Italy. PLoS One 6, e18821.

Mounier, A., Mirazón Lahr, M., 2019. Deciphering African late middle Pleistocene hominin diversity and the origin of our species. Nature Communications 10, 3406.

Mounier, A., Marchal, F., Condemi, S., 2009. Is *Homo heidelbergensis* a distinct species? New insight on the Mauer mandible. Journal of Human Evolution 56, 219-246.

Ni, X., Ji, Q., Wu, W., Shao, Q., Ji, Y., Zhang, C., Liang, L., Ge, J., Guo, Z., Li, J., Li, Q., Grün, R., Stringer, C., in press. Massive cranium from Harbin in northeastern China establishes a new Middle Pleistocene human lineage. The Innovation. DOI: 10.1016/j.xinn.2021.100130.

Nomade, S., Muttoni, G., Guillou, H., Robin, E., Scardia, G., 2011. First $^{40}Ar/^{39}Ar$ age of the Ceprano man (central Italy). Quaternary Geochronology 6, 453-457.

O'Higgins, P., 2000. The study of morphological variation in the hominid fossil record: Biology, landmarks and geometry. Journal of Anatomy 197, 103-120.

O'Higgins, P., Jones, N., 1998. Facial growth in *Cercocebus torquatus*: An application of three-dimensional geometric morphometric techniques to the study of morphological variation. Journal of Anatomy 193, 251-272.

Oyen, O.J., Rice, R.W., Cannon, S.M., 1979. Browridge structure and function in extant primates and Neanderthals. American Journal of Physical Anthropology 51, 83-95.

Oyen, O.J., Walker, A.C., Rice, R.W., 1979. Craniofacial growth in olive baboons (*Papio cynocephalus anubis*): Browridge formation. Growth 43, 174-187.

Picq, P., 1994. Craniofacial size and proportions and the functional significance of the supraorbital region in primates. Zeitschrift Für Morphologie Und Anthropologie 80, 51-63.

Plavcan, J.M., 2012. Body size, size variation, and sexual size dimorphism in early *Homo*. Current Anthropology 53, S409-S423.

Prossinger, H., 2008. Mathematical analysis techniques of frontal sinus morphology, with emphasis on *Homo*. The Anatomical Record: Advances in Integrative Anatomy and Evolutionary Biology 291, 1455-1478.

Prüfer, K., de Filippo, C., Grote, S., Mafessoni, F., Korlević, P., Hajdinjak, M., Vernot, B., Skov, L., Hsieh, P., Peyrégne, S., Reher, D., Hopfe, C., Nagel, S., Maricic, T., Fu, Q., Theunert, C., Rogers, R., Skoglund, P., Chintalapati, M., Dannemann, M., Nelson, B.J., Key, F.M., Rudan, P., Kućan, Ž., Gušić, I., Golovanova, L.V., Doronichev, V.B., Patterson, N., Reich, D., Eichler, E.E., Slatkin, M., Schierup, M.H., Andrés, A., Kelso, J., Meyer, M., Pääbo, S., 2017. A high-coverage Neandertal genome from Vindija Cave in Croatia. Science 358, 655-658.

Prüfer, K., Racimo, F., Patterson, N., Jay, F., Sankararaman, S., Sawyer, S., Heinze, A., Renaud, G., Sudmant, P.H., de Filippo, C., Li, H., Mallick, S., Dannemann, M., Fu, Q., Kircher, M., Kuhlwilm, M., Lachmann, M., Meyer, M., Ongyerth, M., Siebauer, M., Theunert, C., Tandon, A., Moorjani, P., Pickrell, J., Mullikin, J.C., Vohr, S.H., Green, R.E., Hellmann, I., Johnson, P.L.F., Blanche, H., Cann, H., Kitzman, J.O., Shendure, J., Eichler, E.E., Lein, E.S., Bakken, T.E., Golovanova, L.V., Doronichev, V.B., Shunkov, M.V., Derevianko, A.P., Viola, B., Slatkin, M., Reich, D., Kelso, J., Pääbo, S., 2014. The complete genome sequence of a Neanderthal from the Altai Mountains. Nature 505, 43-49.

R Core Team, 2014. R: A language and environment for statistical computing. R Foundation for Statistical Computing, Vienna.

Racimo, F., Sankararaman, S., Nielsen, R., Huerta-Sanchez, E., 2015. Evidence for archaic adaptive introgression in humans. Nature Reviews Genetics 16, 359-371.

Rak, Y., Quam, R., Martínez, I., Gracia, A., Arsuaga, J.L. 2011. Derived characters shared uniquely by Sima de los Huesos mandible sample and *Homo neanderthalensis*. PaleoAnthropology 2011, A28-A29.

Ravosa, M.J., 1988. Browridge development in Cercopithecidae: A test of two models. American Journal of Physical Anthropology 76, 535-555.

Ravosa, M.J., 1991. Interspecific perspective on mechanical and nonmechanical models of primate circumorbital morphology. American Journal of Physical Anthropology 86, 369-396.

Richter, D., Grün, R., Joannes-Boyau, R., Steele, T.E., Amani, F., Rué, M., Fernandes, P., Raynal, J.P., Geraads, D., Ben-Ncer, A., Hublin, J.J., McPherron, S.P., 2017. The age of the hominin fossils from Jebel Irhoud, Morocco, and the origins of the Middle Stone Age. Nature 546, 293-296.

Rightmire, G.P., 1988. *Homo erectus* and later Middle Pleistocene humans. Annual Review of Anthropology 17, 239-259.

Rightmire, G.P., 1996. The human cranium from Bodo, Ethiopia: Evidence for speciation in the Middle Pleistocene? Journal of Human Evolution 31, 21-39.

Rightmire, G.P., 1998. Human evolution in the middle Pleistocene: The role of *Homo heidelbergensis*. Evolutionary Anthropology 6, 218-227.

Rightmire, G.P., 2001. Patterns of hominid evolution and dispersal in the Middle Pleistocene. Quaternary International 75, 77-84.

Rightmire, G.P., 2008. *Homo* in the Middle Pleistocene: Hypodigms, variation, and species recognition. Evolutionary Anthropology 17, 8-21.

Rightmire, G.P., 2013. *Homo erectus* and Middle Pleistocene hominins: Brain size, skull form, and species recognition. Journal of Human Evolution 65, 223-252.

Rightmire, G.P., Lordkipanidze, D., Vekua, A., 2006. Anatomical descriptions, comparative studies and evolutionary significance of the hominin skulls from Dmanisi, Republic of Georgia. Journal of Human Evolution 50, 115-141.

Rightmire, G.P., Margvelashvili, A., Lordkipanidze, D., 2019. Variation among the Dmanisi hominins: Multiple taxa or one species? American Journal of Physical Anthropology 168, 481-495.

Rink, W.J., Schwarcz, H.P., Smith, F.H., Radovcic, J., 1995. ESR ages for Krapina hominids. Nature 378, 24-24.

Rizal, Y., Westaway, K.E., Zaim, Y., van den Bergh, G.D., Bettis, E.A., Morwood, M.J., Huffman, O.F., Grün, R., Joannes-Boyau, R., Bailey, R.M., Sidarto, Westaway, M.C., Kurniawan, I., Moore, M.W., Storey, M., Aziz, F., Suminto, Zhao, J.-x., Aswan, Sipola, M.E., Larick, R., Zonneveld, J.-P., Scott, R., Putt, S., Ciochon, R.L., 2020. Last appearance of *Homo erectus* at Ngandong, Java, 117,000–108,000 years ago. Nature 577, 381-385.

Rohlf, F.J., 1999. Shape statistics: Procrustes superimposition and tangent spaces. Journal of Classification 16, 197-223.

Rohlf, F.J., Slice, D., 1990. Extensions of the Procrustes method for the optimal superimposition of landmarks. Systematic Zoology 39, 40-59.

Rosas, A., Bastir, M., 2002. Thin-plate spline analysis of allometry and sexual dimorphism in the human craniofacial complex. American Journal of Physical Anthropology 117, 236-245.

Russell, M.D., 1982. Tooth eruption and browridge formation. American Journal of Physical Anthropology 58, 59-65.

Russell, M.D., 1985. The supraorbital torus: "A most remarkable peculiarity". Current Anthropology 26, 337-360.

Sánchez-Quinto, F., Lalueza-Fox, C., 2015. Almost 20 years of Neanderthal palaeogenetics: Adaptation, admixture, diversity, demography and extinction. Philosophical Transactions of the Royal Society B 370, 20130374.

Sankararaman, S., Mallick, S., Dannemann, M., Prufer, K., Kelso, J., Pääbo, S., Patterson, N., Reich, D., 2014. The genomic landscape of Neanderthal ancestry in present-day humans. Nature 507, 354-357.

Scerri, E.M.L., Chikhi, L., Thomas, M.G., 2019. Beyond multiregional and simple out-of-Africa models of human evolution. Nature Ecology & Evolution 3, 1370-1372.

Scerri, E.M.L., Thomas, M.G., Manica, A., Gunz, P., Stock, J.T., Stringer, C., Grove, M., Groucutt, H.S., Timmermann, A., Rightmire, G.P., d'Errico, F., Tryon, C.A., Drake, N.A., Brooks, A.S., Dennell, R.W., Durbin, R., Henn, B.M., Lee-Thorp, J., deMenocal, P., Petraglia, M.D., Thompson, J.C., Scally, A., Chikhi, L., 2018. Did our species evolve in subdivided populations across Africa, and why does it matter? Trends in Ecology & Evolution 33, 582-594.Schwartz, J.H., 2016. What constitutes *Homo sapiens*? Morphology versus received wisdom. Journal of Anthropological Sciences 94, 65-80.

Schwartz, J.H., Tattersall, I., 2010. Fossil evidence for the origin of *Homo sapiens*. American Journal of Physical Anthropology 143, 94-121.

Seidler, H., 1997. A comparative study of stereolithographically modelled skulls of Petralona and Broken Hill: Implications for future studies of middle Pleistocene hominid evolution. Journal of Human Evolution 33, 691-703.

Shea, B.T., 1986. On skull form and the supraorbital torus in primates. Current Anthropology 27, 257-260.

Shen, G., Tu, H., Xiao, D., Qiu, L., Feng, Y.-x., Zhao, J.-x., 2014. Age of Maba hominin site in southern China: Evidence from U-series dating of Southern Branch Cave. Quaternary Geochronology 23, 56-62.

Silverman, N., Richmond, B., Wood, B., 2001. Testing the taxonomic integrity of *Paranthropus boisei* sensu stricto. American Journal of Physical Anthropology 115, 167-178.

Simmons, T., Falsetti, A.B., Smith, F.H., 1991. Frontal bone morphometrics of southwest Asian Pleistocene hominids. Journal of Human Evolution 20, 249-269.

Simons, E.L., Pilbeam, D.R., 1965. Preliminary revision of the Dryopithecinae (Pongidae, Anthropoidea). Folia Primatologica 3, 81-152.

Simpson, G.G., 1951. The species concept. Evolution 5, 285-298.

Simpson, G.G., 1961. Principles of Animal Taxonomy. Columbia University Press, New York.

Smith, F.H., Ranyard, G.C., 1980. Evolution of the supraorbital region in Upper Pleistocene fossil hominids from south-central Europe. American Journal of Physical Anthropology 53, 589-610.

Stelzer, S., Neubauer, S., Hublin, J.-J., Spoor, F., Gunz, P., 2019. Morphological trends in arcade shape and size in Middle Pleistocene *Homo*. American Journal of Physical Anthropology 168, 70 - 91.

Stratovan Corporation, 2016. Stratovan Checkpoint. Version 2016.06.28.0428. Jun 28, 2016. Stratovan Corporation, Davis. https://www.stratovan.com/products/checkpoint

Stratovan Corporation, 2018. Stratovan Checkpoint. Version 2018.09.07.0325. Sep 07, 2018. Stratovan Corporation, Davis. https://www.stratovan.com/products/checkpoint

Stringer, C.B., 1983. Some further notes on the morphology and dating of the Petralona hominid. Journal of Human Evolution 12, 731-742.

Stringer, C.B., 2002. Modern human origins: Progress and prospects. Philosophical Transactions of the Royal Society B 357, 563-579.

Stringer, C.B., 2012. The status of *Homo heidelbergensis* (Schoetensack 1908). Evolutionary Anthropology 21, 101-107.

Stringer, C.B., 2016. The origin and evolution of *Homo sapiens*. Philosophical Transactions of the Royal Society B 371, 20150237.

Stringer, C.B., Howell, F.C., Melentis, J.K., 1979. The significance of the fossil hominid skull from Petralona, Greece. American Journal of Physical Anthropology 50, 485.

Sun, X., Yi, S., Lu, H., Zhang, W., 2017. TT-OSL and post-IR IRSL dating of the Dali Man site in central China. Quaternary International 434, 99-106.

Tattersall, I., 1986. Species recognition in human paleontology. Journal of Human Evolution 15, 165-175.

Tattersall, I., 1992. Species concepts and species identification in human evolution. Journal of Human Evolution 22, 341-349.

Tattersall, I., 2005. Species concepts and hominid diversity in Later Pleistocene Europe. Anthropologie (Brno) 43, 207-213.

Tattersall, I., Schwartz, J.H., 2006. The distinctiveness and systematic context of *Homo neanderthalensis*. In: Harvati, K., Harrison, T. (Eds.), Neanderthals Revisited: New Approaches and Perspectives. Springer, Dordrecht, pp. 9-22.

Tattersall, I., Schwartz, J.H., 2008. The morphological distinctiveness of *Homo sapiens* and its recognition in the fossil record: Clarifying the problem. Evolutionary Anthropology 17, 49-54.

Tattersall, I., Schwartz, J.H., 2009. Evolution of the genus *Homo*. Annual Review of Earth and Planetary Sciences 37, 67-92.

Terhune, C.E., Kimbel, W.H., Lockwood, C.A., 2007. Variation and diversity in *Homo erectus*: A 3D geometric morphometric analysis of the temporal bone. Journal of Human Evolution 53, 41-60.

Tückmantel, S., Röllin, A., Müller, A.E., Soligo, C., 2009. Facial correlates of frontal bone pneumatisation in strepsirrhine primates. Mammalian Biology - Zeitschrift für Säugetierkunde 74, 25-35.

Venables, W.N., Ripley, B.D., 2002. Modern Applied Statistics with S, 4th ed. Springer, New York.

Vialet, A., Guipert, G., Jianing, H., Xiaobo, F., Zune, L., Youping, W., Tianyuan, L., de Lumley, M.-A., de Lumley, H., 2010. *Homo erectus* from the Yunxian and Nankin Chinese sites: Anthropological insights using 3D virtual imaging techniques. Comptes Rendus Palevol 9, 331-339.

von Cramon-Taubadel, N., 2009. Revisiting the homoiology hypothesis: The impact of phenotypic plasticity on the reconstruction of human population history from craniometric data. Journal of Human Evolution 57, 179-190.

Wagner, G.A., Krbetschek, M., Degering, D., Bahain, J.J., Shao, Q., Falguères, C., Dolo, J.M., Garcia, T., Rightmire, G.P., 2010. Radiometric dating of the type-site for *Homo heidelbergensis* at Mauer, Germany. Proceedings of the National Academy of Sciences USA 107, 19726-19730.

Weidenreich, F., 1941. The brain and its role in the phylogenetic transformation of the human skull. Transactions of the American Philosophical Society 31, 320-442.

Weidenreich, F., 1947. Facts and speculations concerning the origin of *Homo sapiens*. American Anthropologist 49, 187-203.

Weihs, C., Ligges, U., Luebke, K., Raabe, N., 2005. klaR analyzing German business cycles. In: Baier, D., Decker, R., Schmidt-Thieme, L. (Eds.), Data Analysis and Decision Support. Springer, Berlin, pp. 335-343.

White, S., Gowlett, J.A.J., Grove, M., 2014. The place of the Neanderthals in hominin phylogeny. Journal of Anthropological Archaeology 35, 32-50.

White, S., Soligo, C., Pope, M., Hillson, S., 2020. Taxonomic variation in the supraorbital region of the catarrhine primates. American Journal of Physical Anthropology 171, 198-218.

Wood, B., 1991. A palaeontological model for determining the limits of early hominid taxonomic variability. Palaeontologia Africana 28, 71-77.

Wood, B.A., Li, Y., Willoughby, C., 1991. Intraspecific variation and sexual dimorphism in cranial and dental variables among higher primates and their bearing on the hominid fossil record. Journal of Anatomy 174, 185-205.

Woodward, A., 1921. A new cave man from Rhodesia, South Africa. Nature 108,371-372

Wu, R., 1988. The reconstruction of the fossil human skull from Jinniushan, Yinkou, Liaoning Province and its main features. Acta Anthropologica Sinica 8, 97-102.

Wu, X., Athreya, S., 2013. A description of the geological context, discrete traits, and linear morphometrics of the Middle Pleistocene hominin from Dali, Shaanxi Province, China. American Journal of Physical Anthropology 150, 141-157.

Yokoyama, Y., Nguyen, H.V., 1981. Datation directe de l'Homme de Tautavel parla spectrométrie gamma, non destructive, du crâne humain fossile Arago XXI. Comptes Rendus Académie des Sciences de Paris 292, 741-744.

Yuan, S., Chen, T., Gao, S., 1986. The dating of southern Chinese Palaeolithic sites by uranium method. Acta Anthropologica Sinica 5, 179-190.

Zeitoun, V., 2001. The taxonomical position of the skull of Zuttiyeh. Comptes Rendus de l'Académie des Sciences Paris 332, 521-525.

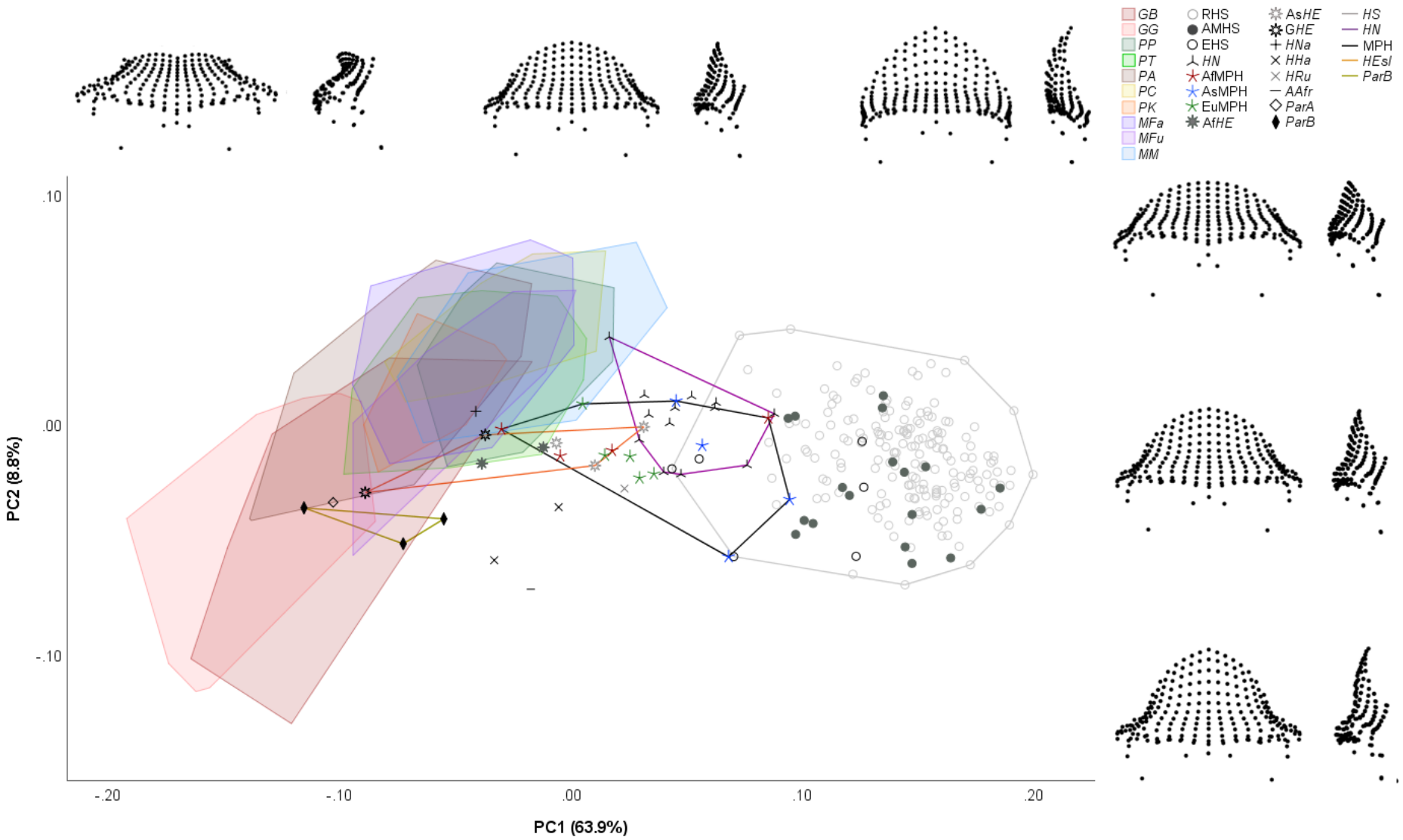
GB
GG
PP
PT
PA
PC
PK
MFa
MFu
MM
RHS
AMHS
EHS
HN
AfMPH
AsMPH
EuMPH
AfHE
AsHE
GHE
HNa
HHa
HRu
AAfr
ParA
ParB
HS
HN
MPH
HEsl
ParB
.10
.00
-.10
PC2 (8.8%)
-.20
-.10
.00
.10
.20
PC1 (63.9%)

Figure 1. Plot of principal component 1 (PC1; x-axis) and principal component 2 (PC2; y-axis), accounting for 72.8% of variation, following principal component analysis. Convex hulls are shown and correspond to species groups. Shape changes are shown for minimum, median, and maximum sample values for both axes, in frontal and left lateral view. Specimens are identified by symbols shown in legend. Abbreviations: GB = *Gorilla beringei*; GG = *Gorilla gorilla*; PP = *Pan paniscus*; PT = *Pan troglodytes*; PA = *Papio anubis*; PC = *Papio cynocephalus*; PK = *Papio kindae*; MFa = *Macaca fascicularis*; MFu = *Macaca fuscata*; MM = *Macaca mulatta*; RHS = recent *Homo sapiens*; AMHS = anatomically modern *H. sapiens*; EHS = early *H. sapiens*; HN = *Homo neanderthalensis*; AfMPH = African Middle Pleistocene hominin remains; AsMPH = Asian Middle Pleistocene hominin remains; EuMPH = European Middle Pleistocene hominin remains; AfHE = African *Homo erectus*; AsHE = Asian *H. erectus*; GHE = Georgian *H. erectus*; HNa = *Homo naledi*; HHa = *Homo habilis*; HRu = *Homo rudolfensis*; AAfr = *Australopithecus africanus*; ParA = *Paranthropus aethiopicus*; ParB = *Paranthropus boisei*.

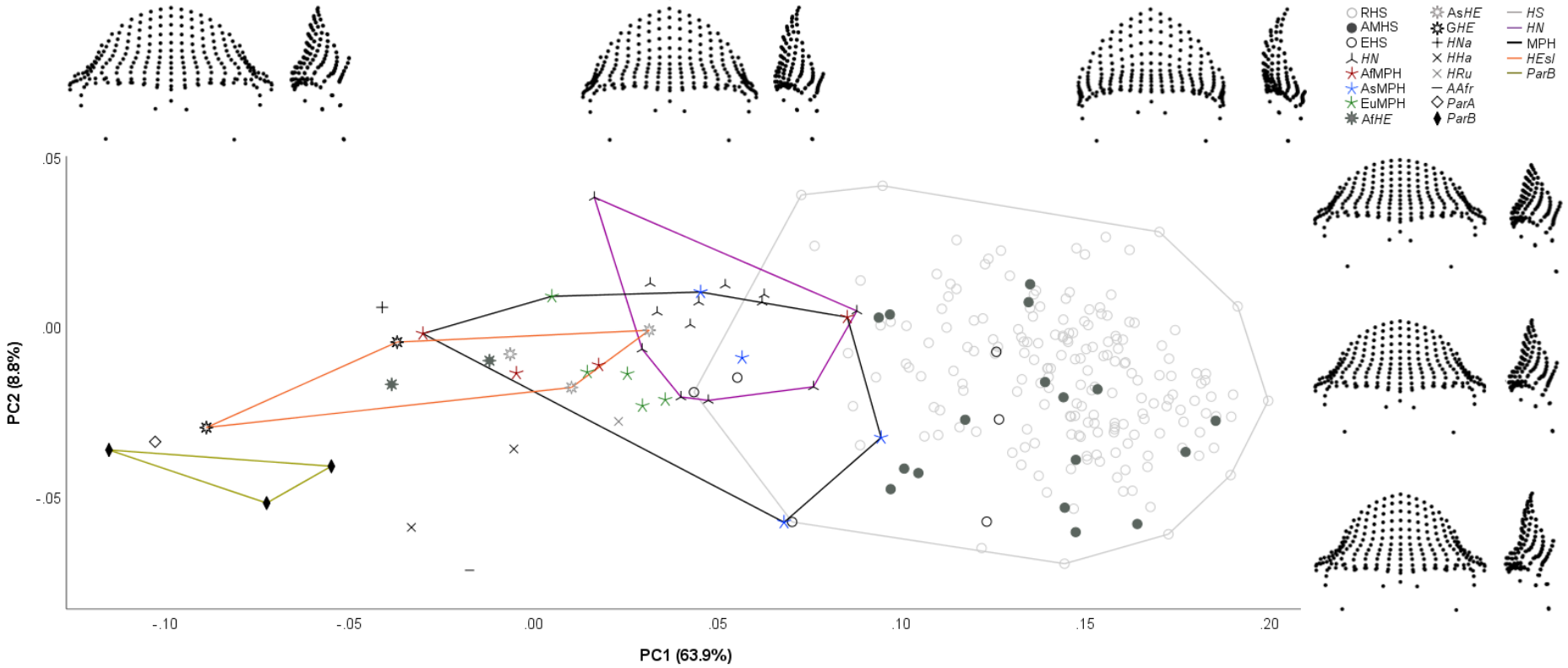

Figure 2. Plot of principal component 1 (PC1; x-axis) and principal component 2 (PC2; y-axis), accounting for 61.4% of variation, following principal component analysis using hominin-only dataset. Convex hulls are shown and correspond to species groups. Shape changes are shown for minimum, median, and maximum sample values for both axes, in frontal and left lateral view. Middle Pleistocene hominins are identified as follows: A = Arago; B = Bodo; C = Ceprano; D= Dali; F = Florisbad; K = Kabwe; M= Maba; N = Narmada; P = Petralona; Sa = Saldanha; SH = Sima de los Huseos 5; St = Steinheim; Z = Zuttiyeh. Legend abbreviations: RHS = recent *Homo sapiens*; AMHS = anatomically modern *H. sapiens*; EHS = early *H. sapiens*; HN = *Homo neanderthalensis*; AfMPH = African Middle Pleistocene hominin remains; AsMPH = Asian Middle Pleistocene hominin remains; EuMPH = European Middle Pleistocene hominin remains;

AfHE = African *Homo erectus*; AsHE = Asian *H. erectus*; GHE = Georgian *H. erectus*; HNa = *Homo naledi*; HHa = *Homo habilis*; HRu = *Homo rudolfensis*; AAfr = *Australopithecus africanus*; ParA = *Paranthropus aethiopicus*; ParB = *Paranthropus boisei.* See SOM Fig. S9 for annotated version.

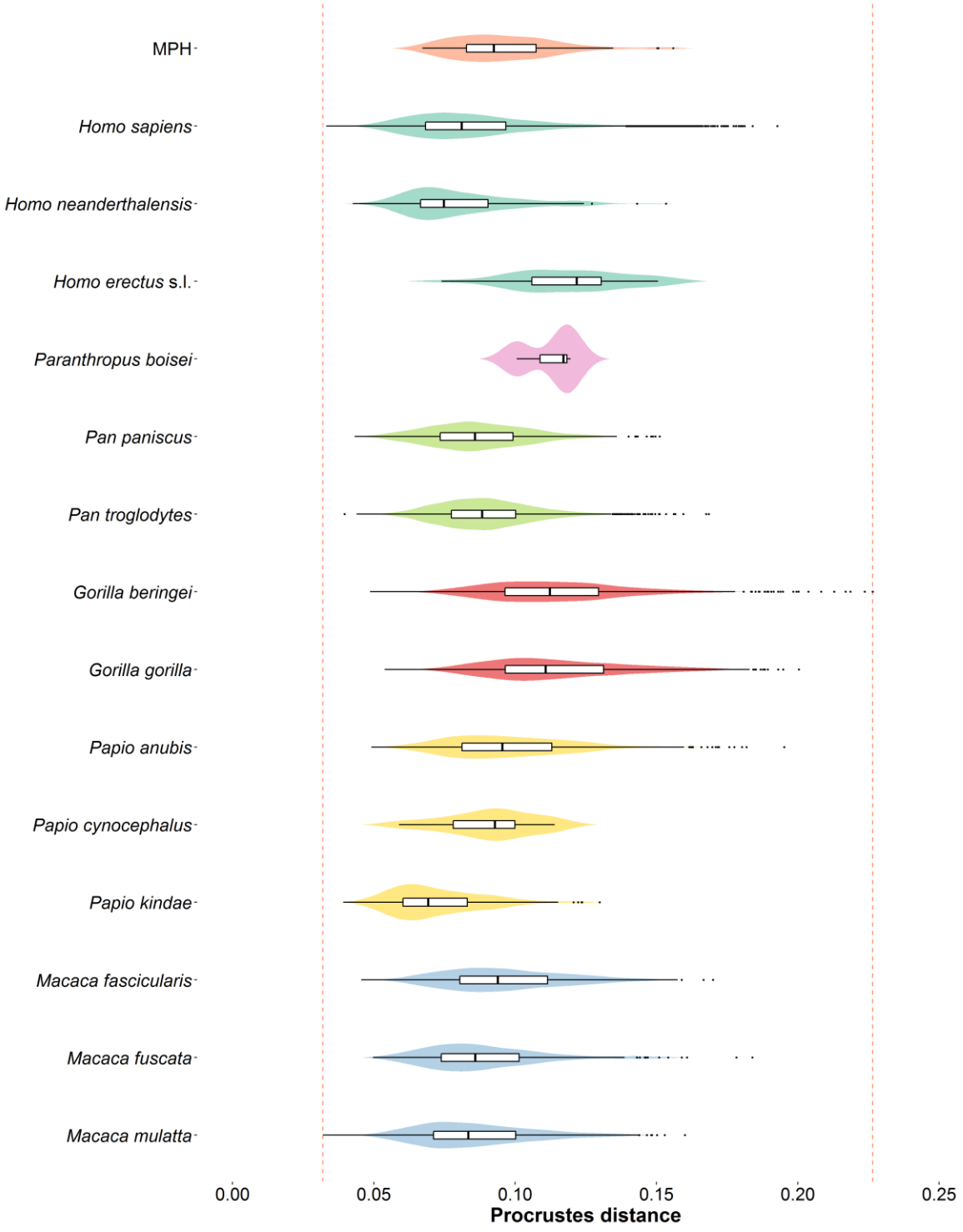

Figure 3. Violin plots of intragroup Procrustes distances for individual groups (species and Middle Pleistocene hominin remains) under main hypothesis. Vertical dashed lines show range of intraspecific Procrustes distances across the sample of non-hominin catarrhines.

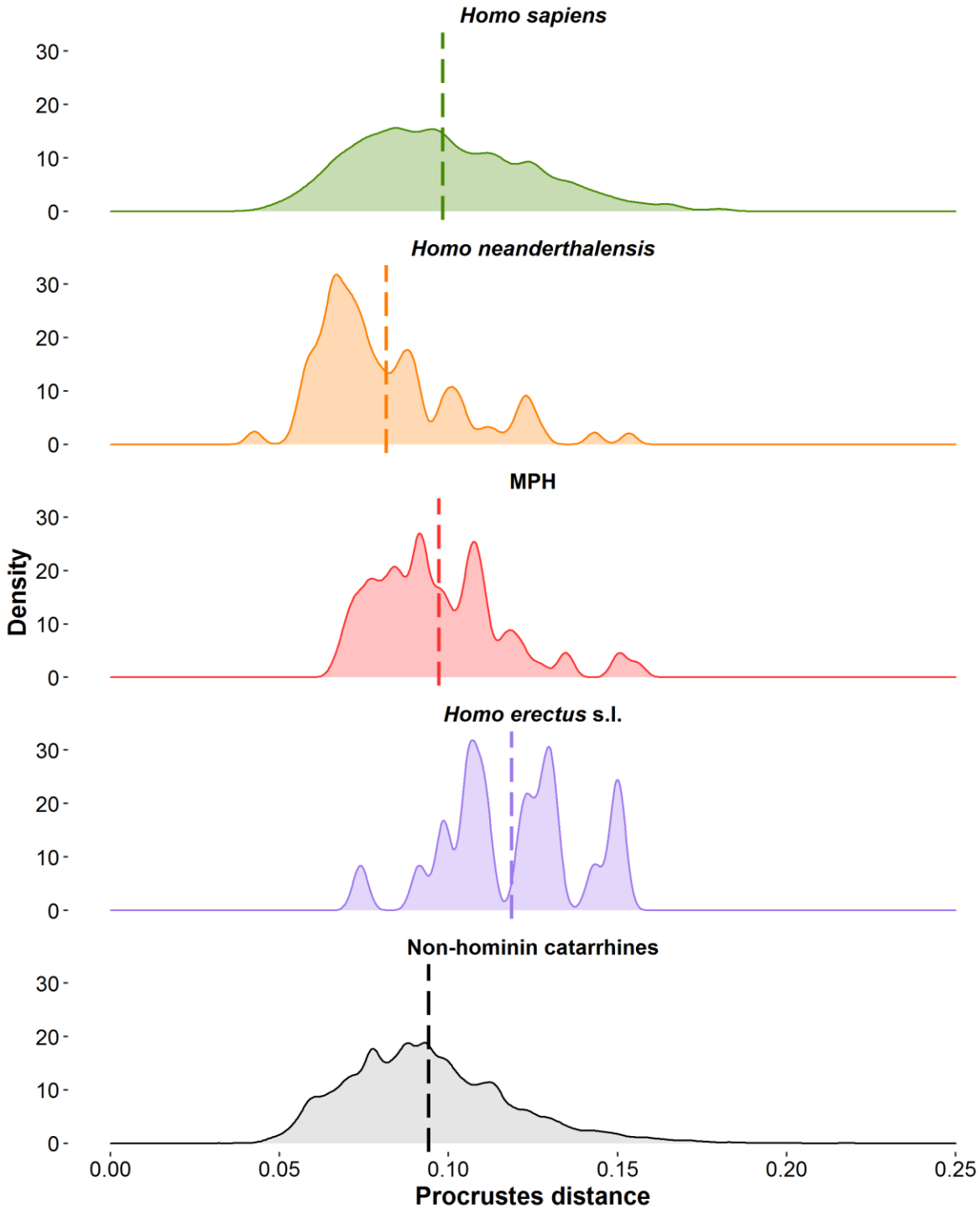

Figure 4. Distribution plots of intragroup (for hominins) and intraspecific (for non-hominin catarrhines) Procrustes distances across 1000 subsamples (n = 7) under main hypothesis. Dashed vertical lines show means for each comparison: *Homo sapiens* $\bar{x}$ = 0.0100; *Homo neanderthalensis* $\bar{x}$ = 0.083; MPH $\bar{x}$ = 0.098; *Homo erectus* s.l. $\bar{x}$ = 0.118; non-hominin catarrhines $\bar{x}$ = 0.094. Abbreviation: MPH = Middle Pleistocene hominins.

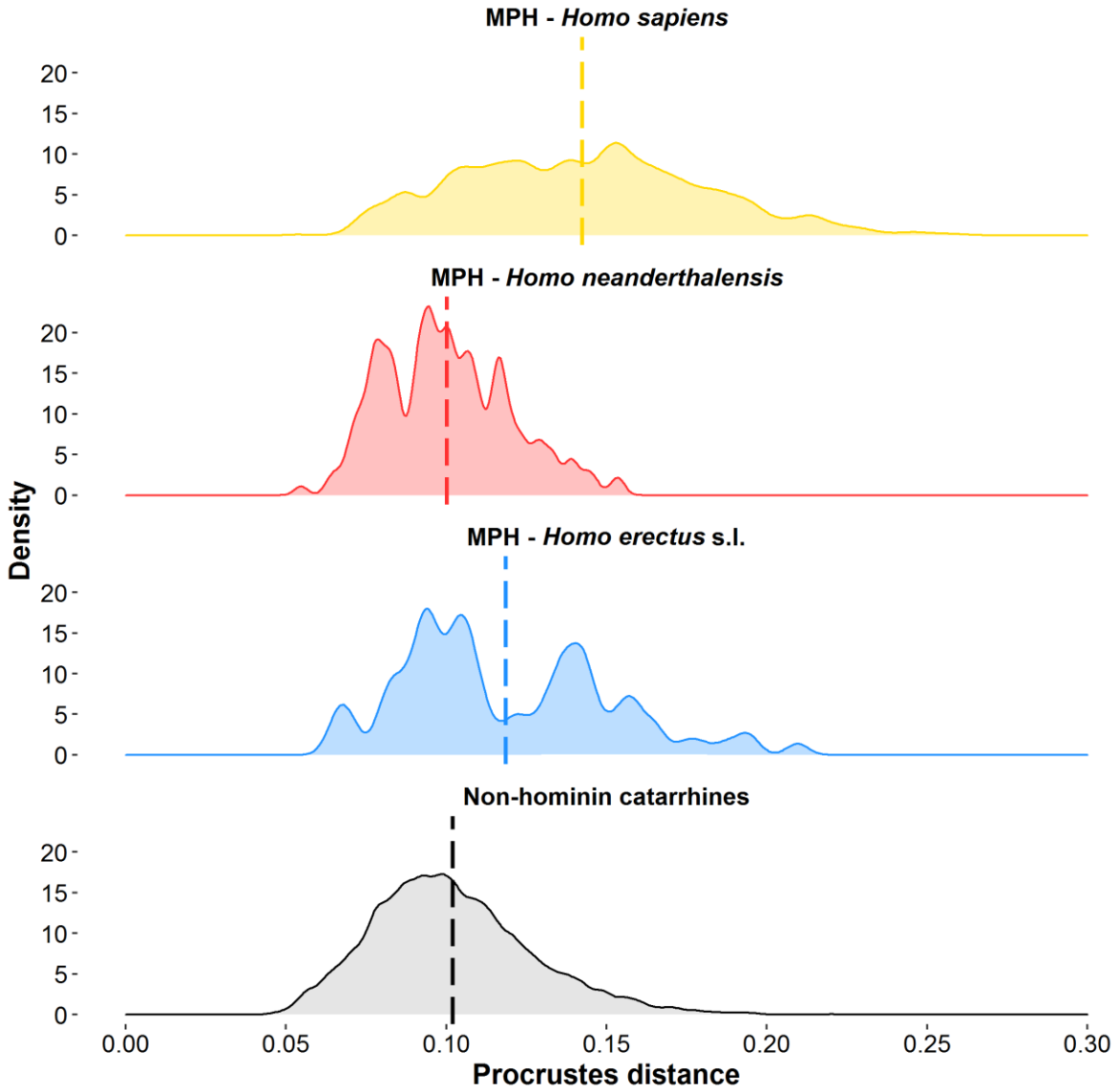

Figure 5. Distribution plots of intergroup (for hominins) and interspecific (for non-hominin catarrhines) Procrustes distances across 1000 subsamples (n = 7) under alternative hypothesis. Dashed vertical lines show means for each comparison: MPH – *Homo sapiens* $\bar{x}$ = 0.141; MPH – *Homo neanderthalensis* $\bar{x}$ = 0.102; MPH – *Homo erectus* s.l. $\bar{x}$ = 0.119; non-hominin catarrhines $\bar{x}$ = 0.101. Abbreviation: MPH = Middle Pleistocene hominins.

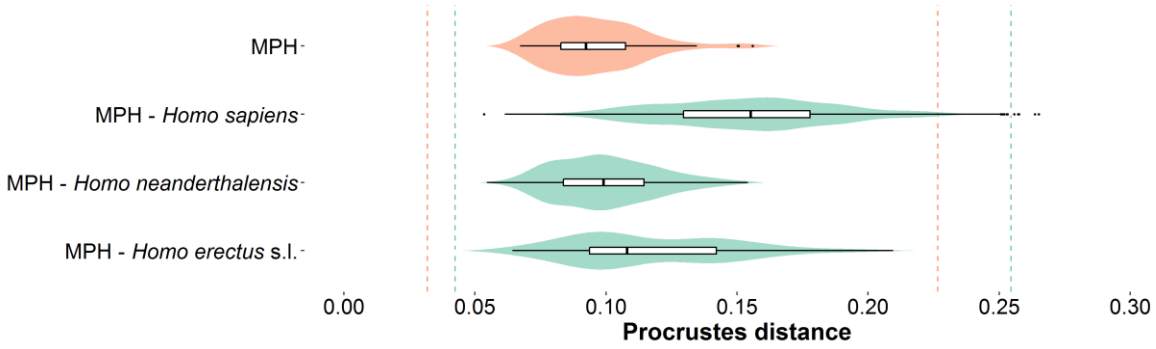

Figure 6. Violin plots of intra- and inter-group Procrustes distances for Middle Pleistocene hominin remains under main hypothesis. Vertical dashed lines show range of intraspecific (orange) and interspecific (turquoise) Procrustes distances across the sample of non-hominin catarrhines.

Table 1

Summary of Middle Pleistocene hominins (MPH) included in this study.

Name	Location	Date (ka)	Reference for date
Arago 21	France	400, 438	Yokoyama and Nguyen (1981), Falguères et al. (2004, 2015)
Bodo	Ethiopia	600	Clark (1994)
Ceprano	Italy	353, 395-435	Nomade et al. (2011), Manzi et al. (2010)
Dali	China	263	Sun et al. (2017)
Florisbad	South Africa	260-280	Kuman (1999), Grün et al. (1996)
Kabwe (Broken Hill) 1	Zambia	299	Grün et al. (2020)
Maba	China	130, >278	Yuan et al. (1986) Shen et al. (2014)
Narmada	India	>236	Cameron et al. (2004)
Petralona	Greece	150-250, >350	Grün (1996), Stringer (1983)
Saldanha	South Africa	600, (400-800)	Klein et al. (2007)
Sima de los Huesos 5 (SH5)	Spain	448	Demuro et al. (2019)
Steinheim	Germany	>225	Czarnetzki (1983)
Zuttiyeh	Israel	200-500	Freidline et al. (2012b)

Table 2

Taxonomic classification for Middle Pleistocene hominins under alternative hypothesis.

Specimen	Classification
Dali	*Homo erectus* s.l.
Maba	*Homo erectus* s.l.
Narmada	*Homo erectus* s.l.
Arago 21	*Homo erectus* s.l.
Ceprano	*Homo erectus* s.l.
Petralona	*Homo erectus* s.l.
Bodo	*Homo erectus* s.l.
Kabwe 1	*Homo erectus* s.l.
Saldanha	*Homo erectus* s.l.
SH5	*Homo neanderthalensis*
Steinheim	*Homo neanderthalensis*
Zuttiyeh[a]	*Homo sapiens/Homo neanderthalensis*
Florisbad	*Homo sapiens*

Abbreviations: SH5 = Sima de los Huesos 5.

[a] Analysis was repeated with Zuttiyeh classified as *Homo sapiens* and *Homo neanderthalensis*, due to unresolved debate over the taxonomic attribution of this fossil.

Table 3
Fossil hominin specimens included in this study. See SOM Table S1 for details and provenance.

	Homo sapiens (HS)
Recent *Homo sapiens* (RHS)[a]	Skull I/Sepulchre, Csokavar, Tepexpan I, Fish Hoek I, Ofnet 4K1802, Ofnet 4K1811, Gambles Cave IV, Combe Capelle, Kennewick, La Brea, Matjes River, Wajak I
Anatomically modern *Homo sapiens* (AMHS)	Keilor, Oberkassel I, Oberkassel II, Furfooz I, Chancelade, Zhoukoudian (ZKD) UC 101, ZKD UC 102, Abri Pataud, Brno II, Brno III, Dolní Věstonice III, Předmostí III, Předmostí IV, Cro-Magnon I, Cro-Magnon II, Mladeč 1[b], Mladeč 2
Early *Homo sapiens* (EHS)	Qafzeh 9, Border Cave 1, Skhūl V[b], Liujiang, Omo 1, Jebel Irhoud 1
	Homo neanderthalensis (HN)
	Gibraltar 1[c], Saint-Césaire I, Spy 1[b], Le Moustier 1, Shanidar I, Shanidar V, Guattari, La Chapelle, Amud 1, La Quina H5, Tabun I, Krapina C, Krapina E
	Middle Pleistocene hominins (MPH)
African	Florisbad, Kabwe 1[c], Bodo[b], Saldanha
Asian	Maba, Zuttiyeh, Dali, Narmada
European	Petralona, Steinheim, Ceprano, Sima de los Huesos 5 (SH5), Arago 21
	Homo erectus sensu lato (HE)
African *Homo erectus* (AfHE)	KNM-ER 3773, KNM-ER 3883
Asian *Homo erectus* (AsHE)	Ngandong 7 (Solo VI), Sangiran 17, Zhoukoudian XII
Georgian *Homo erectus* (GHE)	D4500, D2282
	Homo naledi
	Dinaledi Hominin 1 (DH1)
	Homo habilis
	OH 24, KNM-ER 1813
	Homo rudolfensis
	KNM-ER 1470
	Australopithecus africanus
	Sts 5
	Paranthropus aethiopicus
	KNM-WT 17000
	Paranthropus boisei
	KNM-ER 406, KNM-ER 732, OH 5

Abbreviations: UC = Upper Cave; KNM-ER = Kenya National Museum, East Rudolf; D4500 = Dmanisi hominin 4500; D2282 = Dmanisi hominin 2282; OH = Olduvai Hominid; Sts = Sterkfontein Type Site; KNM-WT = Kenya National Museum, West Turkana.

[a] The RHS sample also includes 172 non-fossil (archaeological and historical) *H. sapiens* specimens (see SOM Table S1).

[b] Specimens for which CT data were used.

[c] Specimens for which surface scans were collected from the original fossil. The rest of the data were collected from research quality casts.

Table 4

Summary of specimens included in this study by taxon and sex, with abbreviations. Data for sex were taken from museum records for all non-hominin catarrhines. Sex of recent *Homo sapiens* was assessed using the standards of Buikstra and Ubelaker (1994) when known sex information was unavailable, using the categories of male, female, or indeterminate. Fossil hominins were treated as being of unknown sex due to issues in generalisability of sex estimation methods based on modern datasets.

Group	Count				Percentage				Total
	F	I	M	U	F	I	M	U	
Gorilla beringei beringei	6		8		42.9%		57.1%		14
Gorilla beringei graueri	23		18		56.1%		43.9%		41
Gorilla gorilla gorilla	25		25		50.0%		50.0%		50
Gorilla gorilla diehli	9		9		50.0%		50.0%		18
Pan paniscus	21		18	4	48.8%		41.9%	9.3%	43
Pan troglodytes troglodytes	25		25		50.0%		50.0%		50
Pan troglodytes schweinfurthii	16		11	3	53.3%		36.7%	8.8%	30
Pan troglodytes verus	6		10		37.5%		62.5%		16
Pan troglodytes ellioti	2		3		40.0%		60.0%		5
Papio anubis	17		25		40.5%		59.5%		42
Papio cynocephalus	2		6		25.0%		75.0%		8
Papio kindae	10		13		43.5%		56.5%		23
Macaca fascicularis	24		25		49.0%		51.0%		49
Macaca fuscata[a]	3		6		33.3%		66.7%		9
Macaca fuscata fuscata	3		1	2	50.0%		16.7%	33.3%	6
Macaca fuscata yakui	5		2		71.4%		28.6%		7
Macaca mulatta	25		19		56.8%		43.2%		44
Homo sapiens	69	26	77	35	33.3%	12.6%	37.2%	16.9%	207
Homo neanderthalensis				13					13
Middle Pleistocene hominins				13					13
Homo erectus sensu lato				7					7
Homo naledi				1					1
Homo rudolfensis				1					1
Homo habilis				2					2
Australopithecus africanus				1					1
Paranthropus aethiopicus				1					1
Paranthropus boisei				3					3
Total									704

Abbreviations: F = female; I = indeterminate; M = male; U = unknown.

[a] Some *Macaca fuscata* and *Papio cynocephalus* sensu lato specimens could not be assigned a subgroup classification.

Table 5

Results of stepwise, jackknife cross-validated discriminant analysis for non-hominin catarrhines, using first 19 principal components that accounted for over 95% of total sample variance from principal component analysis. Table shows mean percentage classification accuracy across the 1000 random subsamples for each group (see SOM Table S10 for additional descriptive statistics). Mean classification accuracy across the groups was 72.3%. Values for correct classification are denoted in bold.

	Gorilla beringei	*Gorilla gorilla*	*Pan paniscus*	*Pan troglodytes*	*Papio anubis*	*Papio cynocephalus*	*Papio kindae*	*Macaca fascicularis*	*Macaca fuscata*	*Macaca mulatta*
Gorilla beringei	**80.3**	15.2	1.3	2.7	0.2			0.1	0.3	
Gorilla gorilla	15.7	**81.1**	0.3	1.5	0.9	0.1	0.2	0.1	0.1	0.1
Pan paniscus	0.6	0.2	**77.8**	20.6	0.1		0.6			0.1
Pan troglodytes	1.3	1.3	19.6	**75.8**	0.1	0.3	0.4	0.1	0.1	1.1
Papio anubis	0.1	0.5			**67.0**	19.2	11.1	0.2	0.6	1.2
Papio cynocephalus				0.1	19.3	**48.6**	22.8	1.0	1.9	6.2
Papio kindae					4.2	8.6	**86.2**	0.1	0.1	0.7
Macaca fascicularis	0.1			0.1	0.6	1.0	0.3	**64.9**	18.9	14.0
Macaca fuscata					0.3	1.1	0.1	15.3	**73.7**	9.5
Macaca mulatta			0.2	0.3	1.4	5.2	2.8	8.1	10.1	**72.0**

Table 6

Results of stepwise, jackknife cross-validated discriminant analysis for hominins, using first 19 principal components that accounted for over 95% of total sample variance from principal component analysis. Table shows mean percentage classification accuracy across the 1000 random subsamples for each group (see SOM Table S11 for additional descriptive statistics). Mean classification accuracy across the groups was 82.4% (75.2% if *Homo habilis* are included). Values for correct classification are denoted in bold.

	Homo sapiens	*Homo neanderthalensis*	Middle Pleistocene hominins	*Homo erectus* sensu lato	*Homo habilis*
Homo sapiens	**85.4**	8.3	6.3		
Homo neanderthalensis	1.5	**90.9**	7.6		
Middle Pleistocene hominins	3.7	9.6	**77.6**	9.1	0.1
Homo erectus sensu lato		1.6	21.2	**75.7**	1.5
Homo habilis		1.5	2.2	50.2	**46.2**

Table 7

Percentage of cases from 1000 random subsamples in which Pleistocene hominins were classified as various groups in stepwise, jackknife cross-validated discriminant analysis using first 19 principal components from principal component analysis. Cases where specimens were classified to a single group in over 50.0% of comparisons are highlighted in bold.

	Group	*n*	HS	HN	MPH	HEsl	HHa
Keilor	AMHS	101	**100.0%**				
Oberkassel I	AMHS	120	**92.5%**	7.5%			
Oberkassel II	AMHS	103	**100.0%**				
Chancelade	AMHS	113	**99.1%**	0.9%			
Furfooz I	AMHS	104	**100.0%**				
ZKD UC 101	AMHS	123	**90.2%**	7.3%	2.4%		
ZKD UC 102	AMHS	126	**100.0%**				
Abri Pataud	AMHS	106	**100.0%**				
Brno II	AMHS	101	**97.0%**	3.0%			
Brno III	AMHS	89	**64.0%**	6.7%	29.2%		
Dolní Věstonice III	AMHS	106	**100.0%**				
Předmostí III	AMHS	129	**92.2%**	7.8%			
Předmostí IV	AMHS	118	**100.0%**				
Cro-Magnon I	AMHS	120	**100.0%**				
Cro-Magnon II	AMHS	105	**100.0%**				
Mladeč 1	AMHS	110	**100.0%**				
Mladeč 2	AMHS	106	**100.0%**				
Qafzeh 9	EHS	347	**100.0%**				
Border Cave 1	EHS	346	49.4%	1.4%	48.8%	0.3%	
Skhūl V	EHS	299	12.4%	34.1%	**53.2%**	0.3%	
Liujiang	EHS	346	**99.4%**	0.6%			
Omo 1	EHS	331	13.9%	**67.4%**	18.7%		
Jebel Irhoud 1	EHS	331	7.9%	**73.1%**	18.7%		
Gibraltar 1	HN	602	0.2%	**98.3%**	1.5%		
Saint-Césaire I	HN	627		**78.5%**	21.4%	0.2%	
Spy 1	HN	618		**97.9%**	2.1%		
Le Moustier 1	HN	625	12.0%	**87.5%**	0.5%		
Shanidar I	HN	619	0.3%	**98.9%**			
Shanidar V	HN	596		**60.9%**	38.9%	0.2%	
Guattari	HN	611	0.5%	**99.5%**			
La Chapelle	HN	640	0.2%	**94.4%**	5.5%		
Amud 1	HN	616	5.0%	**86.5%**	8.4%		
La Quina H5	HN	592		**89.2%**	10.8%		
Tabun I	HN	616	0.2%	**92.7%**	7.1%		
Krapina C	HN	628	0.3%	**98.6%**	1.1%		
Krapina E	HN	613	0.3%	**97.2%**	1.8%	0.7%	
Maba	MPH	624	9.0%	2.9%	**87.0%**	1.1%	
Petralona	MPH	633	0.3%	22.3%	**77.3%**	0.2%	
Zuttiyeh	MPH	611	2.6%	18.2%	**77.6%**	1.3%	0.3%
Dali	MPH	587	0.2%	7.2%	**92.7%**		
Florisbad	MPH	585	37.1%	**59.0%**	3.8%	0.2%	
Kabwe 1	MPH	646		9.9%	**63.5%**	26.5%	
Narmada	MPH	644		0.6%	**98.6%**	0.8%	
Steinheim	MPH	590	0.2%	1.2%	**91.5%**	6.9%	0.2%
Ceprano	MPH	575		1.0%	**96.9%**	2.1%	
SH5	MPH	636		2.0%	**69.8%**	28.1%	
Arago 21	MPH	641			**73.3%**	26.4%	

Bodo	MPH	613	0.2%	4.1%	**80.8%**	14.7%	0.3%
Saldanha	MPH	626		0.6%	**92.8%**	6.5%	
Solo VI	HE	1000		6.2%	**68.8%**	25.0%	
ZKD XII	HE	1000		1.0%	16.3%	**82.6%**	
Sangiran 17	HE	1000		0.2%	12.7%	**85.7%**	1.4%
KNM-ER 3773	HE	1000		2.9%	1.8%	**93.2%**	2.1%
KNM-ER 3883	HE	1000		1.1%	48.0%	**50.9%**	
D2282	HE	1000	0.1%	0.1%	0.4%	**96.3%**	3.1%
D4500	HE	1000			0.1%	**96.2%**	3.7%

Abbreviations: ZKD = Zhoukoudian; UC = Upper Cave; SH5 = Sima de los Huesos 5; KNM-ER = Kenya National Museum, East Rudolf; D2282 = Dmanisi 2282; D4500 = Dmanisi hominin 4500; AMHS = anatomically modern *Homo sapiens*; EHS = early *Homo sapiens*; HN = *Homo neanderthalensis*; MPH = Middle Pleistocene hominin remains; HEsl = *Homo erectus* sensu lato; NHP = non-hominin catarrhine; HS = *Homo sapiens*; HHa = *Homo habilis*.

Table 8

Results of stepwise, jackknife cross-validated discriminant analysis for hominins under alternative hypothesis, using first 19 principal components that accounted for over 95% of total sample variance from principal component analysis. Table shows mean percentage classification accuracy across the 1000 random subsamples for each group. Values are shown with Zuttiyeh assigned to *Homo neanderthalensis* (left) and *Homo sapiens* (right). Mean classification accuracy across the groups was 85.7% (80.3/79.9% if *Homo habilis* are included).

	Homo sapiens		*Homo neanderthalensis*		*Homo erectus* s.l.		*Homo habilis*	
Homo sapiens	**87.7**	**88.7**	9.8	9.6	2.3	1.5	0.2	0.2
Homo neanderthalensis	2.1	2.4	**86.2**	**85.7**	11.7	11.8	0.1	0.2
Homo erectus s.l.	2.7	2.0	12.5	13.0	**83.2**	**82.6**	1.5	2.4
Homo habilis	1.1	1.1	2.8	3.6	32.3	32.8	**63.9**	**62.6**

Table 9

Results of subsampling showing percentage of 1000 repeats in which the Procrustes distances within the 13 Middle Pleistocene hominins were significantly ($p \leq 0.05$; highlighted in bold) or not significantly different to those of random subsamples of 13 specimens from the comparative species.

	No significant difference	Significant difference	
		MPH less variable	MPH more variable
Gorilla beringei	**0.9**	**99.1**	0.0
Gorilla gorilla	7.4	92.6	0.0
Pan paniscus	22.3	0.0	77.7
Pan troglodytes	41.1	0.2	58.7
Papio anubis	75.7	15.9	8.4
Papio cynocephalus[a]	97.1	0.0	2.9
Papio kindae	82.7	12.0	5.3
Macaca fascicularis	77.2	7.7	15.1
Macaca fuscata	54.2	0.0	45.8
Macaca mulatta	71.3	23.9	4.8
Homo sapiens	79.5	16.6	3.9
Homo erectus s.l.[b]	71.8	28.2	0.0

Abbreviations: MPH = Middle Pleistocene hominins.

[a] For comparisons of *Papio cynocephalus* to MPH ($n = 8$).

[b] For comparisons of *Homo erectus* sensu lato to MPH ($n = 7$).

Table 10

Results of subsampling (n = 7) showing percentage of 1000 repeats in which the Procrustes distances between the MPH and closely-related species (columns) were significantly ($p \leq 0.05$; highlighted in bold) or not significantly different to interspecific distances in closely-related non-hominin catarrhines (rows), under main hypothesis.

	MPH – *Homo sapiens*			MPH – *Homo neanderthalensis*			MPH – *Homo erectus* s.l.		
	No significant difference	Significant difference		No significant difference	Significant difference		No significant difference	Significant difference	
		Less	More		Less	More		Less	More
Gorilla beringei – *Gorilla gorilla*	31.2	0.2	68.6	17.7	82.3	0.0	81.8	13.1	5.1
Pan paniscus – *Pan troglodytes*	**0.2**	0.0	**99.8**	66.5	3.7	29.8	10.1	0.0	89.9
Papio anubis – *Papio cynocephalus*	**1.5**	0.0	**98.5**	79.8	7.9	12.3	20.9	0.0	79.1
Papio anubis – *Papio kindae*	15.3	0.1	84.6	63.9	29	7.1	55.0	3.1	41.9
Papio cynocephalus – *Papio kindae*	**0.6**	0.0	**99.4**	73.0	5.3	21.7	19.5	0.0	80.5
Macaca fascicularis – *Macaca fuscata*	**2.9**	0.0	**97.1**	71.5	9.9	18.6	23.7	0.0	76.3
Macaca fascicularis – *Macaca mulatta*	**1.9**	0.1	**98.0**	76.2	9.3	14.5	30.7	0.0	69.3
Macaca fuscata – *Macaca mulatta*	7.6	0.0	92.4	73.0	6.7	20.3	17.6	0.0	82.4

Abbreviations: MPH = Middle Pleistocene hominins.

Table 11

Summary of t and *p* values for independent t-tests across 1000 subsample (n = 7) comparisons of intra- and interspecific Procrustes distances for hominins, under main hypothesis. Figures in bold show majority (for t values) and significance (for *p* values).

		t		*p*		
					Significant difference	
		t < 0	t > 0	No significant difference	Less variable	More variable
Homo sapiens	MPH	**99.5**	0.5	10.3	89.7	0.0
Homo neanderthalensis	MPH	**100.0**	0.0	16.1	83.9	0.0
MPH	*Homo sapiens*	**100.0**	0.0	**0.0**	**100.0**	0.0
	Homo neanderthalensis	**74.5**	25.5	86.1	13.8	0.1
	Homo erectus s.l.	**100.0**	0.0	6.3	93.7	0.0
Homo erectus s.l.	MPH	**60.2**	39.8	99.9	0.1	0.0

Abbreviations: MPH = Middle Pleistocene hominins.

Supplementary Online Material (SOM):

Geometric morphometric variability in the supraorbital and orbital region of Middle Pleistocene hominins: Implications for the taxonomy and evolution of later *Homo*

Suzanna White [a,*], Matt Pope [b], Simon Hillson [b], Christophe Soligo [a]

[a] *Department of Anthropology, University College London, 14 Taviton Street, London, WC1H 0BW, UK*

[b] *Institute of Archaeology, University College London, 31-34 Gordon Square, London, WC1H 0PY, UK*

*Corresponding author.

E-mail address: suzanna.white@ucl.ac.uk (S. White).

SOM S1

Reconstruction

Geometric reconstruction

Geometric reconstruction methods were applied when only a few points were missing. This was performed using the estimate.missing function in the 'geomorph' package v. 3.3.1 (Adams et al., 2013) in R v. 3.6.1 (R Core Team, 2019), with reference samples that were matched by sex and species, for non-hominin catarrhines, and for time period and taxon, for the hominins. 50 of the 704 specimens required this type of reconstruction (SOM Table S12).

Manual virtual reconstruction

After generating 3D models from CT data, some automatic semilandmarks were placed on endocranial surfaces in Checkpoint v. 2016.06.28.0428 or 2018.09.07.0325 (Stratovan Corporation, 2016, 2018). 3D models generated from CT data were put through the 'Mesh Doctor' function in 'Geomagic Wrap' v. 2017 (3D Systems Inc., South Carolina) to fix any errors in the polygon mesh, reducing the number of semilandmarks that were affected. Manual virtual reconstruction methods were used to amend the location of the remaining misplaced semilandmarks, by using the surrounding points and the grid template in Checkpoint. All semilandmarks were put through a sliding algorithm during generalized Procrustes analysis (GPA), which would have negated any effect on homology of points. 61 specimens required this method of reconstruction (SOM Table S13).

Reconstruction by mirroring across an empirical midplane

For specimens which were missing one of a bilateral pair of points, these points were reconstructed using mirroring landmarks across an empirical midplane, estimated with orthogonal regression. This method was used on 14 specimens (SOM Table S14). The midplane was estimated by placing a curve of semilandmarks using three control landmarks: nasion, glabella, and post-toral sulcus. These points were used to generate a plane in Checkpoint which estimated the midsagittal plane. Orthogonal regression was then performed in R.

Digital reconstruction

Specimens with larger areas of damage or distortion were reconstructed by digital reconstruction methods (following White et al., 2020). 37 of the fossil hominin crania required reconstruction, either due to their fragmentary nature or because of taphonomic distortion. Reference specimens were chosen based on species, geographic region, time period, and assessment of overall similarity of form (SOM Table S15). Reflections of specimens were also used when the affected areas were restricted to one side of the cranium. Standard craniofacial landmarks were placed on both the target and reference specimens. Then, either the reference and target surface models were aligned using a GPA in Evan

Toolbox (Phillips et al., 2010), or the reference model was warped onto the target specimen in Evan Toolbox. Resulting reference and target surfaces were then exported and loaded into CloudCompare v. 2.8 beta (CloudCompare, 2016). Distorted or damaged areas were removed on the target model, and the alignment of the two surface models was manually refined. The Mesh Doctor function was then applied to the merged surface model in Geomagic, and the reconstruction was scaled back to its original size in Meshlab v. 1.3.3 (Cignoni et al., 2008). Details of digital reconstruction methods for 27 of the specimens can be found in supplementary materials of White et al. (2020); details for the remaining ten specimens, which were not included in the previous study, are below. Effects of digital reconstruction methods were assessed in White et al. (2020), and found to not have a significant effect on results of analyses.

Ofnet 4K1802 Ofnet 4K1802 showed some damage to the left aspect of the frontal squama and the area around the right temporal lines, and was missing part of the left supraorbital border, immediately lateral to the glabellar region, as well as the nasal column and the medial borders of the orbits. This specimen was reconstructed by using the aligned reflected surface model of the specimen, affecting 22 semilandmarks and two landmarks (left mid-torus anterior and mid-torus inferior). Four points (two semilandmarks and two landmarks: left and right dacryon) were reconstructed using the geometric method (see above) in areas that could not be reliably reconstructed using the digital method.

Combe Capelle The left lateral aspect of the frontal squama is missing on the Combe Capelle specimen. This region was therefore reconstructed by merging the relevant section of an aligned reflected surface model of the specimen. One landmark (left frontotemporale) and 19 semilandmarks were affected by digital reconstruction.

Wajak I Wajak I showed damage to the left frontal squama approximately superior to the supraorbital notch, and the glabella region, extending laterally into the right supraciliary region, and both the area under the right temporal line and the right zygomatic were displaced. These areas were reconstructed by merging the aligned reflected model with the original surface model, after removing damaged areas. Tests were run using reference specimens for the glabellar region, but it was found that the glabellar landmark was placed on the original morphology. 115 semilandmarks and six landmarks (post-toral sulcus, mid-frontotemporale, and right mid-torus inferior, mid-torus anterior, frontotemporale, frontomalare anterior, and frontomalare posterior) were affected, being placed on reflected regions instead of the original surface model.

Keilor Keilor showed slight damage to the lateral aspect of the left supraciliary ridge, and the left lateral aspect of the frontal squama, above the orbital margin. These regions were reconstructed by merging the relevant regions from the righthand side, following reflection with the original surface model. A total of 48 semilandmarks and three landmarks (left mid-torus anterior, mid-torus inferior, and frontomalare anterior) were affected.

Ceprano Ceprano, while mostly intact in the frontal bone, is missing the middle and lower face, with only the superior aspects of both zygoma preserved. This specimen was reconstructed by first warping the SH5 surface model to fit the neurocranial morphology, then by merging the face of the aligned, warped SH5 model with the existing surface model of Ceprano. This reconstruction process affected seven landmarks (nasion, left and right dacryon, left and right ectoconchion, and left and right zygoorbitale).

Maba Maba was missing the lower face, left zygomatic, and portions of the left frontal, and there was damage to the right supraorbital torus, immediately lateral to glabella. This specimen was reconstructed by aligning the original surface model with its reflection. Then, the surface model of Dali was warped to fit the existing morphology of Maba and its reflection, and used to reconstruct the missing and damaged regions. A total of 24 semilandmarks were placed on areas of the supraorbital torus which were reconstructed with the warped Dali surface model, and all left hand landmarks and semilandmarks were placed on the reflected morphology of the Maba specimen.

Narmada Narmada preserved part of the right zygomatic, and most of the right frontal squama and supraorbital torus. This specimen was reconstructed by creating a reflected surface model, and aligning the original and reflected models, using a scaled model of Kabwe 1 as a template. The Kabwe 1 surface model was then warped to fit the morphology of the merged Narmada surface model, and used to reconstruct the missing regions in the midsagittal plane and the lower face. Eight landmarks (all left hand bilateral landmarks) and 64 semilandmarks were placed on the reflected Narmada surface, and four landmarks (mid-frontotemporale, post-toral sulcus, glabella, and nasion) and 79 semilandmarks were placed on areas reconstructed with the warped Kabwe 1 surface.

Saldanha The frontal bone of Saldanha was mostly complete for the area of interest for this study, except for the lateral-most aspect of the left frontal trigone (the two affected semilandmarks on this area were reconstructed using the geometric method; see above) and the lower aspect of the glabella region. The middle and lower face was reconstructed by using the aligned lower face of Kabwe 1. Eight landmarks (glabella, nasion, and left and right dacryon, zygoorbitale, and ectoconchion points) were affected by the reconstruction.

Steinheim Steinheim was missing the left half of the frontal bone, along with the left zygomatic and part of the left maxilla, and was damaged in the medial aspect of the supraorbital torus. This specimen was reconstructed by merging the original with its aligned reflection, then warping the Arago XXI model to reconstruct the damaged areas around glabella. 96 semilandmarks and eight landmarks (left mid-torus anterior, mid-torus inferior, frontotemporale, frontomalare posterior, and frontomalare anterior) were placed on the reflected Steinheim surface, while 14 semilandmarks and one landmark (post-toral sulcus) were placed on the warped Arago XXI surface.

Zuttiyeh Zuttiyeh consists of a largely complete frontal bone, along with part of the nasal bones and the frontal processes of the maxillae. There is some damage to the right frontal squama, but this was

posterior to the recorded area. The lower face was reconstructed by warping the Skhūl V surface model to the Zuttiyeh specimen, affecting six landmarks (nasion and both left and right dacryon, ectoconchion, and zygoorbitale points).

Retrodeformation and reconstruction in ScanStudio

Four specimens required reconstruction by retrodeformation or manipulation of the original ScanStudio file. Two specimens with deformation (Ofnet 4K1811 and Arago 21) were reconstructed by retrodeformation in Landmark Editor v. 3.0 (Wiley et al., 2005), where pairs of bilateral points were plotted and used to estimate the midsagittal plane for the deformed specimen. This plane was then manipulated using the Retrodeform function to form a corrected plane of symmetry, with the morphology of the surface model being corrected using this plane. Two specimens (Florisbad and RMCA 9220, a male *Gorilla beringei graueri* with a gunshot wound) had small defects in their morphology which could be reconstructed in the ScanStudio v. 2.02 software (NextEngine, Inc., 2006-2015). The area of the defect was removed using the Trim function, after which the Fill function was used to fill in the area. This method only works for suitably small areas, and uses the surrounding morphology to generate gaps in the 3D surface model.

SOM S2

Intraobserver Error

Intraobserver error was assessed using a subset of 32 individuals from the total sample (SOM Table S16). Landmarks were placed on these specimens on four different occasions. The intraobserver repeat configurations were added to the dataset of 704 specimens, and put through a GPA (see Materials and methods of the main text). The resulting Procrustes distance matrix was then used to compare intragroup distances for intraobserver repeat specimens, intrasubspecific, and intraspecific comparisons, as well as intersubspecific and interspecific comparisons, using a one-way ANOVA with post-hoc Tukey Honest significant difference tests in SPSS v. 26 (IBM Corp., 2018). For *Homo sapiens* comparisons, only recent *H. sapiens* specimens were used to provide a more conservative comparison. Intertaxonomic comparisons were made between closely related groups (i.e., species within the same genus, subspecies within the same species). Results showed that Procrustes distances for the intraobserver comparisons were significantly (p <0.001) lower than intra- and intertaxonomic comparisons at both levels (SOM Table S4; SOM Fig. S1).

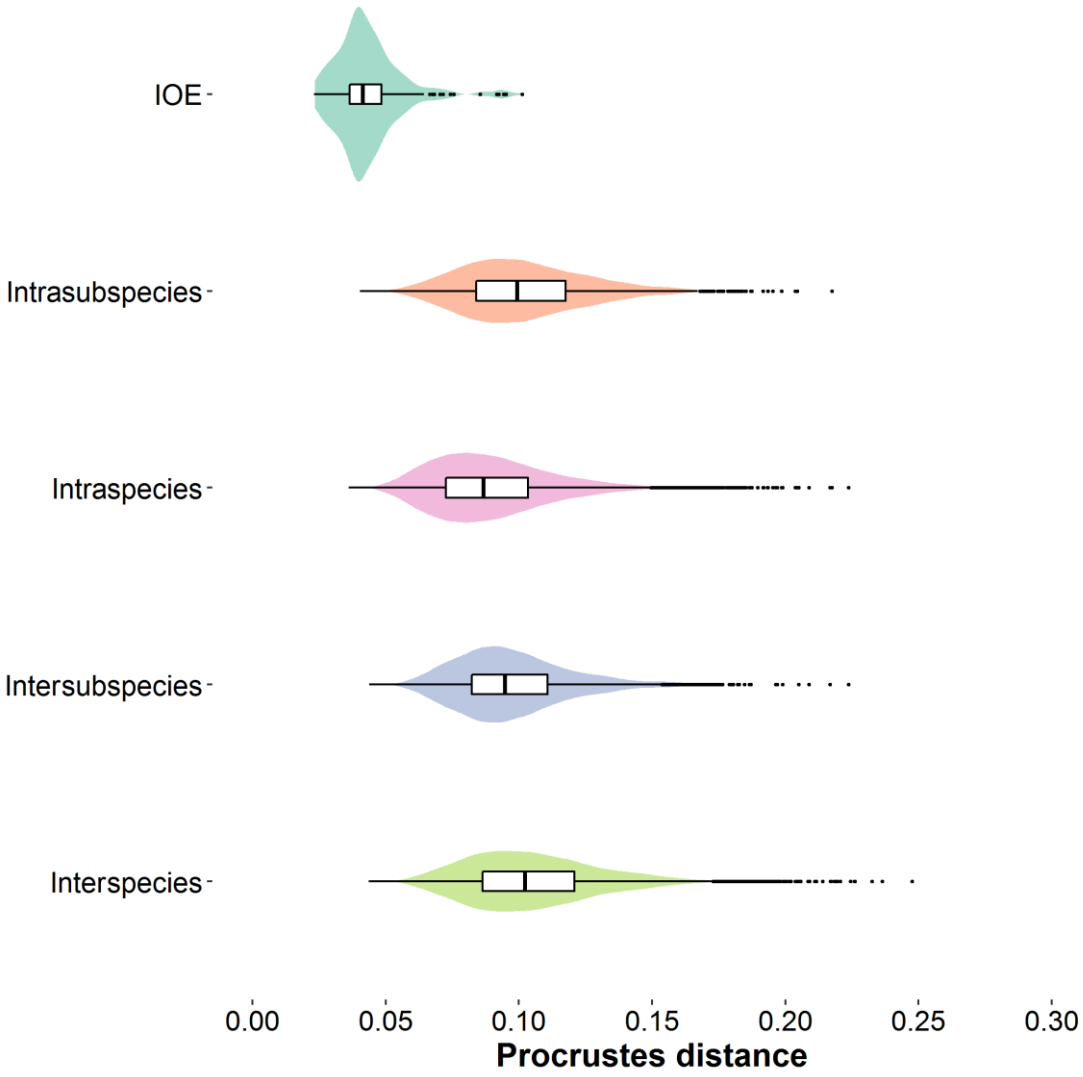

SOM Figure S1. Violin plots of Procrustes distances comparisons for assessment of intraobserver error. Abbreviation: IOE = Intraobserver error.

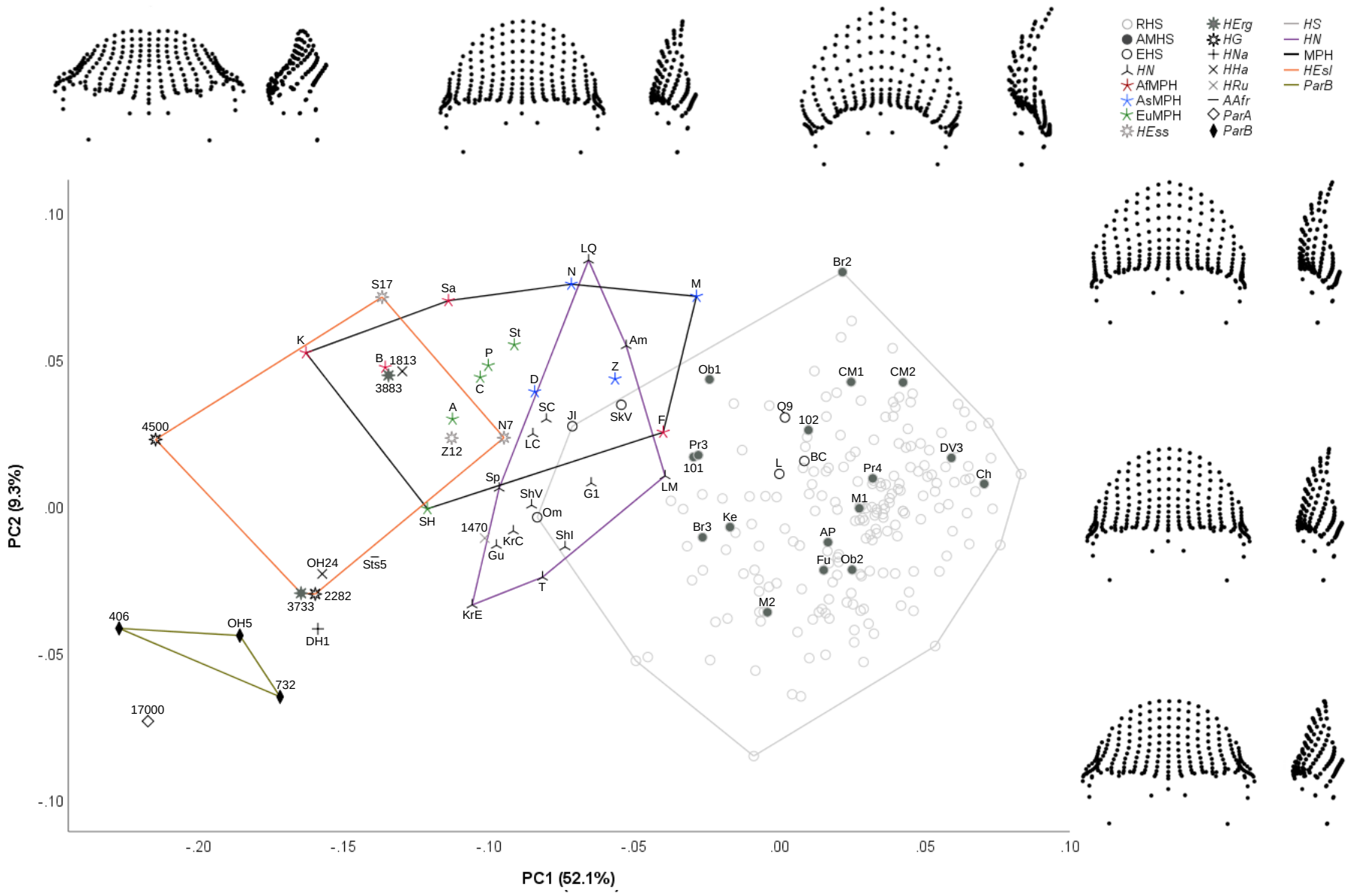
RHS
AMHS
EHS
HN
AfMPH
AsMPH
EuMPH
HEss
HErg
HG
HNa
HHa
HRu
AAfr
ParA
ParB
HS
HN
MPH
HEsl
ParB
PC2 (9.3%)
PC1 (52.1%)
.10
.05
.00
-.05
-.10
-.20
-.15
-.10
-.05
.00
.05
.10
LQ
N
M
S17
Sa
K
St
P
C
B_1813
3883
Am
D
Z
A
Z12
N7
SC
LC
JI
SkV
F
4500
Sp
ShV
Om
G1
LM
SH
1470
KrC
Gu
ShI
T
KrE
OH24
Sts5
3733
2282
406
OH5
DH1
732
17000
Br2
Ob1
CM1
CM2
Q9
102
Pr3
101
L
BC
DV3
Pr4
Ch
M1
Br3
Ke
AP
Fu
Ob2
M2

SOM Figure S2. Plot of principal component 1 (PC1; x-axis) and principal component 2 (PC2; y-axis), accounting for 64.8% of variation, following principal component analysis using hominin-only dataset. Convex hulls are shown and correspond to species groups (see legend). Shape changes are shown for minimum, median, and maximum sample values for both axes, in frontal and left lateral view. Specimens are identified as follows (listed alphabetically): 101 = ZKD UC 101; 102 = ZKD UC 102; 406 = KNM-ER 406; 732 = KNM-ER 732; 1470 = KNM-ER 1470; 1813 = KNM-ER 1813; 2882 = D2282; 3773 = KNM-ER 3733; 3883 = KNM-ER 3883; 4500 = D4500; 17000 = KNM-WT 17000; A = Arago; Am = Amud 1; AP = Abri Pataud; B = Bodo; BC = Border Cave 1; Br2 = Brno II; Br3 = Brno III; C = Ceprano; Ch = Chancelade; CM1 = Cro-Magnon I; CM2 = Cro-Magnon II; D = Dali; DH1 = DH1; DV3 = Dolní Věstonice III; F = Florisbad; Fu = Furfooz I; G1 = Gibraltar 1; Gu = Guattari; H = Herto; JI = Jebel Irhoud 1; K = Kabwe; Ke = Keilor; KrC = Krapina C; KrE = Krapina E; L = Liujiang; LC = La Chapelle; LM = Le Moustier 1; LQ = La Quina H5; M = Maba; M1 = Mladeč 1; M2 = Mladeč 2; N = Narmada; N7 = Ngandong 7; Ob1 = Oberkassel I; Ob2 = Oberkassel II; OH5 = OH 5; OH24 = OH 24; Om = Omo 1; P = Petralona; Pr3 = Předmostí III; Pr4 = Předmostí IV; Q9 = Qafzeh 9; S17 = Sangiran 17; Sa = Saldanha; SC = Saint-Césaire I; SH = Sima de los Huesos 5; ShI = Shanidar I; ShV = Shanidar V; SkV = Skhūl V; Sp = Spy 1; St = Steinheim; Sts5 = Sts 5; T = Tabun I; Z = Zuttiyeh; Z12 = Zhoukoudian XII. Abbreviations: RHS = recent *Homo sapiens*; AMHS = anatomically modern *Homo sapiens*; EHS = early *Homo sapiens*; HN = *Homo neanderthalensis*; AfMPH = African Middle Pleistocene hominin remains; AsMPH = Asian Middle Pleistocene hominin remains; EuMPH = European Middle Pleistocene hominin remains; AfHE = African *Homo erectus*; AsHE = Asian *Homo erectus*; GHE = Georgian *Homo erectus*; HNa = *Homo naledi*; HHa = *Homo habilis*; HRu = *Homo rudolfensis*; AAfr = *Australopithecus africanus*; ParA = *Paranthropus aethiopicus*; ParB = *Paranthropus boisei*.

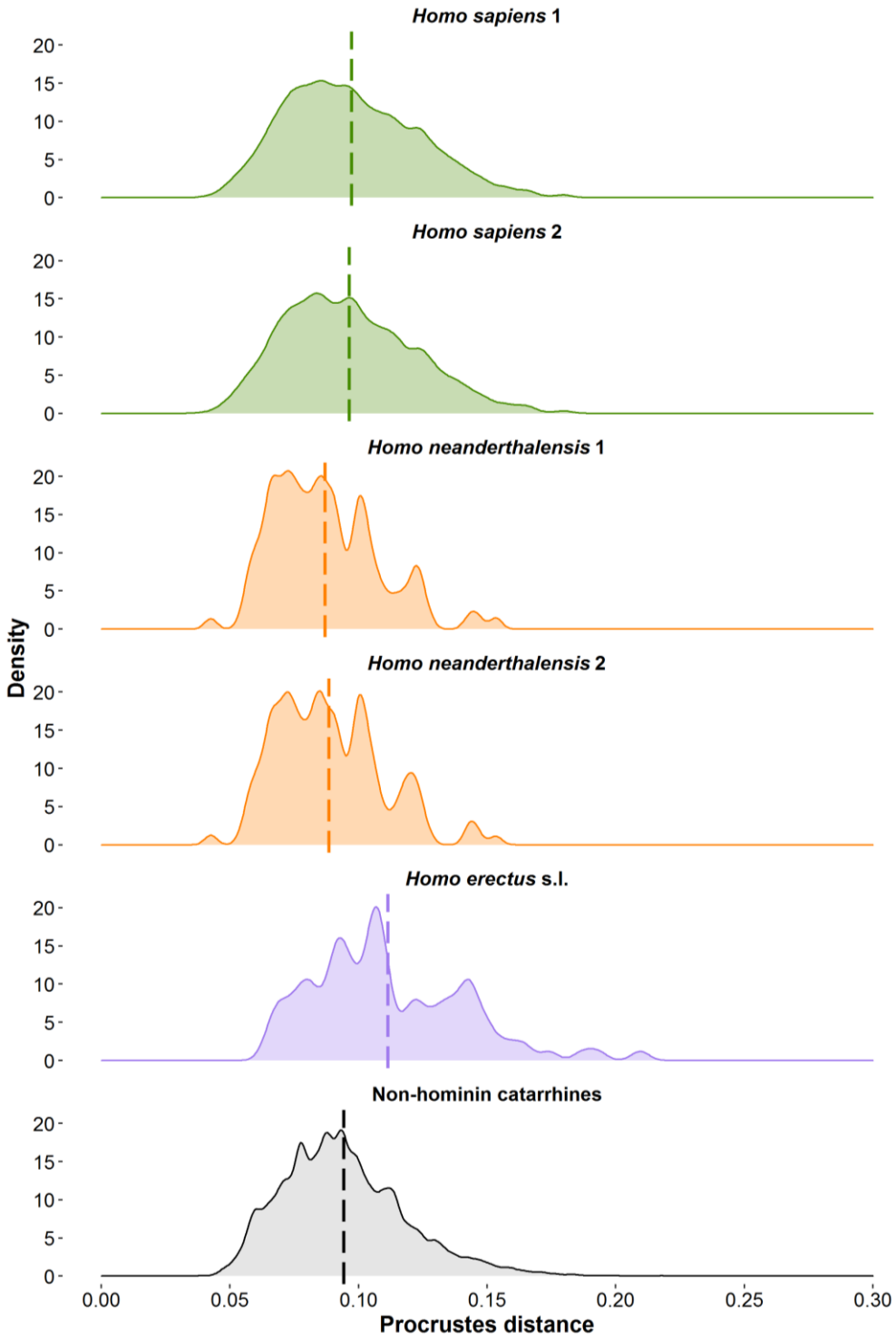

SOM Figure S3. Distribution plots of intragroup (for hominins) and intraspecific (for non-hominin catarrhines) Procrustes distances across 1000 subsamples (n = 8) under alternative hypothesis. Comparisons are shown with Zuttiyeh assigned to *Homo sapiens* (1) and *Homo neanderthalensis* (2). Dashed lines show mean values: *H. sapiens* 1 $\bar{x}$ = 0.097; *H. sapiens* 2 $\bar{x}$ = 0.098; *H. neanderthalensis* 1 $\bar{x}$ = 0.087; *H. neanderthalensis* 1 $\bar{x}$ = 0.090; *Homo erectus* s.l. 1 $\bar{x}$ = 0.111; non-hominin catarrhines $\bar{x}$ = 0.094.

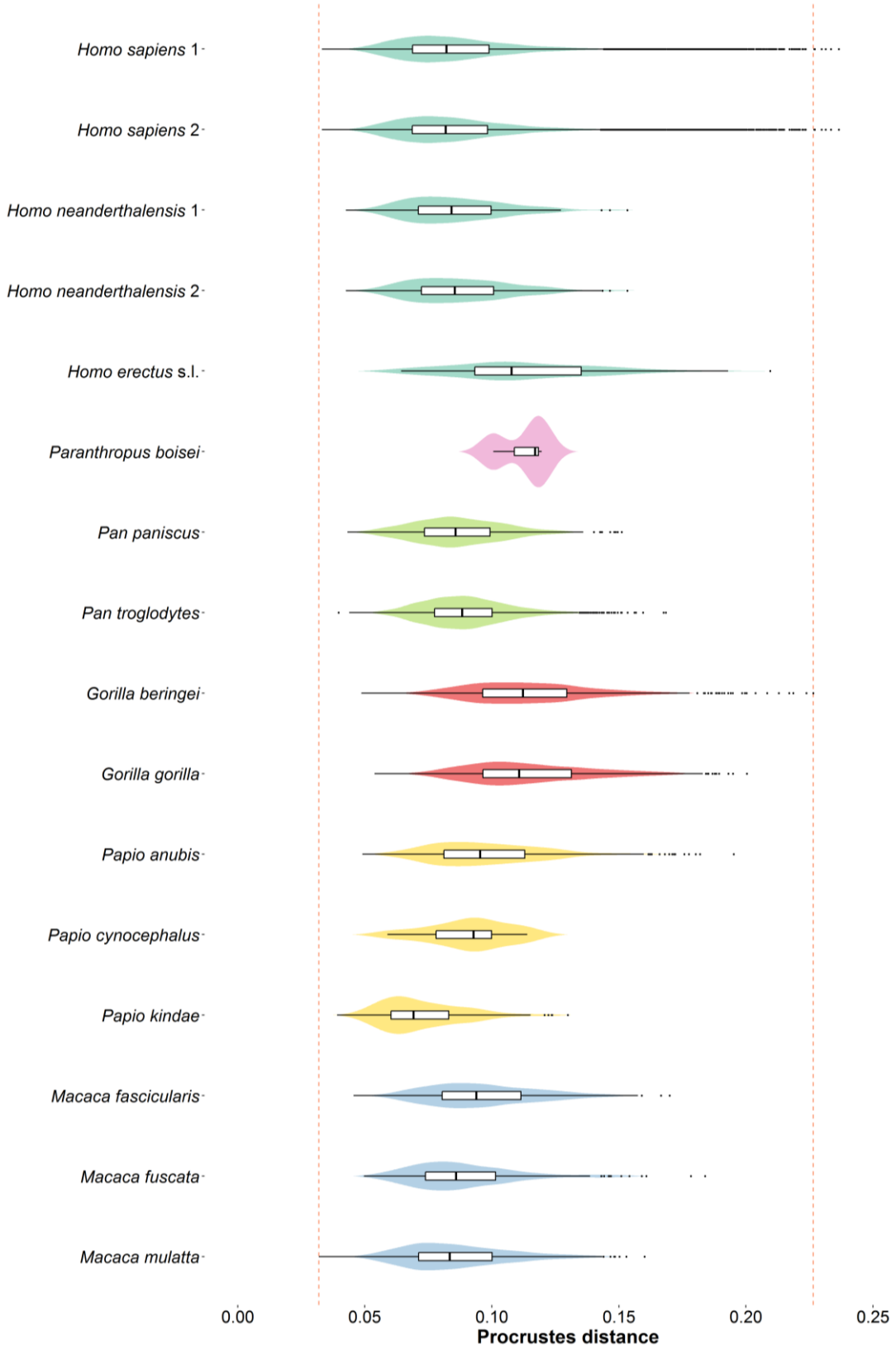

SOM Figure S4. Violin plots of intragroup Procrustes distances for individual groups under alternative hypothesis. Comparisons are shown with Zuttiyeh assigned to *Homo sapiens* (1) and *Homo*

neanderthalensis (2). Vertical dashed lines show range of intraspecific Procrustes distances across the sample of non-hominin catarrhines.

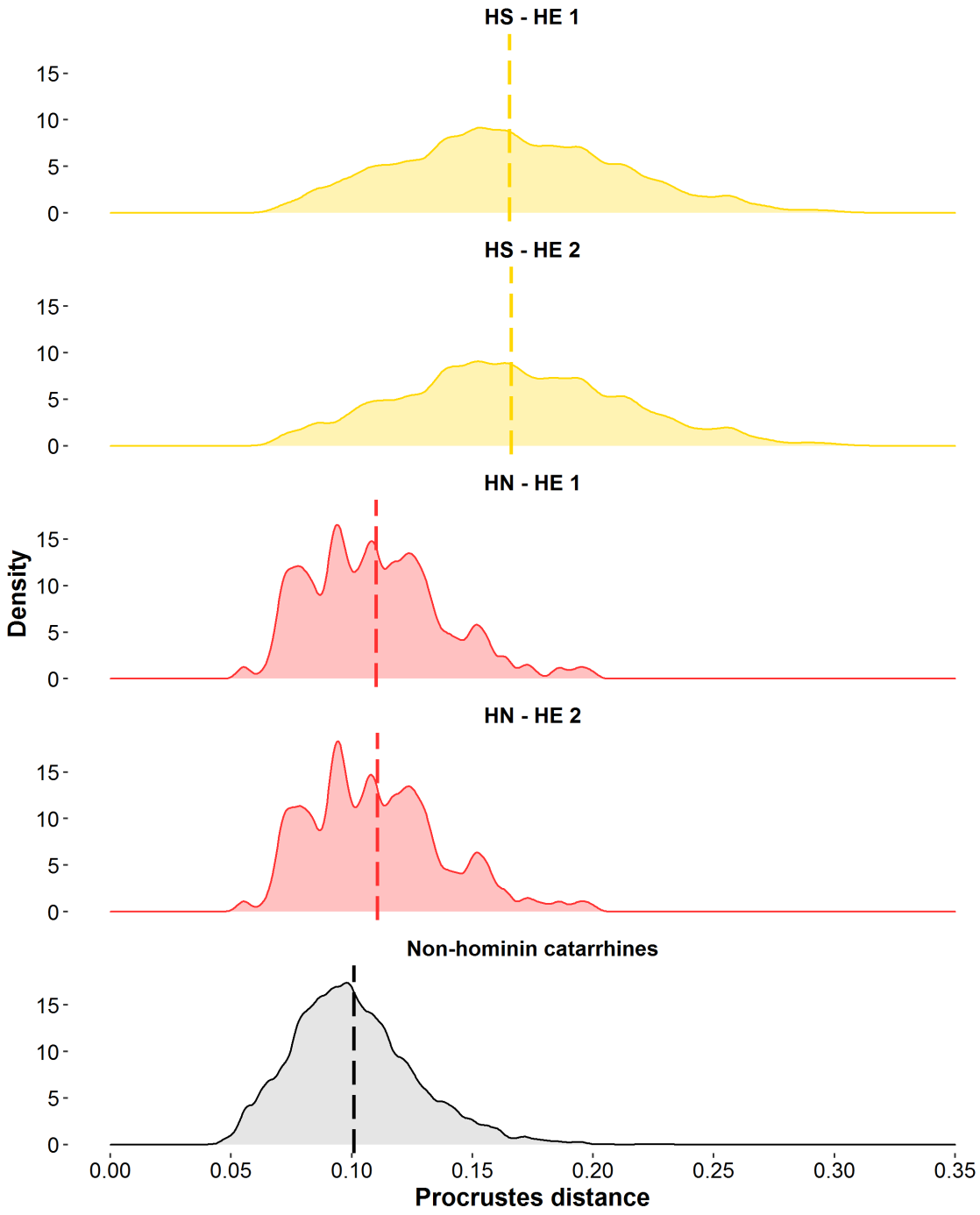

SOM Figure S5. Distribution plots of intergroup (for hominins) and interspecific (for non-hominin catarrhines) Procrustes distances across 1000 subsamples (n = 8) under alternative hypothesis. Comparisons are shown with Zuttiyeh assigned to *Homo sapiens* (1) and *Homo neanderthalensis* (2). Dashed lines show mean values: HS - HE 1 $\bar{x}$ = 0.165; HS - HE 2 $\bar{x}$ = 0.166; HN - HE 1 $\bar{x}$ = 0.110; HN - HE 2 $\bar{x}$ = 0.111; non-hominin catarrhines $\bar{x}$ = 0.101. Abbreviations: HS = *H. sapiens*; HN = *H. neanderthalensis*; HE = *Homo erectus* sensu lato.

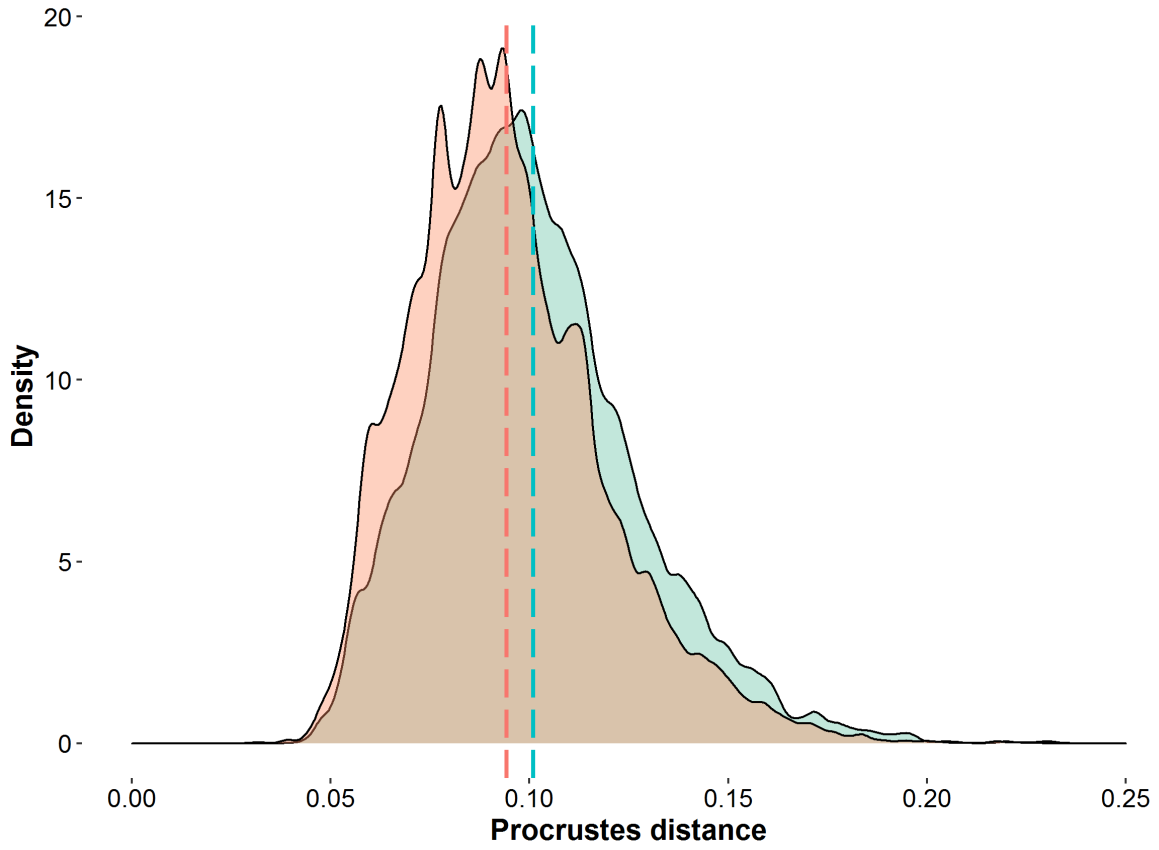

SOM Figure S6. Density plot of intra- (orange) and inter-specific (blue) Procrustes distances across 1000 subsamples (*n* = 8) from non-hominin catarrhine species. Dashed lines show mean values ($\bar{x}$ = 0.094 for intra- and 0.100 for interspecific Procrustes distances).

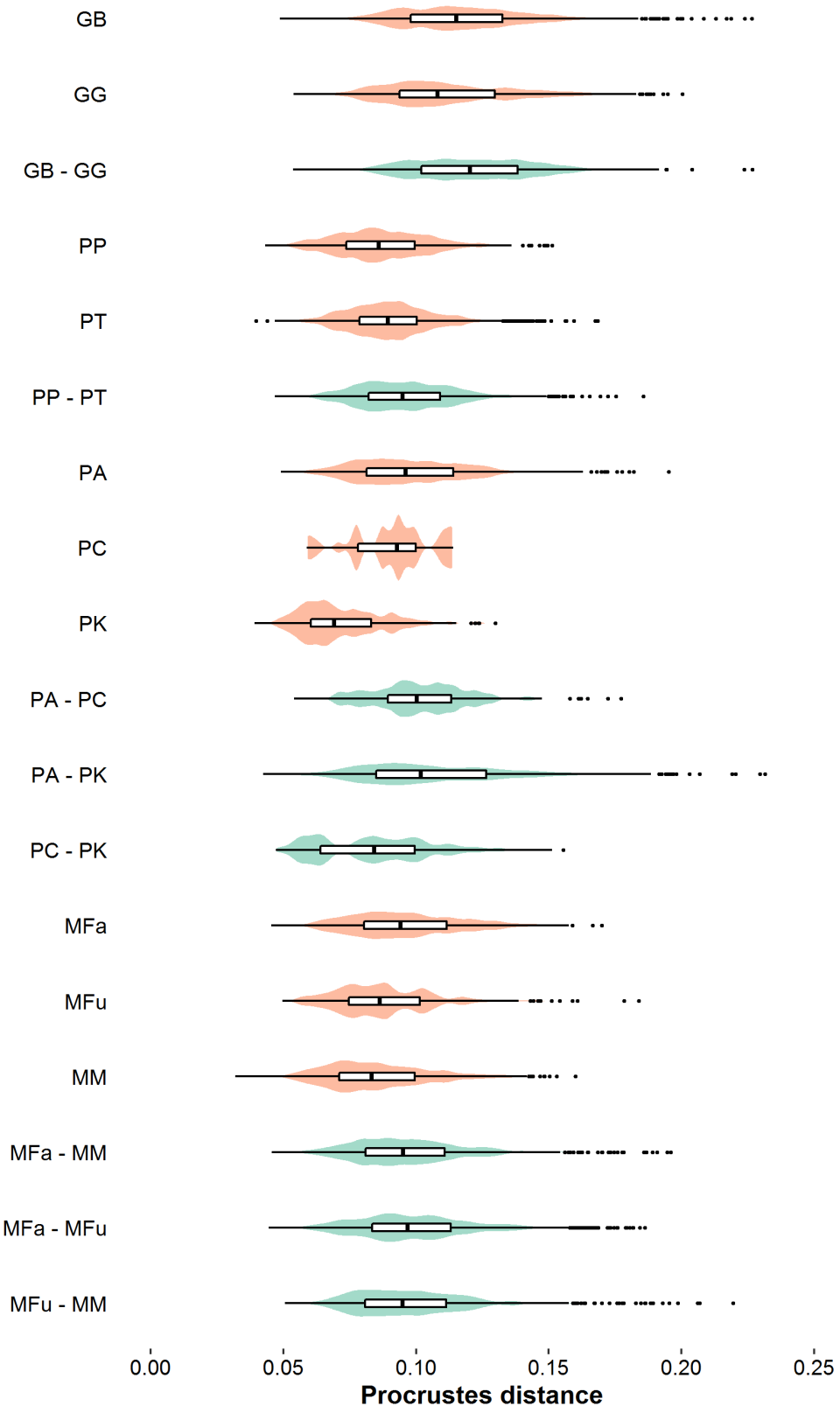

SOM Figure S7. Violin plots of intra- (orange) and inter-specific (blue) Procrustes distances for non-hominin species across 1000 subsamples. Abbreviations: GB = *Gorilla beringei*; GG = *Gorilla*

gorilla; PP = *Pan paniscus*; PT = *Pan troglodytes*; PA = *Papio anubis*; PC = *Papio cynocephalus*; PK = *Papio kindae*; MFa = *Macaca fascicularis*; MFu = *Macaca fuscata*; MM = *Macaca mulatta*.

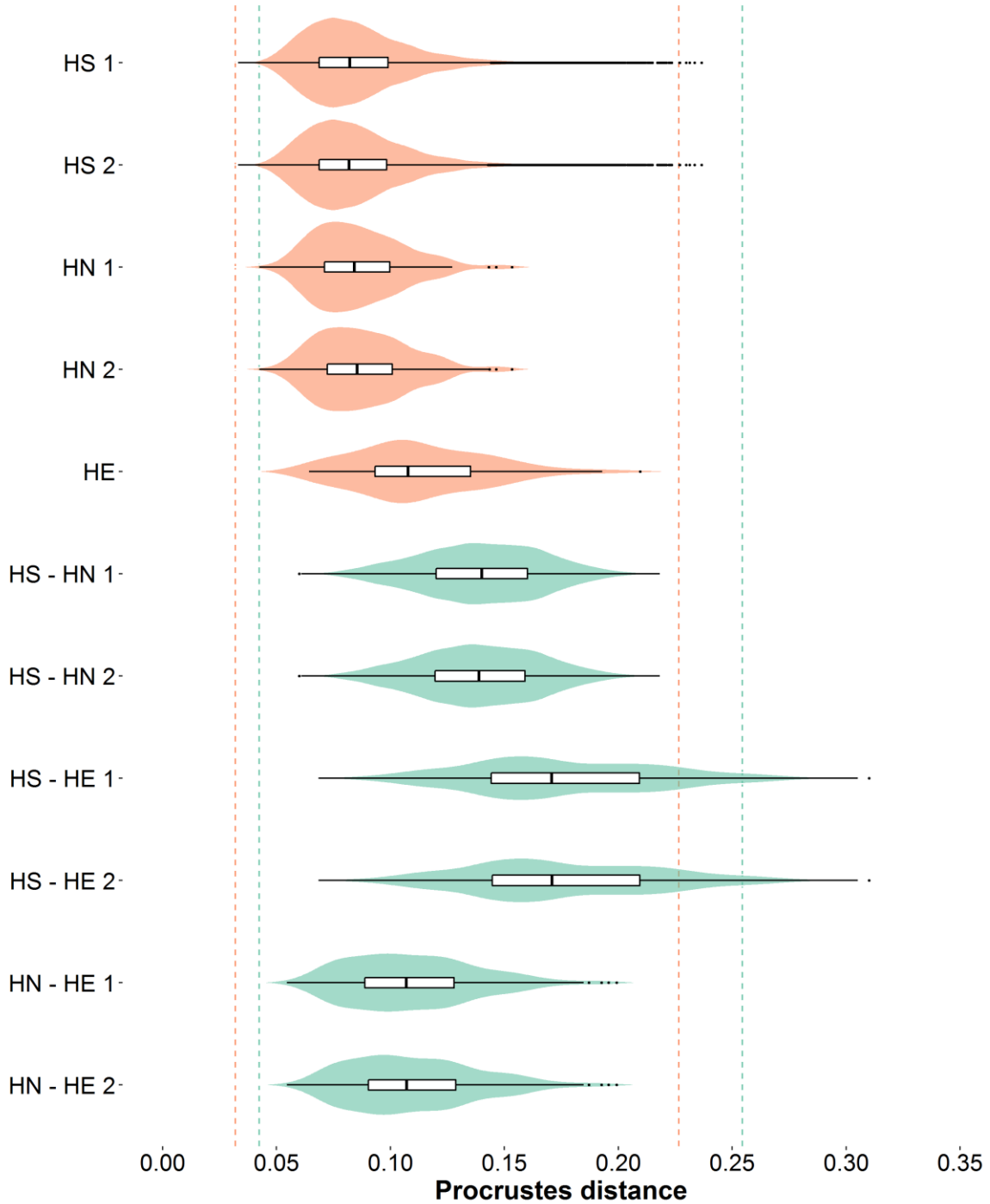

SOM Figure S8. Violin plots of intra- and inter-group Procrustes distances for hominin comparisons under alternative hypothesis. Comparisons are shown with Zuttiyeh assigned to *Homo sapiens* (1) and *Homo neanderthalensis* (2). Vertical dashed lines show range of intraspecific (orange) and interspecific (turquoise) Procrustes distances across the sample of non-hominin catarrhines. Abbreviations: HS = *H. sapiens*; HN = *H. neanderthalensis*; HE = *H. erectus* sensu lato.

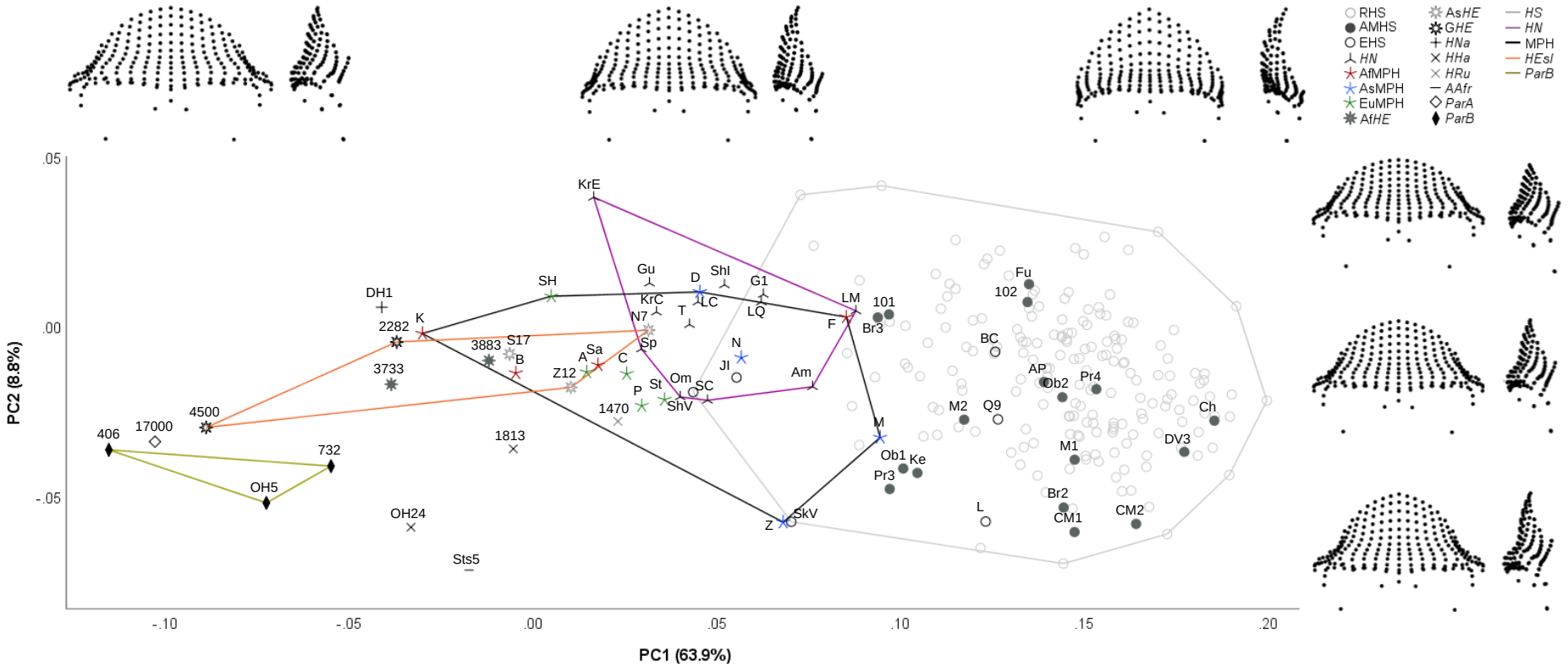

SOM Figure S9. Annotated version of Figure 3, with RHS specimens removed. Specimens are identified as follows (listed alphabetically): 101 = ZKD UC 101; 102 = ZKD UC 102; 406 = KNM-ER 406; 732 = KNM-ER 732; 1470 = KNM-ER 1470; 1813 = KNM-ER 1813; 2882 = D2282; 3773 = KNM-ER 3733; 3883 = KNM-ER 3883; 4500 = D4500; 17000 = KNM-WT 17000; A = Arago; Am = Amud 1; AP = Abri Pataud; B = Bodo; BC = Border Cave 1; Br2 = Brno II; Br3 = Brno III; C = Ceprano; Ch = Chancelade; CM1 = Cro-Magnon I; CM2 = Cro-Magnon II; D = Dali; DH1 = DH1; DV3 = Dolní Věstonice III; F = Florisbad; Fu = Furfooz I; G1 = Gibraltar 1; Gu = Guattari; H = Herto; JI = Jebel Irhoud 1; K = Kabwe; Ke = Keilor; KrC = Krapina C; KrE = Krapina E; L = Liujiang; LC = La Chapelle; LM = Le Moustier 1; LQ = La Quina H5; M = Maba; M1 = Mladeč 1; M2 = Mladeč 2; N = Narmada; N7 = Ngandong 7; Ob1 = Oberkassel I; Ob2 = Oberkassel II; OH5 = OH 5; OH24 = OH 24; Om = Omo 1; P = Petralona; Pr3 = Předmostí III; Pr4 = Předmostí

IV; Q9 = Qafzeh 9; S17 = Sangiran 17; Sa = Saldanha; SC = Saint-Césaire I; SH = Sima de los Huesos 5; ShI = Shanidar I; ShV = Shanidar V; SkV = Skhūl V; Sp = Spy 1; St = Steinheim; Sts5 = Sts 5; T = Tabun I; Z = Zuttiyeh; Z12 = Zhoukoudian XII. Abbreviations: RHS = recent *Homo sapiens*; AMHS = anatomically modern *Homo sapiens*; EHS = early *Homo sapiens*; HN = *Homo neanderthalensis*; AfMPH = African Middle Pleistocene hominin remains; AsMPH = Asian Middle Pleistocene hominin remains; EuMPH = European Middle Pleistocene hominin remains; AfHE = African *Homo erectus*; AsHE = Asian *Homo erectus*; GHE = Georgian *Homo erectus*; HNa = *Homo naledi*; HHa = *Homo habilis*; HRu = *Homo rudolfensis*; AAfr = *Australopithecus africanus*; ParA = *Paranthropus aethiopicus*; ParB = *Paranthropus boisei*.

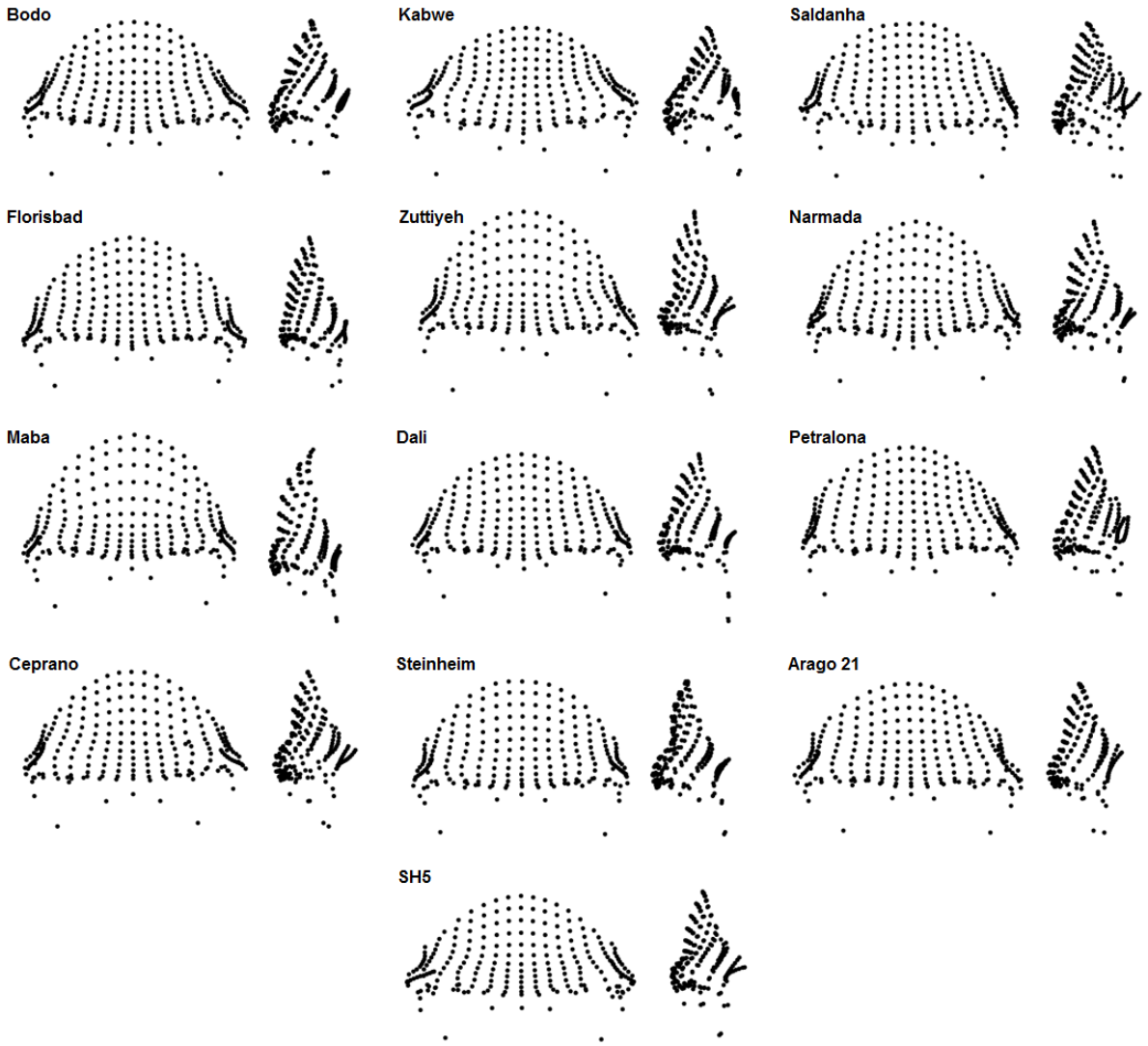

SOM Figure S10. Configurations of 3D landmarks and semilandmarks for 13 Middle Pleistocene hominin remains included in the study following generalized Procrustes analysis, shown from frontal and left lateral view. Abbreviation: SH5 = Sima de los Huesos 5.

SOM Table S1

Details of fossil hominin specimens included in this study.

Name	Species	Subgroup	Country	Institution
Gambles Cave IV	*Homo sapiens*	RHS	Kenya	AMNH (Anth)
Wajak I	*Homo sapiens*	RHS	Indonesia	AMNH (Anth)
Ofnet 4K1802	*Homo sapiens*	RHS	Germany	AMNH (Anth)
Ofnet 4K1811	*Homo sapiens*	RHS	Germany	AMNH (Anth)
La Brea	*Homo sapiens*	RHS	USA	AMNH (Anth)
Kennewick	*Homo sapiens*	RHS	USA	AMNH (Anth)
Csokavar	*Homo sapiens*	RHS	Hungary	AMNH (Anth)
Matjes River	*Homo sapiens*	RHS	South Africa	NHM (Pal)
Skull I/Sepulchre	*Homo sapiens*	RHS	Belgium	AMNH (Anth)
Combe Capelle	*Homo sapiens*	RHS	France	UCL (BioAnth)
Fish Hoek I	*Homo sapiens*	RHS	South Africa	AMNH (Anth)
Tepexpan I	*Homo sapiens*	RHS	Mexico	AMNH (Anth)
Oberkassel I	*Homo sapiens*	AMHS	Germany	AMNH (Anth)
Oberkassel II	*Homo sapiens*	AMHS	Germany	AMNH (Anth)
Keilor	*Homo sapiens*	AMHS	Australia	NHM (Pal)
Zhoukoudian UC 101	*Homo sapiens*	AMHS	China	AMNH (Anth)
Zhoukoudian UC 102	*Homo sapiens*	AMHS	China	AMNH (Anth)
Furfooz I	*Homo sapiens*	AMHS	Belgium	AMNH (Anth)
Brno II	*Homo sapiens*	AMHS	Czech Republic	AMNH (Anth)
Brno III	*Homo sapiens*	AMHS	Czech Republic	AMNH (Anth)
Dolní Věstonice III	*Homo sapiens*	AMHS	Czech Republic	NHM (Pal)
Předmostí III	*Homo sapiens*	AMHS	Czech Republic	UCL (BioAnth)
Předmostí IV	*Homo sapiens*	AMHS	Czech Republic	NHM (Pal)
Abri Pataud	*Homo sapiens*	AMHS	France	NHM (Pal)
Cro-Magnon I	*Homo sapiens*	AMHS	France	UCL (BioAnth)
Cro-Magnon II	*Homo sapiens*	AMHS	France	UCL (BioAnth)
Mladeč 1[a]	*Homo sapiens*	AMHS	Czech Republic	Vienna
Mladeč 2	*Homo sapiens*	AMHS	Czech Republic	NHM (Pal)
Chancelade	*Homo sapiens*	AMHS	France	UCL (BioAnth)
Jebel Irhoud 1	*Homo sapiens*	EHS	Morocco	NHM (Pal)
Omo 1	*Homo sapiens*	EHS	Ethiopia	NHM (Pal)
Liujiang	*Homo sapiens*	EHS	China	NHM (Pal)
Qafzeh 9	*Homo sapiens*	EHS	Israel	UCL (BioAnth)
Skhūl V[a]	*Homo sapiens*	EHS	Israel	Vienna
Border Cave 1	*Homo sapiens*	EHS	South Africa	NHM (Pal)
Bodo[a]	MPH	AfMPH	Ethiopia	Vienna
Kabwe 1[b]	MPH	AfMPH	Zambia	NHM (Pal)
Saldanha	MPH	AfMPH	South Africa	AMNH (Anth)
Florisbad	MPH	AfMPH	South Africa	NHM (Pal)
Dali	MPH	AsMPH	China	AMNH (Anth)
Maba	MPH	AsMPH	China	NHM (Pal)
Narmada	MPH	AsMPH	India	NHM (Pal)
Zuttiyeh	MPH	AsMPH	Israel	UCL (BioAnth)
Petralona	MPH	EuMPH	Greece	UCL (BioAnth)
Arago 21	MPH	EuMPH	France	AMNH (Anth)

Sima de los Huesos 5 (SH5)	MPH	EuMPH	Spain	NHM (Pal)
Steinheim	MPH	EuMPH	Germany	NHM (Pal)
Ceprano	MPH	EuMPH	Italy	NHM (Pal)
Tabun I	*Homo neanderthalensis*		Israel	AMNH (Anth)
La Quina H5	*Homo neanderthalensis*		France	AMNH (Anth)
Spy 1 [a]	*Homo neanderthalensis*		Belgium	NESPOS
La Chapelle	*Homo neanderthalensis*		France	UCL (Anth)
Guattari	*Homo neanderthalensis*		Italy	NHM (Pal)
Gibraltar 1 [b]	*Homo neanderthalensis*		Gibraltar	NHM (Pal)
Le Moustier 1	*Homo neanderthalensis*		France	UCL (Anth)
Amud 1	*Homo neanderthalensis*		Israel	UCL (Anth)
Krapina C	*Homo neanderthalensis*		Croatia	NHM (Pal)
Krapina E	*Homo neanderthalensis*		Croatia	AMNH (Anth)
Saint-Césaire I	*Homo neanderthalensis*		France	AMNH (Anth)
Shanidar I	*Homo neanderthalensis*		Iraq	AMNH (Anth)
Shanidar V	*Homo neanderthalensis*		Iraq	AMNH (Anth)
KNM-ER 3773	*Homo erectus* sensu lato	AfHE	Kenya	NHM (Pal)
KNM-ER 3883	*Homo erectus* sensu lato	AfHE	Kenya	NHM (Pal)
Ngandong 7 (Solo VI)	*Homo erectus* sensu lato	AsHE	Indonesia	NHM (Pal)
Sangiran 17	*Homo erectus* sensu lato	AsHE	Indonesia	MorphoSource
Zhoukoudian XII	*Homo erectus* sensu lato	AsHE	China	UCL (Anth)
Dinaledi Hominin 1 (DH1)	*Homo naledi*		South Africa	MorphoSource
KNM-ER 1813	*Homo habilis*		Kenya	UCL (Anth)
OH 24	*Homo habilis*		Tanzania	UCL (Anth)
KNM-ER 1470	*Homo rudolfensis*		Kenya	UCL (Anth)
Sts 5	*Australopithecus africanus*		South Africa	Vienna
KNM-WT 17000	*Paranthropus aethiopicus*		Kenya	AfricanFossils.org
KNM-ER 406	*Paranthropus boisei*		Kenya	AfricanFossils.org
KNM-ER 732	*Paranthropus boisei*		Kenya	AfricanFossils.org
OH 5	*Paranthropus boisei*		Tanzania	UCL (Anth)

Abbreviations: UC = Upper Cave; KNM-ER = Kenya National Museum, East Rudolf; OH = Olduvai Hominid; Sts = Sterkfontein Type Site; KNM-WT = Kenya National Museum, West Turkana; MPH = Middle Pleistocene hominin remains; RHS = recent *Homo sapiens*; AMHS = anatomically modern *H. sapiens*; EHS = early *H. sapiens*; AfMPH = African Middle Pleistocene hominin remains; AsMPH = Asian Middle Pleistocene hominin remains; EuMPH = European Middle Pleistocene hominin remains; AfHE = African *Homo erectus*; AsHE = Asian *H. erectus*; GHE = Georgian *H. erectus*; AMNH (Anth) = American Museum of Natural History (Anthropology Department); NHM (Pal) = Natural History Museum, London (Palaeontology Department); UCL (BioAnth) = University College London, Biological Anthropology collection

[a] Specimens for which CT data were used.

[b] Specimens for which surface scans were collected from the original fossil. All other data were collected from research quality casts.

SOM Table S2

Details of 172 archaeological and historical *H. sapiens* specimens included in this study. Sex estimates are reported, using the methods of Buikstra and Ubelaker (1994). See White et al. (2020) for details on non-hominin catarrhine specimens. Available location information is indicated in parentheses when exact provenance was unknown.

Accession number	Category	Provenance	Sex	Institution
242	RHS	UK	F	DW
443	RHS	UK	F	DW
961	RHS	(Europe)	F?	DW
1029	RHS	UK	I	DW
1174	RHS	(N Europe)	F?	DW
1177	RHS	Finland	F	DW
1233	RHS	Syria	M	DW
1241	RHS	Jordon	F	DW
1242	RHS	Dutch	M	DW
1248	RHS	Spain	M?	DW
1583	RHS	Egypt	F	DW
1627	RHS	Egypt	M	DW
1703	RHS	India	F	DW
1705	RHS	India	M	DW
1717	RHS	Tenerife	M	DW
1727	RHS	Mozambique	F	DW
1731	RHS	Angola	M	DW
1749	RHS	Congo	F	DW
1761	RHS	China	F	DW
1773	RHS	Egypt	I	DW
1777	RHS	(Congo)	M?	DW
1778	RHS	Ivory Coast	F?	DW
1783	RHS	Madagascar	F?	DW
1785	RHS	Madagascar	F	DW
1791	RHS	Philippines	M	DW
2202	RHS	Sumatra	F	DW
3275	RHS	Egypt	F	DW
3276	RHS	Egypt	M	DW
4194	RHS	Japan	F?	DW
4211	RHS	China	F	DW
4220	RHS	(Canaan)	F	DW
4300	RHS	Egpyt	M	DW
5039	RHS	Senegal	I	DW
5041	RHS	Madagascar	F	DW
5053	RHS	(W Africa)	F	DW
5060	RHS	Gabon	M	DW
5064	RHS	Crete	I	DW
5096	RHS	Syria	I	DW
5332	RHS	Siberia	M	DW
5343	RHS	Sudan	I	DW
5424	RHS	Nigeria	M?	DW

5428	RHS	Nigeria	F?	DW
6094	RHS	Uganda	M	DW
1082/BK.FOL.63	RHS	Kenya	F?	DW
1168/2133	RHS	Australia	M	DW
1178/1205	RHS	Sweden	M	DW
1204/SAS 13	RHS	Pakistan	F	DW
1250/SAS15	RHS	Pakistan	M	DW
1739/AF 1144	RHS	South Africa	I	DW
1755/AF 1102	RHS	South Africa	F	DW
1798/POL 067	RHS	Tahiti	F?	DW
1811/POL 105	RHS	Rotuma	F	DW
1812/POL 099	RHS	Rotuma	M	DW
1830/NA 147	RHS	(Eskimo)	M	DW
1838/NA 083	RHS	Huron	M	DW
1842/NA 071	RHS	USA	M	DW
1849/ NA 092	RHS	Canada	I	DW
2117/AUS 89	RHS	Australia	M	DW
2394/SA 020	RHS	Peru	I	DW
3315/SAS 07	RHS	Sri Lanka	M	DW
3317/SAS 9	RHS	Sri Lanka	M	DW
4213/EAS 15	RHS	China	I	DW
4434/AF 1195	RHS	Ghana	I	DW
4503/POL 019	RHS	New Zealand	M?	DW
4556/SEA 045	RHS	Malaysia	I	DW
4576/SEA 065	RHS	Malaysia	F?	DW
5291/MEL 206	RHS	Papua New Guinea	F	DW
5423/AF 1177	RHS	Nigeria	F?	DW
6073/MIC 001	RHS	Gilbert Islands	M	DW
99/6689	RHS	Canada	M	AMNH (Anth)
99/6690	RHS	Canada	M	AMNH (Anth)
AF 1376	RHS	Sudan	M	DW
AF.11.5.328	RHS	Egypt	F	DW
AF.15.0.14	RHS	Somalia	F?	DW
AF.21.0.52	RHS	Kenya	F	DW
AF.21.0.6/AF 886	RHS	Kenya/Ethiopia	I	DW
AF.23.0.19	RHS	Tanzania	I	DW
AM.0.0.1/NA 136	RHS	(Eskimo)	F	DW
AM.0.0.2/NA 137	RHS	(Eskimo)	F	DW
AM.15.0.11/NA 072	RHS	USA	M?	DW
AM.44.0.2	RHS	Chile	F	DW
AM.45.0.1	RHS	Tierra del Fuego	F	DW
ANI 047	RHS	Nicobar Islands	F	DW
ANI 23	RHS	Andaman Islands	F?	DW
AS.17.0.1	RHS	Tibet	I	DW
AS.17.0.2/EAS 21	RHS	Tibet	F	DW
AS.21.0.6/EAS 6	RHS	China	F?	DW
AS.45.0.1/SEA 162	RHS	Philippines	M?	DW
AS.57.0.14/BU 14	RHS	(Unknown)	M	DW
AS.57.0.45/BU 45	RHS	(Unknown)	I	DW

AS.66.0.74/AR 4	RHS	Saudi Arabia?	F?	DW
CA 004/AM.21.0.1	RHS	Guatemala	F	DW
CA 010	RHS	Lesser Antilles	I	DW
EAS 24	RHS	Japan	M	DW
ESC11 SK1105	RHS	UK	M?	UCL (IoA)
ESC11 SK1606	RHS	UK	F	UCL (IoA)
ESC11 SK2241	RHS	UK	F?	UCL (IoA)
ESC11 SK2322	RHS	UK	I	UCL (IoA)
ESC11 SK2504	RHS	UK	M?	UCL (IoA)
ESC11 SK3310	RHS	UK	M	UCL (IoA)
ESC11 SK3638	RHS	UK	F?	UCL (IoA)
ESC11 SK4309	RHS	UK	M?	UCL (IoA)
ESC11 SK4606	RHS	UK	F	UCL (IoA)
ESC11 SK4611	RHS	UK	F?	UCL (IoA)
ESC11 SK5183	RHS	UK	F?	UCL (IoA)
EU.1.1.113	RHS	UK	F?	DW
EU.1.1.27	RHS	UK	M	DW
EU.1.1.9	RHS	UK	M	DW
EU.1.2.225	RHS	UK	F	DW
EU.1.2.266	RHS	UK	F?	DW
EU.1.2.284	RHS	UK	M	DW
EU.1.2.362	RHS	UK	M	DW
EU.1.3.172	RHS	UK	M	DW
EU.1.3.196	RHS	UK	M?	DW
EU.1.3.240	RHS	UK	M?	DW
EU.1.3.278	RHS	UK	M	DW
EU.1.3.5	RHS	UK	F	DW
EU.1.4.20	RHS	UK	F	DW
EU.1.4.3	RHS	UK	M	DW
EU.1.4.92	RHS	UK	F	DW
EU.1.4.96	RHS	UK	M	DW
EU.1.5.076	RHS	UK	M	DW
EU.1.5.082/39	RHS	UK	M	DW
EU.1.5.105	RHS	UK	F	DW
EU.3.5.01/712	RHS	UK	M?	DW
EU.31.0.1	RHS	Russia	M	DW
EU.34.4.1	RHS	Italy?	I	DW
EU.42.00.2	RHS	Italy	I	DW
EU.45.4.1	RHS	Minorca	M?	DW
F 161	RHS	Egypt?	F	DW
JT12/198	RHS	UK	M	DW
Kiyono-27	RHS	Jomon	M?	KUM
Kiyono-34	RHS	Jomon	F	KUM
Kiyono-61	RHS	Jomon	M	KUM
Kiyono-66	RHS	Jomon	M?	KUM
Kiyono-70	RHS	Jomon	F?	KUM
KUA-103	RHS	China	M	KUM
KUA-1047	RHS	China	F	KUM
KUA-1070	RHS	China	M	KUM

KUA-1407	RHS	China	I	KUM
KUA-1416	RHS	China	F	KUM
KUA-1618	RHS	China	M	KUM
KUA-2573	RHS	China	I	KUM
KUA-2783	RHS	China	M	KUM
KUA-3012	RHS	China	F	KUM
KUA-867	RHS	China	F	KUM
MEL 110	RHS	Papua New Guinea	M	DW
MEL 382	RHS	Solomon Islands	M	DW
MEL 396	RHS	Solomon Islands	M	DW
MEL 406/OC.14.0.2	RHS	Santa Cruz	M	DW
MEL 478	RHS	New Caledonia	F?	DW
MEL 483/OC.19.0.1	RHS	Fiji	M	DW
NA 015/AM.15.1.15	RHS	USA	F	DW
NA 068/AM.15.0.9	RHS	USA	F?	DW
NA 087/1861	RHS	USA	M	DW
OC.3.0.3	RHS	Australia	F	DW
RCSOM/B 1	RHS	UK	M?	RCS
RCSOM/B 105 Part 1	RHS	UK	I	RCS
RCSOM/B 110	RHS	UK	M?	RCS
RCSOM/B 124	RHS	UK	F?	RCS
RCSOM/B 14	RHS	UK	M	RCS
RCSOM/B 17	RHS	UK	M	RCS
RCSOM/B 27	RHS	UK	F	RCS
RCSOM/B 57	RHS	UK	M	RCS
RCSOM/B 71	RHS	UK	M?	RCS
RCSOM/B 94	RHS	UK	M?	RCS
RCSOM/B nn28	RHS	UK	M?	RCS
SA 006/2017	RHS	Chile	I	DW
SA 008	RHS	Chile	M	DW
SEA 061	RHS	Malaysia	M	DW
SEA 133	RHS	Malaysia	I	DW
TORR 060	RHS	Torres Strait	I	DW

Abbreviations: RHS = Recent *Homo sapiens*; F = female; F? = probably female; I = indeterminate sex; M = male; M? = probable male; DW = Duckworth Laboratory, Cambridge; AMNH (Anth) = American Museum of Natural History (Anthropology Department); UCL (IoA) = University College London, Institute of Archaeology collections; KUM = Kyoto University Museum; RCS = Royal College of Surgeons, Odontological collection, London.

SOM Table S3

Definitions of landmarks used in the present study. Taken from White et al. (2020).

Landmark	Definition
Auriculare[a]	The point vertically above the midpoint of the external auditory meatus on the zygomatic root
Dacryon	The point where a line from ectoconchion dividing the orbit into two along the long axis intersects with the medial orbital margin
Ectoconchion	The intersection of the most anterior surface of the lateral border of the orbit and a line bisecting the orbit along the long axis
Frontomalare anterior	The point where the frontomalare suture intersects with the lateral orbital margin
Frontomalare posterior	The most posterior point on the frontomalare suture of the zygomatic process
Frontotemporale	The most medial point on the lateral curve of the frontal bone, when viewed from *norma verticalis*
Glabella	The most anterior point on the frontal bone, between the supraorbital tori, on the midsagittal plane
Mid-frontotemporale	The point where a line between the frontotemporale points intersects with the midsagittal plane
Mid-torus anterior	The most anterior point on the frontal bone directly above the midpoints of the orbit
Mid-torus inferior	The point on the superior orbital margin, at the midpoint of the orbit
Nasion	The point where the nasofrontal suture intersects the midsagittal plane
Orbitale	The most inferior point on the infraorbital margin
Post-toral sulcus	The most inferior point on the region posterior to glabella, in the midsagittal plane

[a] Auriculare points were not included in the final configuration.

SOM Table S4

Results of Games-Howell post-hoc comparisons of Procrustes distances between groups for assessment of intraobserver error significance.

	Mean difference	SE	*p*	95% CI	
Intrasubspecies	-0.058	0.002	<0.001	-0.063	-0.053
Intersubspecies	-0.054	0.002	<0.001	-0.059	-0.049
Intraspecies	-0.046	0.002	<0.001	-0.051	-0.041
Interspecies	-0.061	0.002	<0.001	-0.066	-0.057

SOM Table S5

Descriptive statistics for 1000 repeats of stepwise, jackknife cross-validated discriminant analysis for non-hominin catarrhines.

	Mean	Minimum	Maximum	SD
Gorilla beringei	80.3%	37.5%	100.0%	13.1%
Gorilla gorilla	81.1%	25.0%	100.0%	12.7%
Pan paniscus	77.8%	37.5%	100.0%	13.4%
Pan troglodytes	75.8%	0.0%	100.0%	14.1%
Papio anubis	67.0%	0.0%	100.0%	14.8%
Papio cynocephalus	48.6%	12.5%	87.5%	13.4%
Papio kindae	86.2%	25.0%	100.0%	10.9%
Macaca fascicularis	64.9%	0.0%	100.0%	15.5%
Macaca fuscata	73.7%	25.0%	100.0%	14.6%
Macaca mulatta	72.0%	25.0%	100.0%	15.4%
All	72.7%	0.0%	100.0%	17.2%

SOM Table S6

Descriptive statistics for 1000 repeats of stepwise, jackknife cross-validated discriminant analysis for hominins.

	Mean	Minimum	Maximum	SD
Homo sapiens	85.4%	62.5%	100.0%	9.0%
Homo neanderthalensis	90.9%	50.0%	100.0%	9.1%
Middle Pleistocene hominins	77.6%	37.5%	100.0%	13.4%
Homo erectus s.l.	75.7%	28.6%	100.0%	10.4%
Homo habilis	46.2%	0.0%	100.0%	24.9%
All	75.1%	0.0%	100.0%	21.3%

SOM Table S7

Results of subsampling (n = 7) showing percentage of 1000 repeats in which the Procrustes distances within the hominin groups, including the MPH, were significantly ($p \leq 0.05$; highlighted in bold) or not significantly different intraspecific distances in the non-hominin catarrhine species, under the main hypothesis.

	Homo sapiens			*Homo neanderthalensis*			MPH			*Homo erectus* s.l.		
	No significant difference	Significant difference		No significant difference	Significant difference		No significant difference	Significant difference		No significant difference	Significant difference	
		Less variable	More variable		Less variable	More variable		Less variable	More variable		Less variable	More variable
Gorilla beringei	39.6	59.9	0.5	**3.3**	**96.7**	0.0	30.2	69.6	0.2	84.6	4.2	11.2
Gorilla gorilla	50.1	48.5	1.4	8.8	91.2	0.0	40.7	58.6	0.7	72.9	2.2	24.9
Pan paniscus	56.5	1.6	41.9	65.2	30.8	4.0	53.9	1.1	45	**0.8**	0.0	**99.2**
Pan troglodytes	63.7	3.6	32.7	58.2	40.8	1.0	66.3	2.0	31.7	**1.2**	0.0	**98.8**
Papio anubis	76.7	12.9	10.4	36.2	63.8	0.0	77.8	13.2	9.0	23.3	0.0	76.7
Papio cynocephalus	75.4	2.1	22.5	57.6	42.4	0.0	80.7	0.2	19.1	**0.0**	0.0	**100.0**
Papio kindae	11.6	0.2	88.2	60.2	2.2	37.6	6.1	0.0	93.9	**0.0**	0.0	**100.0**
Macaca fascicularis	75.6	9.6	14.8	43.0	56.4	0.6	78.5	9.9	11.6	15.7	0.0	84.3
Macaca fuscata	58.3	1.9	39.8	65.9	32	2.1	56.8	1.8	41.4	4.5	0.0	95.5
Macaca mulatta	59.3	1.3	39.4	69.1	26.6	4.3	58.9	0.5	40.6	**1.0**	0.0	**99.0**

Abbreviation: MPH = Middle Pleistocene hominins.

SOM Table S8

Results of subsampling (n = 8) showing percentage of 1000 repeats in which the Procrustes distances within the hominin groups were significantly ($p \leq 0.05$; highlighted in bold) or not significantly different to intraspecific distances in the non-hominin catarrhine species, under alternative hypothesis. In each column, Under the alternative hypothesis, results are shown with Zuttiyeh assigned toclassified as both *Homo sapiens* (left) and *Homo neanderthalensis* (right).

	Homo sapiens						*Homo neanderthalensis*						*Homo erectus* s.l.		
	No significant differences		Significant differences				No significant differences		Significant differences				No significant differences	Significant differences	
			Less variable		More variable				Less variable		More variable			Less variable	More variable
Gorilla beringei	26.7	25.4	73.1	74.4	0.2	0.2	**3.7**	**4.6**	**96.3**	**95.4**	0.0	0.0	70.0	25.0	5.0
Gorilla gorilla	45.5	38.6	53.8	60.3	0.7	1.1	10.0	14.8	90.0	85.2	0.0	0.0	71.2	16.2	12.6
Pan paniscus	54.3	59.2	2.6	1.8	43.1	39.0	69.4	67.7	17.2	14.4	13.4	17.9	14.7	0.1	85.2
Pan troglodytes	61.0	67.2	3.9	3.6	35.1	29.2	70.5	70.6	24.0	20.1	5.5	9.3	18.1	0.0	81.9
Papio anubis	75.4	72.4	15.1	18.9	9.5	8.7	48.3	52.5	50.9	46.3	0.8	1.2	51.1	1.9	47.0
Papio cynocephalus	71.2	74.8	2.8	2.3	26.0	22.9	75.6	81.6	23.8	16.8	0.6	1.6	15.6	0.0	84.4
Papio kindae	6.7	9.6	0.0	0.1	93.3	90.3	30.0	25.5	0.1	0.1	69.9	74.4	**0.1**	0.0	**99.9**
Macaca fascicularis	72.9	74.1	13.2	12.8	13.9	13.1	52.1	58.2	45.6	38.6	2.3	3.2	44.6	1.0	54.4
Macaca fuscata	58.8	61.2	2.6	4.1	38.6	34.7	68.6	71.1	21.6	15.6	9.8	13.3	20.8	0.3	78.9
Macaca mulatta	52.7	56.1	2.4	2.6	44.9	41.3	72.5	71.5	13.1	9.7	14.4	18.8	15.5	0.0	84.5

SOM Table S9

Results of subsampling (n = 8) showing percentage of 1000 repeats in which the Procrustes distances between the hominin groups were significantly ($p \leq 0.05$; highlighted in bold) or not significantly different to interspecific distances in the non-hominin catarrhines, under alternative hypothesis. In each column, results are shown with Zuttiyeh assigned to both *Homo sapiens* (left) and *Homo neanderthalensis* (right).

	Homo sapiens - *Homo erectus* s.l.						*Homo neanderthalensis* - *Homo erectus* s.l.					
	No significant difference		Significant difference				No significant difference		Significant difference			
			Sig. less		Sig. more				Sig. less		Sig. more	
Gorilla beringei – Gorilla gorilla	**0.8**	**1.2**	0.0	0.0	**99.2**	**98.8**	52.6	53.8	46.2	44.0	1.2	2.2
Pan paniscus – Pan troglodytes	**0.0**	**0.0**	0.0	0.0	**100.0**	**100.0**	30.8	29.9	0.4	0.5	68.8	69.6
Papio anubis – Papio cynocephalus	**0.0**	**0.0**	0.0	0.0	**100.0**	**100.0**	53.6	52.1	1.9	1.5	44.5	46.4
Papio anubis – Papio kindae	**1.2**	**1.3**	0.0	0.0	**98.8**	**98.7**	64.2	64.6	12.2	11.7	23.6	23.7
Papio cynocephalus – Papio kindae	**0.0**	**0.0**	0.0	0.0	**100.0**	**100.0**	**4.0**	**2.7**	0.0	0.0	**96.0**	97.3
Macaca fascicularis – Macaca fuscata	**0.0**	**0.0**	0.0	0.0	**100.0**	**100.0**	41.9	40.8	1.3	1.0	56.8	58.2
Macaca fascicularis – Macaca mulatta	**0.0**	**0.1**	0.0	0.0	**100.0**	**99.9**	47.2	46.0	1.9	1.8	50.9	52.2
Macaca fuscata – Macaca mulatta	**1.6**	**2.3**	0.0	0.1	**98.4**	**97.6**	40.6	37.8	0.7	0.8	58.7	61.4

Abbreviation: Sig. = significantly.

SOM Table S10

Summary of t and *p* values for independent t-tests across 1000 subsample ($n = 8$) comparisons of intra- and interspecific Procrustes distances for non-hominin catarrhines. Figures in bold show majority (for t values) and significance (for *p* values).

		t		*p*		
		< 0	> 0	No significant differences	Significant differences	
					Less	More
Gorilla beringei	*Gorilla gorilla*	**68.6**	31.4	85.1	13.2	1.7
Gorilla gorilla	*Gorilla beringei*	**78.8**	21.2	63.4	35.9	0.7
Pan paniscus	*Pan troglodytes*	**89.0**	11.0	55.7	43.9	0.4
Pan troglodytes	*Pan paniscus*	**79.9**	20.1	64.8	33.6	1.6
Papio anubis	*Papio cynocephalus*	**68.4**	31.6	86.8	12.5	0.7
	Papio kindae	**76.2**	23.8	65.8	32.9	1.3
Papio cynocephalus	*Papio anubis*	**99.4**	0.6	37.9	62.1	0.0
	Papio kindae	8.7	**91.3**	76.2	0.0	23.8
Papio kindae	*Papio anubis*	**100.0**	0.0	**0.9**	**99.1**	0.0
	Papio cynocephalus	**97.9**	2.1	44.6	55.4	0.0
Macaca fascicularis	*Macaca fuscata*	**52.2**	47.8	80.6	13.7	5.7
	Macaca mulatta	**64.2**	35.8	81.1	16.4	2.5
Macaca fuscata	*Macaca fascicularis*	**91.7**	8.3	62.8	37.0	0.2
	Macaca mulatta	**81.4**	18.6	57.2	41.3	1.5
Macaca mulatta	*Macaca fascicularis*	**93.9**	6.1	42.5	57.3	0.2
	Macaca fuscata	**94.1**	5.9	53.7	46.1	0.2

SOM Table S11

Summary of t and *p* values for independent t-tests across 1000 subsample (n = 8) comparisons of intra- and interspecific Procrustes distances for hominins, under alternative hypothesis. Figures in bold show majority (for t values) and significance (for *p* values). Under the alternative hypothesis, results are shown with Zuttiyeh assigned to *Homo sapiens* (left) and *Homo neanderthalensis* (right).

		t				*p*					
		< 0		> 0		No significant difference		Significant difference			
								Less		More	
Homo sapiens	*Homo neanderthalensis*	**99.9**	**100.0**	0.1	0.0	**1.2**	**1.2**	**98.8**	**98.8**	0.0	0.0
	Homo erectus s.l.	**100.0**	**100.0**	0.0	0.0	**0.0**	**0.0**	**100.0**	**100.0**	0.0	0.0
Homo neanderthalensis	*Homo sapiens*	**100.0**	**100.0**	0.0	0.0	**0.0**	**0.0**	**100.0**	**100.0**	0.0	0.0
	Homo erectus s.l.	**100.0**	**99.8**	0.0	0.2	**4.6**	7.4	**95.4**	92.6	0.0	0.0
Homo erectus s.l.	*Homo sapiens*	**100.0**	**100.0**	0.0	0.0	**0.0**	**0.0**	**100.0**	**100.0**	0.0	0.0
	Homo neanderthalensis	41.3	49.6	**58.7**	**50.4**	95.6	94.4	3.3	4.5	1.1	1.1

SOM Table S12

Details of 50 specimens for which landmarks and semilandmarks were reconstructed using geometric method, showing number of points which were reconstructed with this method.

Specimen	Number of reconstructed (semi)landmarks	Group	Sex
USNM 545030	1	*Gorilla gorilla beringei*	F
RMCA 29538	1	*Gorilla gorilla graueri*	F
RMCA 29104	1	*Gorilla gorilla graueri*	F
USNM 252575	4	*Gorilla gorilla gorilla*	F
F.C. 130	4	*Gorilla gorilla gorilla*	M
USNM 599172	3	*Pan troglodytes troglodytes*	M
USNM 236971	4	*Pan troglodytes schweinfurthii*	F
M-16115	2	*Papio anubis*	F
M-82097	1	*Papio anubis*	F
ZD.1908.8.9.41	6	*Papio anubis*	F
ZD.1924.8.6.16	6	*Papio anubis*	F
ZD.1930.12.1.2	2	*Papio anubis*	F
ZD.1964.2194	4	*Papio anubis*	F
USNM 397476	1	*Papio anubis*	F
M-55446	2	*Papio anubis*	M
ZD.1899.7.8.1	2	*Papio anubis*	M
ZD.1900.3.18.1	1	*Papio anubis*	M
ZD.1902.9.2.1	2	*Papio anubis*	M
ZD.1922.12.19.6	3	*Papio anubis*	M
ZD.1924.2.25.1	1	*Papio anubis*	M
ZD.1939.1033	3	*Papio anubis*	M
ZD.1973.1291	2	*Papio anubis*	M
Cam.II.85	2	*Papio anubis*	M
ZD.1961.758	3	*Papio cynocephalus*	F
ZD.1961.768	5	*Papio cynocephalus*	F
ZD.1897.10.1.11	2	*Papio cynocephalus*	M
ZD.1924.1.1.7	2	*Papio cynocephalus*	M
ZD.1961.782	1	*Papio cynocephalus*	M
ZD.1967.1658	1	*Papio cynocephalus*	M
M-107100	1	*Macaca fascicularis*	F
ZD.1894.6.12.13	4	*Macaca fascicularis*	F
ZD.1951.67	2	*Macaca fascicularis*	F
M-102015	1	*Macaca fascicularis*	M
M-106565	1	*Macaca fascicularis*	M
ZD.1876.10.4.9	1	*Macaca fascicularis*	M
ZD.1909.11.1.2	1	*Macaca fascicularis*	M
ZD.1955.1508	1	*Macaca fascicularis*	M
ZD.1955.1518	1	*Macaca fascicularis*	M
ZD.1842.1.19.95	6	*Macaca fuscata*	M
ZD.1931.1.11.26	1	*Macaca mulatta*	F
M-54816	3	*Macaca mulatta*	M
ZD.1921.7.9.3	1	*Macaca mulatta*	M
ZD.1923.11.4.1	1	*Macaca mulatta*	M
T4-8	6	*Macaca mulatta*	M

Ofnet 4K1802	4	*Homo sapiens*	U
Tabun	4	*Homo neanderthalensis*	U
La Quina H5	3	*Homo neanderthalensis*	U
La Chapelle	2	*Homo neanderthalensis*	U
Shanidar V	5	*Homo neanderthalensis*	U
Saldanha	2	MPH	U

Abbreviations: USNM = United States National Museum; RMCA = Royal Museum for Central Africa, Tervuren; F.C. = French Congo; M = Mammalogy; ZD = Zoological Department; Cam = Cambridge; MPH = Middle Pleistocene hominin remains; F = female; M = male; U = unknown sex.

SOM Table S13

Details of 61 specimens for which landmarks and semilandmarks were reconstructed using a manual digital reconstruction technique, showing number of points which were reconstructed using this method.

Specimen	Number of (semi)landmarks	Group	Sex
USNM 545030	10	*Gorilla beringei beringei*	F
USNM 545026	6	*Gorilla beringei beringei*	F
USNM 545029	10	*Gorilla beringei beringei*	F
USNM 395636	6	*Gorilla beringei beringei*	M
USNM 396934	8	*Gorilla beringei beringei*	M
USNM 545028	1	*Gorilla beringei beringei*	M
USNM 545034	19	*Gorilla beringei beringei*	M
USNM 545035	17	*Gorilla beringei beringei*	M
USNM 260582	11	*Gorilla beringei graueri*	F
USNM 590946	1	*Gorilla gorilla diehli*	F
USNM 590947	1	*Gorilla gorilla diehli*	F
USNM 590948	5	*Gorilla gorilla diehli*	F
USNM 590951	3	*Gorilla gorilla diehli*	F
USNM 590956	4	*Gorilla gorilla diehli*	F
USNM 590963	12	*Gorilla gorilla diehli*	F
USNM 590950	5	*Gorilla gorilla diehli*	M
USNM 590953	3	*Gorilla gorilla diehli*	M
USNM 590955	9	*Gorilla gorilla diehli*	M
USNM 590958	5	*Gorilla gorilla diehli*	M
USNM 590959	6	*Gorilla gorilla diehli*	M
USNM 590967	10	*Gorilla gorilla diehli*	M
USNM 590968	15	*Gorilla gorilla diehli*	M
USNM 252575	1	*Gorilla gorilla gorilla*	F
USNM 220380	10	*Gorilla gorilla gorilla*	F
USNM 252576	7	*Gorilla gorilla gorilla*	F
USNM 252579	10	*Gorilla gorilla gorilla*	F
USNM 252580	12	*Gorilla gorilla gorilla*	F
USNM 252577	19	*Gorilla gorilla gorilla*	F
USNM 174714	21	*Gorilla gorilla gorilla*	M
USNM 176206	33	*Gorilla gorilla gorilla*	M
USNM 176207	8	*Gorilla gorilla gorilla*	M
USNM 176209	13	*Gorilla gorilla gorilla*	M
USNM 176213	18	*Gorilla gorilla gorilla*	M
USNM 176216	21	*Gorilla gorilla gorilla*	M
USNM 220324	10	*Gorilla gorilla gorilla*	M
USNM 174701	1	*Pan troglodytes troglodytes*	F
USNM 174702	3	*Pan troglodytes troglodytes*	F
USNM 174707	3	*Pan troglodytes troglodytes*	F
USNM 174710	1	*Pan troglodytes troglodytes*	F
USNM 220062	4	*Pan troglodytes troglodytes*	F
USNM 599172	6	*Pan troglodytes troglodytes*	M
USNM 220327	11	*Pan troglodytes troglodytes*	M

USNM 220326	1	*Pan troglodytes troglodytes*	M
USNM 220065	4	*Pan troglodytes troglodytes*	M
USNM 176242	3	*Pan troglodytes troglodytes*	M
USNM 176240	1	*Pan troglodytes troglodytes*	M
USNM 176228	2	*Pan troglodytes troglodytes*	M
USNM 174704	2	*Pan troglodytes troglodytes*	M
USNM 236971	7	*Pan troglodytes schweinfurthii*	F
USNM 477333	2	*Pan troglodytes verus*	F
USNM 481803	3	*Pan troglodytes verus*	F
USNM 162899	11	*Papio anubis*	M
Wajak I	1	*Homo sapiens*	U
Keilor	1	*Homo sapiens*	U
Liujiang	5	*Homo sapiens*	U
Skhūl V	8	*Homo sapiens*	U
Spy 1	12	*Homo neanderthalensis*	U
D2282	5	*Homo erectus* s.l.	U
Sangiran 17	1	*Homo erectus* s.l.	U
KNM-ER 1813	12	*Homo habilis*	U
Sts 5	8	*Australopithecus africanus*	U

Abbreviations: USNM = United States National Museum; D2282 = Dmanisi hominin 2282; KNM-ER = Kenya National Museum, East Rudolf; Sts = Sterkfontein Type Site; F = female; M = male; U = unknown.

SOM Table S14

Details of 14 specimens for which single landmarks were reconstructed using the method of reflection across an empirical midplane, showing number of landmarks which were reconstructed using this method.

Specimen	Number of landmarks	Group	Sex
ZD.1961.737	1	*Papio cynocephalus*	Female
M-102018	1	*Macaca fascicularis*	Female
M-103652	1	*Macaca fascicularis*	Female
M-107095	1	*Macaca fascicularis*	Female
M-107559	1	*Macaca fascicularis*	Male
Ofnet 4K1811	1	*Homo sapiens*	Unknown
Tepexpan	1	*Homo sapiens*	Unknown
RCSOM/B.94	2	*Homo sapiens*	Male?
RCSOM/B.124	2	*Homo sapiens*	Female?
Kiyono-34	1	*Homo sapiens*	Female
Kiyono-66	2	*Homo sapiens*	Male?
Kiyono-70	2	*Homo sapiens*	Female?
Dali	1	MPH	Unknown
Tabun	1	*Homo neanderthalensis*	Unknown

Abbreviations: ZD = Zoological Department; M= Mammalogy; RCSOM = Royal College of Surgeons Odontological Material; MPH = Middle Pleistocene hominin remains.

SOM Table S15

Details of 37 fossil specimens which were digitally reconstructed. Reference specimen(s) indicates the specimens that were used to guide reconstruction.

Specimen	Group	Reference specimen(s)
Ofnet 4K1802	*Homo sapiens*	Ofnet 4K1802
Combe Capelle	*Homo sapiens*	Combe Capelle
Wajak I	*Homo sapiens*	Wajak I
Keilor	*Homo sapiens*	Keilor
Brno II	*Homo sapiens*	Brno II, Brno III
Předmostí IV	*Homo sapiens*	Předmostí III
Cro-Magnon II	*Homo sapiens*	Cro-Magnon II
Mladeč 2	*Homo sapiens*	Mladeč 1
Liujiang	*Homo sapiens*	Liujiang
Qafzeh 9	*Homo sapiens*	Qafzeh 9
Jebel Irhoud 1	*Homo sapiens*	Jebel Irhoud 1
Gibraltar 1	*Homo neanderthalensis*	Gibraltar 1
Guattari	*Homo neanderthalensis*	Guattari
Krapina C	*Homo neanderthalensis*	Krapina C, Shanidar 1
Krapina E	*Homo neanderthalensis*	Krapina E, Shanidar 1
Le Moustier 1	*Homo neanderthalensis*	Le Moustier 1
Saint Césaire	*Homo neanderthalensis*	Sainte Césaire, Shanidar 1
Shanidar V	*Homo neanderthalensis*	Shanidar V
Spy 1	*Homo neanderthalensis*	Spy 1, La Chapelle
Bodo	MPH	Bodo, Kabwe 1
Ceprano	MPH	Sima de los Huesos 5
Maba	MPH	Maba, Dali
Narmada	MPH	Narmada, Kabwe 1
Saldanha	MPH	Kabwe 1
SH5	MPH	SH5
Steinheim	MPH	Arago 21
Zuttiyeh	MPH	Skhūl V
Solo VI	*Homo erectus* s.l.	Solo VI, Sangiran 17
Zhoukoudian XII	*Homo erectus* s.l.	Zhoukoudian XII
KNM-ER 3733	*Homo erectus* s.l.	KNM-ER 3733
KNM-ER 3883	*Homo erectus* s.l.	KNM-ER 3883
D2282	*Homo erectus* s.l.	D2282, D4500
KNM-ER 1813	*Homo habilis*	KNM-ER 1813
KNM-ER 1470	*Homo habilis*	KNM-ER 1470
KNM-WT 17000	*Paranthropus aethiopicus*	KNM-WT 17000
KNM-ER 406	*Paranthropus boisei*	KNM-ER 406
KNM-ER 732	*Paranthropus boisei*	KNM-ER 732

Abbreviations: KNM-ER = Kenya National Museum, East Rudolf; KNM-WT = Kenya National Museum, West Turkana; MPH = Middle Pleistocene hominin remains; SH5 = Sima de los Huesos 5; D2282 = Dmanisi hominin 2282; D4500 = Dmanisi hominin 4500.

SOM Table S16

Details of 32 specimens used for intraobserver error assessment.

Number	Specimen	Species	Sex
IOE1	RMCA 2260	*Gorilla beringei beringei*	Male
IOE2	RMCA 27840	*Gorilla beringei graueri*	Female
IOE3	USNM 590946	*Gorilla gorilla dielhi*	Female
IOE4	ZD.1878.12.14.1	*Gorilla gorilla gorilla*	Male
IOE5	RMCA 27012	*Pan paniscus*	Female
IOE6	RMCA 29036	*Pan paniscus*	Male
IOE7	RMCA 29074	*Pan troglodytes schweinfurthii*	Female
IOE8	ZD.1939.3365	*Pan troglodytes troglodytes*	Male
IOE9	ZD.1908.8.9.42	*Papio anubis*	Female
IOE10	ZD.1925.5.12.1	*Papio anubis*	Male
IOE11	ZD.1961.772	*Papio kindae*	Female
IOE12	ZD.1961.734	*Papio kindae*	Male
IOE13	M-30622	*Macaca fascicularis*	Female
IOE14	ZD.1919.11.12.8	*Macaca fascicularis*	Male
IOE15	ZD.1905.11.3.2	*Macaca fuscata*	Male
IOE16	KAS-290	*Macaca fuscata yakui*	Female
IOE17	ZD.1914.7.10.3	*Macaca mulatta*	Female
IOE18	ZD.1931.1.11.8	*Macaca mulatta*	Male
IOE19	RCSOM/B 57	*Homo sapiens*	Male[a]
IOE20	ESC11 SK2332	*Homo sapiens*	Intermediate[a]
IOE21	Kiyono-61	*Homo sapiens*	Unknown[a]
IOE22	AS.17.0.2	*Homo sapiens*	Female[a]
IOE23	1717	*Homo sapiens*	Male[a]
IOE24	EU.1.5.082	*Homo sapiens*	Male[a]
IOE25	Zhoukoudian UC 101	*Homo sapiens*	Unknown
IOE26	Border Cave 1	*Homo sapiens*	Unknown
IOE27	Gibraltar 1	*Homo neanderthalensis*	Unknown
IOE28	Bodo	MPH	Unknown
IOE29	KNM-ER 3733	*Homo erectus* s.l.	Unknown
IOE30	D4500	*Homo erectus* s.l.	Unknown
IOE31	OH 24	*Homo habilis*	Unknown
IOE32	KNM-ER 732	*Paranthropus boisei*	Unknown

Abbreviations: IOE = Intraobserver error; RMCA = Royal Museum for Central Africa, Tervuren; USNM = United States National Museum; ZD = Zoological Department; M = Mammalogy; KAS = Kyoto University; RCSOM = Royal College of Surgeons Odontological Material; AS = Asia; EU = Europe; UC = Upper Cave; KNM-ER = Kenya National Museum, East Rudolf; D4500 = Dmanisi hominin 4500; OH = Olduvai hominid; MPH = Middle Pleistocene hominin remains.

[a] Based on sex assessment, not known sex values.

SOM References

Adams, D.C., Otárola-Castillo, E., Paradis, E., 2013. Geomorph: An R package for the collection and analysis of geometric morphometric shape data. Methods in Ecology and Evolution 4, 393-399.

Cignioni, P., Callieri, M., Corsini, M., Dellepiane, M., Ganovello, F., Ranzuglia, G., 2008. MeshLab: An open-source mesh processing tool. In: Scarano, V., Chiara, R.D., Erra, U. (Eds.), Eurographics Italian Chapter Conference. Eurographics, Salerno, pp. 129-136

CloudCompare, 2016. GPL software version 2.8 beta. http://www.cloudcompare.org/

IBM Corp., 2018. IBM SPSS Statistics for Windows, Version 26.0. IBM Corp., Armonk.

NextEngine, Inc., 2006-2015. ScanStudio, Version 2.0.2. NextEngine, Inc., Santa Monica, CA

Phillips, R., O'Higgins, P., Bookstein, F.L., 2010. EVAN (European Virtual Anthropology Network) toolbox. In: Green, B., Gunnaron, H., Shady, Y., Dalge, V., Gowigati, R. (Eds.), European Virtual Anthropology Network - EVAN and the EVAN-Society. EVAN, Vienna. https:// www.evan.at.

R Core Team, 2019. R: A language and environment for statistical computing. R Foundation for Statistical Computing, Vienna.

Stratovan Corporation, 2016. Stratovan Checkpoint. Version 2016.06.28.0428. Jun 28, 2016. Stratovan Corporation, Davis. https://www.stratovan.com/products/checkpoint

Stratovan Corporation, 2018. Stratovan Checkpoint. Version 2018.09.07.0325. Sep 07, 2018. Stratovan Corporation, Davis. https://www.stratovan.com/products/checkpoint

White, S., Soligo, C., Pope, M., Hillson, S., 2020. Taxonomic variation in the supraorbital region of the catarrhine primates. American Journal of Physical Anthropology 171, 198-218.

Wiley, D., Wiley, N., Amenta, D., Ghosh, W., Ghosh, W., Delson, F.J., Delson, F.J., Harcourt Smith, B., Rohlf, Hamann. 2005. Evolutionary morphing. UC Davis–Institute for Data Analysis and Visualisation, Davis. Retrieved from https://escholarship.org/uc/item/4k5991zk